2016

Development and Application of Gadolinium Free Cardiac Magnetic Resonance Fibrosis Imaging for Multiscale Study of Heart Failure in Patients with End Stage Renal Disease

Tori A. Stromp
University of Kentucky, tstromp@gmail.com
Digital Object Identifier: https://doi.org/10.13023/ETD.2016.443

STUDENT AGREEMENT:

I represent that my thesis or dissertation and abstract are my original work. Proper attribution has been given to all outside sources. I understand that I am solely responsible for obtaining any needed copyright permissions. I have obtained needed written permission statement(s) from the owner(s) of each third-party copyrighted matter to be included in my work, allowing electronic distribution (if such use is not permitted by the fair use doctrine) which will be submitted to UKnowledge as Additional File.

I hereby grant to The University of Kentucky and its agents the irrevocable, non-exclusive, and royalty-free license to archive and make accessible my work in whole or in part in all forms of media, now or hereafter known. I agree that the document mentioned above may be made available immediately for worldwide access unless an embargo applies.

I retain all other ownership rights to the copyright of my work. I also retain the right to use in future works (such as articles or books) all or part of my work. I understand that I am free to register the copyright to my work.

REVIEW, APPROVAL AND ACCEPTANCE

The document mentioned above has been reviewed and accepted by the student's advisor, on behalf of the advisory committee, and by the Director of Graduate Studies (DGS), on behalf of the program; we verify that this is the final, approved version of the student's thesis including all changes required by the advisory committee. The undersigned agree to abide by the statements above.

Tori A. Stromp, Student

Dr. Moriel Vandsburger, Major Professor

Dr. Kenneth Campbell, Director of Graduate Studies

DEVELOPMENT AND APPLICATION OF GADOLINIUM FREE CARDIAC MAGNETIC RESONANCE FIBROSIS IMAGING FOR MULTISCALE STUDY OF HEART FAILURE IN PATIENTS WITH END STAGE RENAL DISEASE

DISSERTATION

A dissertation submitted in partial fulfillment of the requirements for the degree of Doctor of Philosophy in the College of Medicine at the University of Kentucky.

By:

Tori Ann Stromp

Co-Directors: Dr. Moriel Vandsburger,
Professor of Physiology and Biomedical Engineering
and Dr. Brian Delisle, Professor of Physiology

Lexington, Kentucky
2016

ABSTRACT OF DISSERTATION

DEVELOPMENT AND APPLICATION OF GADOLINIUM FREE CARDIAC MAGNETIC RESONANCE FIBROSIS IMAGING FOR MULTISCALE STUDY OF HEART FAILURE IN PATIENTS WITH END STAGE RENAL DISEASE

Cardiac magnetic resonance (CMR) is a powerful tool to noninvasively image ventricular fibrosis. Late gadolinium enhancement (LGE) CMR identifies focal and, with T1 mapping, diffuse fibrosis. Despite prevalent cardiac fibrosis and heart failure, patients with end stage renal disease (ESRD) are excluded from LGE. Absence of a suitable diagnostic has limited the understanding of heart failure and obstructed development of therapies in the setting of ESRD. A quantitative, gadolinium free fibrosis detection method could overcome this critical barrier, propelling the advancement of diagnostic, monitoring, and therapy options. This project describes the development of a gadolinium free CMR technique and application for cardiac fibrosis measurement in patients with ESRD.

Magnetization transfer (MT) occurs during standard cine balanced steady state free precession (bSSFP) CMR, where extracellular matrix protons exchange magnetization with water molecules. Extracellular water volume expansion, concomitant with fibrosis, reduces MT and subtly elevates signal intensity. Our technique, 2-pt bSSFP, extracts endogenous contrast sensitive to tissue fibrosis by obtaining pairs of high and low MT-weighted images and calculating normalized signal differences, denoted by $\Delta S/S_o$.

We tested 2-pt bSSFP in patients referred for CMR and found excellent agreement spatially with LGE and quantitatively with extracellular volume fraction. Diagnostic and clinical application of 2-pt bSSFP was comparable to LGE. We applied 2-pt bSSFP to patients with ESRD for multiscale comparison with correlates of fibrosis ranging from blood biomarkers to whole organ function. Patients with ESRD displayed hypertrophy with reduced contraction, but elevated $\Delta S/S_o$ and fibrosis. Some biomarkers correlated with both hypertrophy and fibrosis, highlighting the need to distinguish between hypertrophic and fibrotic remodeling. We monitored fibrosis over 1 year using 2-pt bSSFP in a cohort of

patients with ESRD. $\Delta S/S_o$ and fibrotic burden increased substantially, despite minor changes in structure and function.

Collectively these studies validate and apply 2-pt bSSFP for gadolinium free fibrosis CMR in patients with ESRD. While ventricular structure and function are commensurate with progression toward heart failure, it is now possible to specifically describe global and focal patterns of cardiac fibrosis in ESRD, along with comparisons to blood biomarkers which may lead to improved diagnostics and molecular treatment targets.

KEYWORDS: Cardiac Fibrosis, Magnetic Resonance Imaging, End Stage Renal Disease, Hemodialysis

Tori Stromp

28 Nov 2016
Date

DEVELOPMENT AND APPLICATION OF GADOLINIUM FREE CARDIAC MAGNETIC RESONANCE FIBROSIS IMAGING FOR MULTISCALE STUDY OF HEART FAILURE IN PATIENTS WITH END STAGE RENAL DISEASE

By

Tori Ann Stromp

Moriel Vandsburger, PhD
Co-Director of Dissertation

Brian Delisle, PhD
Co-Director of Dissertation

Kenneth Campbell, PhD
Director of Graduate Studies

28 Nov 2016
Date

ACKNOWLEDGEMENTS

I owe immeasurable gratitude to the following individuals, among many others, for their impact on my training and this project.

I am truly grateful for the guidance of my primary mentor and Dissertation Chair, Dr. Moriel Vandsburger. His unmatched intelligence, unwavering assurance, and unending positivity have driven my eternal pursuit of inquiry and success with an ingrained, genuine optimism. I aspire to someday achieve the caliber of scientist and mentor that I was so fortunate to encounter.

I gratefully acknowledge my Dissertation Committee—Dr. Brian Delisle (Co-Chair), Dr. Brian Jackson, Dr. Susan Smyth, and Dr. Gregory Graf—for their constant challenge and direction, which have improved me as a scientist through this process. I thank Dr. Misung Jo for serving as the external examiner for my dissertation defense.

Dr. Steve Leung deserves the utmost appreciation for his detailed training. He taught me the balance of technical skill, troubleshooting, and patient rapport which merely scratches the surface of his professional and scientific prowess. Many thanks to Dr. Vincent Sorrell for his mentorship and assistance with our protocols, and the cardiac MRI technicians—Becca Egli, Joe Jenkins, John Green and Karsten Colwell —for their assistance in image acquisition. I am grateful for the contributions of Tyler Spear, Becca Kidney, Kristin Andres, and Josh Kaine, who were game-changers at pivotal points throughout this work. Each has truly improved the course of this research. It was a privilege to work with these young stars who are destined to impact the future of science and medicine.

Finally, I extend my deepest gratitude to the dedicated participants of this research. The altruism of these volunteers exhibits their commitment to the progress of science and medicine. While many will never witness or benefit from the improvements we aim to make in clinical care, their time, data, and insight will forever impact our understanding of disease and drive advances in diagnostic and treatment options. They are, after all, why I became a scientist.

TABLE OF CONTENTS

LIST OF TABLES

LIST OF FIGURES

CHAPTER 1: INTRODUCTION

Heart Failure

Epidemiology, Etiology, and Clinical Presentation

Heart disease is currently the leading cause of death in the United States [1]. The prevalence of heart failure remains high at over 5.5 million adults in the United States [2]. Over $20 billion in medical expenses are attributed to heart failure. By the year 2030, the projected prevalence of heart failure is expected to exceed 8 million Americans costing over $53 billion [3]. This is driven by both the increasing incidence in a growing elderly population and improved survival due to advances in detection and treatments [3].

Heart failure is defined as the inability of the heart to pump enough blood to meet the metabolic demands of the body. The etiology and clinical features are complex. Heart failure can result from filling and/or ejection abnormalities, caused by conduction, structural and/or functional alterations in the pericardium, myocardium, endocardium, valves, or vasculature [4,5]. Signs and symptoms are similarly complex and not specific to heart failure. Patients may present with dyspnea, exercise intolerance, fatigue, and fluid retention, although their manifestations are highly varied [4,6]. Many patients with heart failure remain asymptomatic.

The majority of signs and symptoms of heart failure are caused by reduced left ventricular (LV) function. In fact, LV ejection fraction (EF) of <35% or <40% is often used as a cutoff to classify heart failure with reduced EF (HFrEF)

versus heart failure with preserved EF (HFpEF) [4,6]. HFrEF, or systolic heart failure, comprises about half of the heart failure population and is better understood than HFpEF, or diastolic heart failure [5]. This cutoff is prognostic and often used for enrollment into randomized controlled clinical trials [5], meaning efficacy for new treatments has been shown in HFrEF patients only [4]. The major influence of the LV in heart failure development, prognosis, and treatment is the motivation for focusing this project on investigating the LV only.

Cardiac Remodeling

Cardiac remodeling is the alteration of the structure (geometry, shape, and mass) and ultimately physiological function (contraction and relaxation) of the heart [7]. Particularly in the LV, remodeling is now appreciated as an important determinant in the progression and severity of heart disease to heart failure. Remodeling is a physiologic or pathophysiologic process mainly affecting the myocytes, but also the interstitium, fibroblasts, collagen, and vasculature in the ventricle [7]. Causes include, but are not limited to, myocardial infarction, volume or pressure overload, and inflammation.

Following initial myocardial infarct, myocyte necrosis leaves reduced cellular mass and an area of thinned LV wall. In the first hours to weeks, the infarct region typically undergoes disproportionate thinning and dilation, known as infarct expansion [8-10], with a loss of regional myocardial mass [11]. Chronically, whole chamber dilation may follow, leading to increased end diastolic (EDV) and end systolic volumes (ESV) while restoring myocardial mass

to pre-infarct levels [12,13]. Increased chamber volume leads to volume overload in remote areas, causing hypertrophy in non-infarct zones [9]. These remodeling events aid in the maintenance of ejection fraction [12] and cardiac output [14], despite reduced contractility of the infarct segments, but at the cost of increased chamber volumes. Some patients may eventually progress to noncompensatory dilation and remodeling which leads to reduced EF [14] and can proceed to HFrEF.

Hemodynamic overload increases myocyte stretch, a mechanical signal that initiates a complex intercellular cascade leading to cardiomyocyte growth and hypertrophy [15]. Systemic hypertension leads to pressure overload, causing elevated LV wall stress. This is counteracted by increasing wall thickness and mass. The resulting structural pattern is labeled concentric hypertrophy, in which LV chamber size, EDV and ESV [16], and cardiac output are reduced [15]. Thickened walls may also be stiffer thus unable to relax and fill with blood, leading to diastolic heart failure. Another pattern of LV growth—eccentric hypertrophy—is characterized by increased chamber size in conjunction with increased LV mass [15,16]. Often caused by volume overload, the LV wall responds by dilating, allowing preserved cardiac output and relatively normal wall thickness [16]. A third pattern of remodeling—concentric remodeling—has been described as normal LV mass with increased wall thickness [16]. While mass is unchanged, the decrease in chamber size leads to reduced cardiac output. Overall LV mass increases, independent of body size, as measured by left ventricular mass index (LVMI) are prognostic of clinical events and cardiac death

[17,18]. To support hypertrophic cardiomyocytes and their coordinated contraction, connective tissues of the extracellular matrix must remodel in parallel [19]. While initially adaptive, this matrix remodeling process can become pathological and lead to increased deposition of collagen in conjunction with hypertrophy (see *Cardiac Fibrosis* below).

Additional causes can lead to pathological remodeling similar to those described above. Dilated cardiomyopathy, for example, may be idiopathic or due to non-ischemic influences such as heredity or alcoholism [20]. Hypertrophic cardiomyopathy may also be idiopathic or inherited [7,21]. Following hemodynamic or injurious insult, however, remodeling is an adaptive process to maintain cardiac function. The transition from compensatory to maladaptive remodeling may contribute to heart failure progression and deteriorating prognosis [7].

Cardiac Fibrosis

In healthy hearts, cardiomyocytes are surrounded by a lattice-like matrix of proteins and molecules along with other cell types like cardiac fibroblasts [22]. This extracellular matrix provides a scaffold for shape and structure and is required for proper function of the ventricles by assisting conduction and force generation. The equilibrium of the extracellular matrix, which consists primarily of collagen type I, is responsible for maintaining proper cardiac stiffness for efficient contraction and relaxation [23]. Cardiac fibrosis occurs from the remodeling of extracellular matrix and subsequent increase in collagen deposition.

Similar to and often in conjunction with structural remodeling, collagen deposition is a compensatory process to maintain proper ventricular stiffness. This is evident in myocardial infarction where necrotic cardiomyocytes are replaced with collagen [24] to form a dense scar. Fibrotic tissue protects the ventricle from rupture [25] and increases stiffness to maintain pump function. This replacement fibrosis process is typically characterized by a dense, focal pattern of scar.

Reactive fibrosis is a progressive process that develops from an increase in collagen production by cardiac fibroblasts [26]. Unlike replacement fibrosis, reactive fibrosis is characterized by a diffuse interstitial distribution. Hypertension, diabetes [27], and aging [22] contribute to the expansion of extracellular matrix and subsequent collagen deposition. Pressure overload induced hypertrophy (as seen in hypertension [28]) and hypertrophic cardiomyopathy [29] are also associated with diffuse, reactive fibrosis. Fibrosis has also been identified in volume overload-induced ventricular dilation without ischemia [30] and in dilated cardiomyopathy [31]. As described previously, infarcted hearts may also develop hypertrophy in remote zones [9] requiring subsequent adaptation by the extracellular matrix. Thus increased collagen content may also arise in this non-infarcted tissue of ischemic hearts [31,32], particularly in areas of hypertrophy.

While reactive fibrosis can occur simultaneously or subsequently in structural remodeling, there is discrepancy whether dilation or hypertrophy directly correlates with fibrosis. An increase in collagen content is not absolute in areas of hypertrophy following myocardial infarction [24] or hypertension [33].

Septal thickness and overall heart size are common clinical indicators of hypertrophy and often used as surrogates for fibrosis, yet some have found a lack of association with fibrotic burden [33]. While fibrosis is presumed to follow hypertrophy, there is also evidence that fibrosis can actually precede some forms of hypertrophy [34]. Particularly in the context of hypertrophy, then, myocardial fibrosis is not directly explained merely by growing cardiomyocytes [33]. Other unknown factors must be contributing to the development of reactive fibrosis.

Importantly, fibrosis can lead to ventricular stiffening [35,36], which impacts pump function. Progressive collagen deposit causes stiffening, which typically affects diastolic relaxation followed by systolic contraction [37]. Fibrosis also disrupts the syncytium formed by healthy cardiomyocytes by isolating bundles of cardiomyocytes and disrupting gap junctions. The physical separation and disconnection of cardiomyocytes slows conduction and wave propagation, increasing the susceptibility to conduction block, which can initiate reentry and arrhythmia [38]. Thus, increased fibrosis is linked to worsening heart failure, arrythmogenesis, mortality risk [33], and sudden cardiac death [39].

Chronic Kidney Disease and End Stage Renal Disease

Epidemiology and Etiology

Over 13% of the United States adult population has persistent reduction of kidney function, or chronic kidney disease (CKD) [40]. Commensurate with current national health epidemics, primary risk factors for CKD include diabetes, hypertension, cardiovascular disease, and obesity [40]. Likely due to these

comorbidities, Blacks/African Americans are disproportionately affected by CKD. The severity of CKD is categorized by stages based on estimated glomerular filtration rate (eGFR) and albumin clearance. Patients are diagnosed with CKD if eGFR <60 ml/min/1.73m^2 or urine albumin/creatinine ratio >30mg/g over persistent measurements. Patients who reach eGFR<15ml/min/m^2 are considered CKD Stage 5, or complete renal failure. At this point, patients may be classified as end stage renal disease (ESRD), which indicates that they require renal replacement therapy for survival [41].

ESRD affects over 600,000 American adults and lends over $87 billion to total Medicare costs [42]. While overall incidence has plateaued, incident cases in middle aged and especially elderly populations are on the rise [40,41]. The leading primary causes of ESRD are diabetes, hypertension, glomerulonephritis, and cystic kidney disease [40]. Diabetes and hypertension as primary cause of ESRD are drastically higher in Blacks/African Americans than any other race [40].

Treatments

Each year, over 100,000 patients begin renal replacement therapy for treatment of ESRD [40,42,43]. Of patients initiating renal replacement therapy, nearly 90% receive hemodialysis treatment, but peritoneal dialysis (9%) and kidney transplants (3%) are increasing [42], especially in younger patients [40]. In patients on hemodialysis, death rates are highest in the first year of treatment, then after a drastic drop at year 2, steadily increase over at least the next 5 years

[42]. Cardiovascular events are the leading cause of deaths in patients on hemodialysis for ESRD, encompassing over 50% of the known causes of death [44]. Within 3 years of ESRD therapy, only about 50% of patients are still alive [41].

End Stage Renal Disease and Cardiac Risk

The term cardiorenal syndrome has been used to describe the combined failure of both heart and kidneys [45]. Five types have been identified based on the influence of and outcome in each organ. Cardiorenal Type IV comprises CKD as an independent cause of heart failure [45]. Renal dysfunction worsens hypertension, increases fluid retention, and elevates circulating uremic toxins. Thus, ESRD contributes to volume overload, pressure overload, and cardiomyopathy [46]. These are the fundamental causes of cardiac remodeling, resulting in eccentric hypertrophy, concentric hypertrophy, and dilation, respectively, and promote the transition toward heart failure and possibly death. In fact, cardiovascular disease is the leading cause of death in patients with ESRD [42]

Hemodialysis exacerbates many cardiovascular risks in patients with ESRD. One in 4 patients on hemodialysis will die from sudden cardiac death [43]. For long term hemodialysis patients, risk of cardiovascular mortality is 10-20 times greater than the general population [47]. Unique risk factors for sudden cardiac death include hyperphysiologic swings in electrolytes and blood volume

[48,49]. Extreme blood volume removal during hemodialysis may also lead to hypotension, cardiac stunning [50], and repeated ischemic events [45].

End State Renal Disease and Cardiac Fibrosis

Patients with ESRD almost ubiquitously develop dilation [51] and/or hypertrophic [52] remodeling but fibrosis is not certain. Hypertrophy seems to develop early in CKD, prior to hemodialysis initiation [53] and progresses with deteriorating eGFR [54]. Previous reports describe a varied but large proportion—up to 91% [55]—of hemodialysis patients who are hypertrophic [56-58]. In hemodialysis patients, hypertrophy is associated with poorer systolic function [58] and worse prognosis. Elevated blood pressure and ventricular dilation—likely from chronic volume overload—associates with increased LV mass [56,57], making the interplay between patterns of structural remodeling complex.

Myocardial infarction prevalence is about 14% in hemodialysis patients, yet cause of death is most often attributed to sudden cardiac death, not myocardial infarction [47]. While a fraction of patients on hemodialysis develop replacement fibrosis following myocardial infarction, a larger proportion develop reactive fibrosis, which can occur with or without infarct [59].

Similar to the cardiac patient population, CKD patients can demonstrate fibrosis irrespective of hypertrophy [60]. It has been shown that diffuse fibrosis may not correlate with systolic function or low EF [58]. While an autopsy study revealed an association between fibrosis and hemodialysis vintage [61] (time of

hemodialysis treatment) others have not found a similar correlation [58]. It is understood that patients on hemodialysis with a greater fibrotic burden (>30% of tissue area) have significantly worse prognosis [51], despite the lack of association with systolic dysfunction. In fact, in a multivariate analysis including hypertension, diabetes, ejection fraction, LV dilation, and cardiomyocyte hypertrophy as predictors, only the percent area of LV fibrosis emerged as an independent predictor of cardiac death [51]. An experimental model in rabbits also linked induced renal failure to arrhythmias and increased fibrosis [62]. Therefore, cardiac fibrosis is an independent risk factor for death above and beyond the structural remodeling seen in patients with ESRD. As articulated by McCullogh et al., cardiac fibrosis is a common and significant substrate for pump dysfunction and sudden cardiac death due to arrhythmia, the two leading mechanisms of death in ESRD [45].

Measuring Cardiac Fibrosis

Tissue Biopsy

Since fibrosis is a crucial element in cardiac disease and heart failure, accurate measurement is essential for proper diagnosis, treatment selection, and survival—particularly in the ESRD population. The historical gold standard for fibrosis identification is collagen volume fraction measured by myocardial tissue biopsy. Biopsy studies in ESRD patients have identified cardiomyocyte hypertrophy along with replacement [50] and diffuse fibrosis [51,63,64]. Unfortunately, this technique is prone to falsely report the absence of fibrosis

[65], likely due to the heterogeneity of the disease. Additionally, clinicians must assume fibrotic content of non-biopsied regions from small tissue samples. Aoki et al. report a mean percent area of fibrosis in myocardial samples in hemodialysis patients that is only slightly elevated (22%) compared to controls (21%) [51], which highlights that wide distribution of fibrosis leaves biopsy susceptible to false underestimations of true, global fibrotic burden. The invasiveness of the biopsy procedure also renders it unsuitable for serial measurements, which is critical for monitoring the actively remodeling hearts of patients with ESRD.

Echocardiography

Echocardiography is a widely available technology with the ability to rapidly acquire measurements of LV mass and monitor systolic and diastolic function. Due to the prevalence of LV hypertrophy in the ESRD population, echocardiography has been widely adopted for measurement of cardiac remodeling and dysfunction. Measures of mass and volume are obtained for assessment of hypertrophy and dilation as well as LV function assessed by EF [66]. Using deformation imaging, echocardiography can measure LV dysfunction through strain and strain rate measurement in radial, circumferential, and longitudinal directions to identify systolic dysfunction [67]. Diastolic dysfunction can be assessed by comparing early (E) and late (A) diastolic strain via the E/A ratio and is predictive of outcomes [67]. Location and extent of infarct patterns may be identified by wall reduced tissue velocity [66].

Due to the potential correlation between hypertrophy, dysfunction, and fibrosis, echocardiography has been extended to the assessment of fibrosis in patients with ESRD. The unique and hyperphysiologic hemodynamic variations experienced by patients with ESRD can influence the accuracy of echocardiography. Measurements via echocardiography depend on both loading conditions and an assumed symmetric geometry of the LV [52], which is problematic for the dynamically shifting blood volumes and remodeling ESRD heart. It has been shown that echocardiography systematically overestimates LV mass and volumes in patients on hemodialysis [52,68]. Since hypertrophy is often used as a correlate for fibrosis, this overestimation not only impacts the understanding of structural remodeling, but also the assumption of cardiac fibrotic burden in ESRD. While this noninvasive method is preferred over biopsy, echocardiographic functional biomarkers such as E/A ratio may be unable to distinguish cardiac fibrosis as measured by histology [51], leaving this technology unsuitable for fibrosis identification in patients with ESRD.

Contrast Enhanced Cardiac Magnetic Resonance Imaging

Cardiac magnetic resonance imaging (CMR) with gadolinium contrast agents has emerged as the new clinical standard for detecting fibrosis, particularly following myocardial infarction, using a technique called late gadolinium enhancement (LGE) [69-71]. Gadolinium is an extracellular contrast agent, delivered intravenously. Upon perfusion into the myocardium, gadolinium accumulates in areas of expanded interstitial space, which occurs during the

development of fibrosis [72]. It shortens the T1 (longitudinal) relaxation of protons associated with nearby water molecules, leading to an increase in signal intensity in magnetic resonance imaging (MRI). Slower kinetics and increased concentrations of gadolinium in fibrotic areas can be detected as enhancement on images 5-20 min after contrast agent injection [72]. Thus, LGE creates contrast between fibrotic and healthy myocardial tissue, where gadolinium washes out more quickly.

While adequate for identifying focal fibrosis, relatively low levels of signal enhancement preclude the identification of diffuse fibrosis by LGE [63]. Combining LGE with T1 mapping techniques allows for calculation of extracellular volume fraction and determination of diffuse fibrosis [73-76]. T1 relaxation time is shortened in proportion to the local concentration of gadolinium. The absolute T1 time in all myocardial voxels is measured to expose subtle changes in gadolinium concentration due to interstitial volume expansion and fibrosis [72]. Gadolinium distributes into all extracellular fluid in the body, so by correcting for hematocrit, the extracellular volume (ECV) fraction of the myocardium can be calculated. ECV represents a quantitative measure of fibrotic burden and has been applied in a wide range of cardiac diseases [77] and validated with histological comparison of collagen volume fraction [63,78]. Increased ECV is also associated with mortality in cardiac patients [79]. Shortened post-contrast T1 times and increased ECV, consistent with diffuse fibrosis, have been correlated with ventricular stiffness, or diastolic dysfunction [64,80].

Contrast enhanced CMR plays an important role in tissue characterization and therefore differential diagnosis for cardiac patients with a wide variety of pathologies [72]. Reactive fibrosis in non-infarcted myocardium as measured by ECV is prognostic and has been associated with heart failure and death, independent of EF [81]. ECV measurement of fibrosis may also add incremental prognostic value on top of the well-established clinical risk factors for heart failure such as reduced EF, renal dysfunction, heart failure severity, and age.

Contrast enhanced CMR has been used to define patterns of fibrosis in patients with ESRD. Schietinger et al. described prevalent enhancement at LGE in hemodialysis patients, specifically identifying 3 patterns of fibrosis: (1) transmural enhancement consistent with an infarct pattern, and the more frequent non infarct-related (2) circumferential, diffuse enhancement, and (3) focal enhancement of the midwall [59]. In this study, LGE correlated with hypertrophy and systolic dysfunction on a global and segmental level, while a nonsignificant trend emerged for LGE and hemodialysis vintage. In a similar study, Mark et al. described 2 patterns of LGE, corresponding to ischemic (replacement) and non-ischemic (reactive) causes with high prevalence in ESRD patients [58]. Either type of LGE correlated with greater LV mass and dilation. Focal LGE associated with systolic dysfunction, while diffuse fibrosis did not. It is clear that a high rate of cardiac fibrosis is present in the ESRD population with varying structural and functional correlates.

In 2006, the U.S. Food and Drug Administration (FDA) issued several public health advisories resulting in updated product labeling and exclusion of

patients with renal insufficiency from gadolinium based imaging techniques [82,83]. These warnings resulted from the observation of nephrogenic systemic fibrosis in patients with ESRD supposedly caused by gadolinium [84] . Further evidence has established a causative role for gadolinium in the development of nephrogenic systemic fibrosis [84-87]. Despite the overwhelming benefits of LGE CMR for the identification of fibrotic burden and patterning, it is now unsuitable for use in patients with ESRD.

Given the severe limitations in direct fibrosis measurement, the current dogma leans on the potential correlation between fibrosis and hypertrophy or dysfunction to predict fibrosis in patients with ESRD. The field has now reverted to non-contrast CMR or echocardiographic measurements of increased myocardial mass and reduced strain as surrogate measures of fibrosis.

Non Contrast Cardiac MRI

Native T1 mapping without gadolinium is emerging as a non-contrast technique for tissue characterization [88,89], with valuable application for patients with ESRD [90]. As mentioned previously, T1 relaxation time measures the longitudinal relaxation of protons associated with water molecules. T1 is calculated using a curve-fitting algorithm based on samples taken at multiple inversion times [91]. The interstitial expansion occurring concomitantly with fibrosis development leads to an increase in extracellular water fraction, which can be detected as lengthened T1 times compared to healthy tissue. Modified Look-Locker inversion recovery (MOLLI) sequences are now widely used to

measure and map native T1 relaxation in a single acquisition during in CMR [92]. Using a threshold technique, native T1 mapping can distinguish infarcted tissue from normal tissue, in agreement with LGE, to identify replacement fibrosis [93]. Maps of T1 relaxation time allow both visual and quantitative analysis of fibrosis and have been correlated with histology [94] and contrast enhanced CMR measures of ECV [95,96]. T1 mapping in non-ischemic cardiomyopathy was correlated with dilation, ECV, and dysfunction [97], revealing a potential prognostic value for native T1 mapping. Others have shown no correlation between native T1 and histology [63] or calculation of ECV [98] though.

In a large study of patients with early CKD but not yet on dialysis, native T1 was increased and correlated with reduced strain but not LV mass [60]. Smaller reports of myocardial native T1 studies in patients on hemodialysis for ESRD are beginning to emerge [90,99]. Rutherford et al. demonstrated prolonged native T1 times along with hypertrophy and reduced strain in patients on hemodialysis [90]. Elevated T1 correlated with ventricular mass but not reduced strain. A recent case report also demonstrated the identification of non-ischemic, reactive fibrosis patterns in one hemodialysis patient [99], demonstrating the utility of native T1 to identify specific patterns of fibrosis. Larger studies are warranted to investigate the role of T1 mapping in hemodialysis patients and its correlation with other cardiac remodeling measures.

T1 mapping sequences are highly variable across centers resulting in varied reports of healthy myocardial T1 times [100]. T1 times in disease states

may be even more variable than healthy populations [101], leading to uncertainty in the accuracy for fibrosis identification. Ongoing efforts aim to standardize acquisition procedures and improve accuracy of normal myocardial T1 times so comparisons between sites and studies are more robust [96,100,102]. Heart rate variability, a common occurrence in ESRD, is a concern in T1 mapping, especially for long T1 values [91]. Additionally, the need to sample over multiple inversions, through a number of cardiac cycles, requires aggressive motion correction to be employed [103]. Due to motion correction artifacts, T1 quantitative analysis has been predominantly limited to the interventricular septum [94,95,104]. It is known that patients on hemodialysis also tend to develop anemia which can exacerbate hypertrophy [105] and arbitrarily elevate native T1 times. Without correction for hematocrit, T1 mapping may not be an accurate fibrosis measurement option in this group.

Another non-contrast technique—magnetization transfer (MT) MRI—is emerging for myocardial tissue characterization. During standard clinical imaging using cine balanced steady state free precession (bSSFP) MRI, the transfer of saturated magnetization from extracellular matrix macromolecules to the surrounding bulk water occurs through a process called magnetization transfer (MT) [106], which reduces the myocardial signal intensity [107,108]. Expansion of extracellular water volume, which occurs concomitantly with progression of fibrosis, causes reduction in MT and subtle elevation of myocardial signal intensity. This endogenous contrast mechanism can be exploited for gadolinium free CMR fibrosis imaging.

Simple visual identification of these myocardial signal elevations is challenging because of the subtle differences between healthy and fibrotic tissue. Advanced analysis of bSSFP images is required to extract the differences in MT caused by fibrosis. Two images with high and low MT-weighting are required. MT-weighting can be modulated by altering the radiofrequency (RF) pulse duration or flip angle such that long RF pulse duration or high flip angles (to a threshold) generate greater amounts of MT [108]. A pair of images is acquired with and without an off-resonance RF pulse [109] or at low and high flip angles to produce weak and strong MT effects, respectively. Effects of MT are typically measured as a ratio of signal intensity (SI) and presented as a percent following the formula: MT ratio=$(SI_{weakMT} - SI_{strongMT})/ SI_{weakMT}$ x100% [107]. Voxel-wise maps of MT ratio are generated to visually represent the alterations in myocardial MT allowing quantitative analysis per segment, slice, or whole ventricle. Notably, since MT-CMR is conducted using standard clinical bSSFP images, concurrent assessment of ventricular tissue characterization, structure, and function is possible.

MT effects have been investigated in select studies for cardiac fibrosis identification. In an experimental myocardial infarction model in rats, nuclear magnetic resonance measured the reduction of MT in acute and chronic myocardial infarction [110]. Vandsburger et al. described the identification and monitoring of scar formation by measurement of reduced MT ratio following induced myocardial infarction in mice [111]. MT-CMR showed excellent spatial association with LGE in this model. A study by Weber et al. in human participants

demonstrated uniform MT ratio in healthy myocardium, decreased MT ratio in infarcted tissue, and strong spatial agreement with LGE [108]. MT-CMR shows substantial promise for gadolinium free myocardial fibrosis measurement in patients with ESRD. The ability to combine structural, functional, and tissue characterization measurement in a single imaging technique means MT-CMR may be the key to multiscale study of fibrosis and its association with ventricular remodeling and dysfunction in hemodialysis patients with ESRD.

Summary

Patients with ESRD experience unique risk factors of heart failure and sudden cardiac death, unlike the general cardiac patient population. Clinical predictors of heart failure and sudden cardiac death are well established for cardiac patients but are complicated by comorbidities and unique exposures introduced by ESRD and hemodialysis treatment. Though these patients are highly attended in frequent hemodialysis treatment, the understanding of heart failure and sudden cardiac death in patients with ESRD remains obscure. Patients with ESRD, clearly suffer from a unique cardiomyopathy that is linked to their complex disease and treatment states. The current dogma treats hypertrophy or reduced strain as reliable surrogate measures of cardiac fibrosis in patients on hemodialysis. Conflicting evidence in a variety of studies illustrates the complex interaction and independence between structural remodeling, contractile dysfunction, and fibrosis while highlighting the inappropriateness of these dogmatic surrogate measures for fibrosis identification. While highly

related, hypertrophy, strain, and fibrosis should be treated as separate manifestations of a multifaceted disease.

The exclusion of patients with ESRD from gadolinium enhanced CMR greatly hinders the capacity to safely identify and monitor fibrosis. Absence of a suitable cardiac fibrosis diagnostic has limited the understanding of heart failure in the setting of ESRD and obstructed development and testing of potential therapies in this unique population. Development of a gadolinium free and quantitative method of fibrosis detection could overcome this critical barrier and present better diagnostic and monitoring options to propel the development of targeted therapies. Accurate and safe measurement of fibrotic burden and distribution could inform appropriate pharmaceutical interventions or serve as selection criteria for alternative treatments such as radiofrequency ablation and implantable cardioverter-defibrillator to prevent arrhythmias and ultimately reduce the risk of sudden cardiac death in patients with ESRD. The following project describes the development of a gadolinium free, MT-CMR technique and its application for cardiac fibrosis measurement and monitoring in patients with ESRD.

CHAPTER 2: GADOLINIUM FREE CARDIAC MAGNETIC RESONANCE IMAGING WITH 2-POINT CINE BALANCED STEADY STATE FREE PRECESSION

Preface

This chapter is reprinted from: Stromp TA, Leung SW, Andres KN, Jing L, Fornwalt BK, Charnigo RJ, Sorrell VL, and Vandsburger MH. Gadolinium Free Cardiac Magnetic Resonance Imaging with 2-point Cine Balanced Steady State Free Precession. *Journal of Cardiovascular Magnetic Resonance. 2015; 17.*

Alterations were made in agreement with the formatting requirements dictated by the University of Kentucky Graduate School and for clarity and continuity of this dissertation.

Synopsis

***Background*:** MRI of ventricular structure and function is widely performed using cine balanced steady state free precession (bSSFP) MRI. The bSSFP signal of myocardium is weighted by magnetization transfer (MT) and T1/T2-relaxation times. In edematous and fibrotic tissues, increased T2 and reduced MT lead to increased signal intensity on images acquired with high excitation flip angles. We hypothesized that acquisition of two differentially MT-weighted bSSFP images (termed 2-point bSSFP) can identify tissue that would enhance with gadolinium similar to standard of care late gadolinium enhancement (LGE).

***Methods*:** Cine bSSFP images (flip angles of 5º and 45º) and native-T1 and T2 maps were acquired in one mid-ventricular slice in 47 patients referred for cardiac MRI and 10 healthy controls. Afterwards, LGE images and post-contrast T1 maps were acquired and gadolinium partition coefficient (GPC) was calculated. Maps of $\Delta S/S_o$ were calculated as $(S_{45}-S_5)/S_5*100$ (%), where S_{flip_angle} is the voxel signal intensity.

***Results*:** Twenty three patients demonstrated areas of myocardial hyper-enhancement with LGE. In enhanced regions, $\Delta S/S_o$, native-T1, T2, and GPC were heightened ($p<0.05$ vs. non-enhanced tissues). $\Delta S/S_o$, native-T1, and T2 all demonstrated association with GPC, however the association was strongest for $\Delta S/S_o$. Bland-Altman analysis revealed a slight bias towards larger volume of enhancement with $\Delta S/S_o$ compared to LGE, and similar transmurality. Subjective

analysis with 2-blinded expert readers revealed agreement between $\Delta S/S_o$ and LGE of 73.4%, with false positive detection of 16.7% and false negative detection of 15.2%.

***Conclusions*:** Gadolinium free 2-point bSSFP identified tissue that enhances at LGE with strong association to GPC. Our results suggest that with further development, MT-weighted CMR could be used similar to LGE for diagnostic imaging.

Background

Cardiac magnetic resonance imaging (CMR) has become a reference standard modality to image ventricular structure, contractile function, and perfusion [112]. Combined with intravenous administration of gadolinium contrast agents, late gadolinium enhancement (LGE) – CMR has become the standard of care to identify myocardial edema, necrosis, and focal fibrosis. The presence of LGE correlates with significantly increased risk of adverse cardiac events and mortality [113]. Recent studies that identify diffuse fibrosis through measurement of gadolinium partition coefficient (GPC) or the extracellular volume fraction (ECV) [77,114] have similarly demonstrated a strong correlation between diffuse fibrosis and increased mortality [115]. However, residual concerns surrounding gadolinium and nephrogenic systemic fibrosis [116] have spurred the development of gadolinium free methods to identify diseased myocardium.

Both edematous and fibrotic myocardium are characterized by an increased extracellular volume fraction, which results in lengthened native-T1 and T2-relaxation times compared to healthy myocardium. These changes have been used to identify edema in acute MI [117,118] and fibrosis in select cardiomyopathies [119-121]. Recent studies using native T1-mapping to identify fibrosis are highly promising [122-124]. However, measured myocardial T1-relaxation times vary between T1-mapping pulse sequences [125] and myocardial regions [126], require special sequence modifications to reduce arrhythmia sensitivity [127], and reconstruction of T1-maps requires motion correction [128] that has limited some prior measurements to the septum

[119,121,129,130]. In contrast, cine balanced steady state free precession (bSSFP) is ubiquitously used to image ventricular structure and function. While weighting of the bSSFP signal by a factor of √T2/T1 is established, modulation of the bSSFP signal by magnetization transfer (MT) from extracellular matrix macromolecules has only recently been understood [131,132]. Specifically, myocardium characterized by increased ECV demonstrates reduced MT compared to healthy myocardium, as demonstrated in a prior study of acute-MI [131]. However, whether MT-weighted CMR can be used to identify tissues that would enhance with gadolinium across a range of cardiomyopathies similar to LGE has not been examined.

We hypothesized that acquisition of bSSFP cine image sets with different MT-weighting (termed 2-point bSSFP) could combine the changes in signal intensity due to both lengthened T1/T2-relaxation and reduced MT to identify tissue that would enhance with gadolinium in close agreement to LGE. We compared tissue characterization with 2-point bSSFP, native-T1 and T2-mapping to LGE in 47 patients referred for cardiac MRI at our institution. Our results demonstrate robust agreement between gadolinium free 2-point bSSFP imaging and standard of care LGE, with a strong association between 2-point bSSFP and GPC.

Methods

Patient Selection, Ethics, Consent and Permissions

Fifty non-consecutive patients referred for clinically indicated CMR with gadolinium contrast were prospectively enrolled, however 3 were excluded due to inability to maintain breath-holds. All patients referred for CMR with gadolinium contrast at our institution over a six month period were approached for study participation, with the forty seven included in the study representing those that consented to participate. Afterwards, ten healthy age-matched controls were recruited but did not receive gadolinium. The research protocol was approved by our institutional review board (IRB 13-0914-F2L) and informed consent was obtained from all subjects for participation and publication of findings. Demographic characteristics are summarized in Table 1. Clinical CMR reports were used to obtain ejection fraction (EF), end-diastolic volume (EDV), and CMR diagnosis.

Cardiac MRI Protocol

CMR was performed on a 1.5T Siemens MAGNETOM Aera scanner (Siemens Medical Imaging Solutions, Erlanger, Germany) using an 18 channel body coil and 12 channel spine coil. A short-axis stack of bSSFP cine images were obtained with prospective ECG triggering to cover the entire heart (TE: 1.2ms TR: 3.2ms, bandwidth: 930Hz, field of view: 260x260mm, slice thickness: 8mm, flip angle: 50°, 256x256matrix, GRAPPA 2), from which one mid-ventricular slice was identified for further imaging. The signal intensity of bSSFP

images acquired with high excitation flip angles and short repetition times is heavily weighted by MT, T1 and T2, while identical images acquired with low flip angles reflect proton density weighting with minimal contributions from MT. In the identified slice, pairs of bSSFP cine images were acquired with excitation flip angles of 5° (proton density reference) and 45° (MT, T1, T2-weighted) during end-expiratory breath-holds. Native myocardial T1-relaxation times were assessed using a modified Look-Locker imaging (MOLLI) sequence (5(3)3, TE:1.1ms, TR:2.7ms, flip angle:35°, bandwidth:1085Hz, field of view:272x 272mm, slice thickness:8mm, 256 matrix with 66% phase resolution, partial Fourier transform 7/8, GRAPPA 2). T2-relaxation times were assessed using a gradient echo readout (T2 preparations of: 0ms, 25ms, 55ms with 3 heart beat recovery in between, TE:1.1ms, TR:3.2ms, bandwidth:1184Hz, field of view:272x272mm, slice thickness:8mm, 192 matrix with 75% phase resolution, partial Fourier transform 6/8, GRAPPA 2) in the same short axis slice during diastasis. Afterwards, gadolinium (0.2mmol/kg Gd-DTPA) was administered intravenously as a bolus (rates ranged from 2ml/s to 5ml/s) and after 15 minutes LGE images were obtained using segmented gradient recalled echo inversion recovery (TE:3.2ms, TR:8.3ms, flip angle:25°, Bandwidth:140Hz) with inversion time set to optimally null the myocardium. Finally, post-contrast MOLLI (4(1)3(1)2, TE: 1.1ms, TR: 2.7ms, flip angle: 35°, field of view: 272 x 272mm, GRAPPA 2) images were obtained in the same slice position as pre-contrast images. Normal volunteers only underwent non-contrast portions of the protocol.

Image Analysis

Maps of T1 and T2-relaxation times were automatically reconstructed after motion correction using non-rigid body correction. The reproducibility of breath-hold position and the degree of mis-alignment between 5° and 45° scans was assessed via calculation of the DICE similarity coefficient for both complete images and segmented images in which only the heart was included. 2-point bSSFP data was analyzed by calculating the normalized change in signal between images as $(\Delta S/S_o)_i=[(S_{45}-S_5)/S_5]_i$, where S_{45} and S_5 represent the signal intensity for 45° and 5° excitations respectively for each cardiac phase (*i*). For each patient $\Delta S/S_o$ maps from 3 diastolic phases without cardiac motion were averaged together to reduce random noise. Maps of GPC were calculated as $GPC=(\Delta R_{1,myocardium}/\Delta R_{1,blood})$ from reconstructed T1-maps.

Data from patients receiving gadolinium were divided and analyzed in a double-blinded manner. An SCMR level-III reader (SWL) used a custom designed MATLAB script to segment the myocardium and define a non-enhanced region of interest (ROI) in each LGE image. Myocardial voxels with signal intensity greater than 5 standard deviations (SD) above the mean of the defined ROI were classified as enhanced at LGE. Maps defining LGE-enhanced and non-enhanced regions were saved, transmitted to MHV, and used to segment $\Delta S/S_o$, native-T1, T2, and GPC maps. To avoid partial volume errors and account for minor differences in spatial resolution, endocardial and epicardial borders were slightly adjusted to remove the blood pool and pleural space. Measurements in healthy

controls and patients without LGE-enhancement were performed over all voxels in the myocardium.

In data acquired from patients demonstrating enhancement at LGE, the enhanced area was calculated as the percentage of all myocardial voxels classified within the enhanced ROI. To calculate the enhanced area from maps of $\Delta S/S_o$, a threshold value of 197% (representing the mean + 3 standard deviations of the mean from the healthy control cohort) was applied and used to calculate the fraction of myocardial voxels above the threshold. Transmurality was calculated as the percentage of enhancement along the radial direction at the center of the area of enhancement for LGE and $\Delta S/S_o$ maps.

Figures were prepared using a median filter with a 3x2 kernel. The color scheme for maps of $\Delta S/S_o$ and native-T1 used in Figures 2.1-2.5 has been designed to emulate LGE, with non-enhanced tissue appearing dark, enhanced tissue appearing bright, and tissue that would demonstrate diffuse “gray” enhancement appearing red/yellow.

Subjective Assessment by Blinded Readers

Subjective assessment of 2-point bSSFP in comparison to LGE was performed by two blinded readers with 1 and over 10 years’ experience. All $\Delta S/S_o$ maps and LGE images were compiled separately and randomized. The readers were asked to identify the presence, location, and type (focal vs. diffuse) of enhancement, and to delineate the extent of enhancement on each image.

Statistics

Numeric data are summarized as mean ± SD. For outcome variables we used Version 9.3 of SAS software (SAS Institute, Cary NC) to fit a linear mixed model comparing mean levels across four groups of heart tissue: healthy controls (Group I), patients without LGE-enhancement in the imaged slice (Group II), non-enhanced regions of interest from patients with LGE-enhancement (Group III), and enhanced regions of interest from patients with LGE-enhancement (Group IV). We included random effects for subjects to account for correlations between measurements on non-enhanced and enhanced tissue from the same patient with LGE-enhancement. Linear contrasts were used for pairwise comparisons. Demographic variables were analyzed using SPSS (IBM Corp., 2013). The Shapiro-Wilk method was used to test normality of numeric data. Age, body mass index (BMI), and race were compared across all participants using the Kruskal-Wallis method. Fisher's exact tests were used to compare gender across all participants and CMR diagnosis between the two patient groups. Differences in EF were compared via Mann-Whitney and EDV was analyzed by student's t-test. Statistical significance in pairwise comparisons was defined by a p-value < 0.05 divided by the number of comparisons to control Type I testing error through Bonferroni adjustment. Otherwise, a p-value<0.05 defined statistical significance.

Results

Demographics and Ventricular Structure and Function

Amongst 23 patients who demonstrated LGE-enhancement in the imaged slice, EDV trended higher and EF trended lower compared to patients who did not demonstrate LGE-enhancement (**Table 2.1**). There were no significant differences in age or BMI between patients with and without LGE enhancement. Control participants differed only in BMI compared to patients ($p<0.001$ for all).

MR Tissue Characterization

The DICE similarity coefficient measured across all patients was 0.995 ± 0.004 when comparing entire 5° and 45° images. Comparison of the same images following segmentation of only the heart revealed a DICE similarity coefficient of 0.991± 0.015. Representative bSSFP images and maps of $\Delta S/S_o$ in a healthy control subject and a patient without LGE-enhancement revealed uniformly low $\Delta S/S_o$ values across both hearts (Figure 2.1). In patients with acute (Figure 2.2-2.3) and chronic MI (Figure 2.4), CMR tissue characterization with 2-point bSSFP demonstrated heightened $\Delta S/S_o$ values in close spatial agreement with LGE-CMR enhancement patterns. Representative images acquired in two patients with non-ischemic dilated cardiomyopathy demonstrate the accurate detection of fibrotic tissue using 2-point bSSFP (Figure 2.5). Elevated native T1-relaxation times were also observed in agreement with LGE following MI (Figures 2.2 and 2.4).

Average myocardial $\Delta S/S_o$, native-T1 and T2 relaxation-times were significantly higher in LGE-enhanced regions (Group IV) compared to all non-enhanced regions (Groups II and III) and healthy controls (Group I, Figure 2.6).

The mean of the standard deviation of $\Delta S/S_o$ values amongst healthy controls was 27.1 ± 8.1 (%) in absolute terms. Segmentation of the heart into twelve equal circumferentially spaced sectors revealed moderately lower average $\Delta S/S_o$ values (118.8 ± 14.7 (%)) in the anterior-lateral wall compared to the rest of the myocardium. Additionally, GPC was significantly elevated in LGE-enhanced regions (Figure 2.6). Native-T1 and T2-relaxation times and $\Delta S/S_o$ did not differ significantly between non-enhanced myocardium in patients (Groups II and III) and healthy controls (Group I, Figure 2.6). Native-T1, T2 and $\Delta S/S_o$ all demonstrated strong association with GPC (Figure 2.7).

Quantification of the percent of myocardium classified as enhanced at 2-point bSSFP demonstrated a strong association ($R^2 = 0.84$) with the percent of myocardium classified as enhanced at LGE (Figure 2.8), however a slight bias towards over-estimation of the enhanced area in patients with a higher percentage of enhancement was observed. Bland-Altman analysis (Figure 2.8) revealed a coefficient of covariance of 0.204. Measurement of the transmurality of enhancement was similar between 2-point bSSFP and LGE ($R^2 = 0.73$), and Bland-Altman analysis revealed a coefficient of covariance of 0.0875 (Figure 2.8).

Subjective Assessment

Analysis of $\Delta S/S_o$ maps and LGE images by 2 blinded readers revealed an average agreement of 73.4% between methods. Among the patients demonstrating enhancement at LGE, the extent of enhancement on $\Delta S/S_o$ maps

was identified as the same in an average of 67.2% of individuals. The extent of enhancement was identified as greater in $\Delta S/S_o$ maps in 20.8% of individuals, and smaller in $\Delta S/S_o$ maps in 12.0% of individuals. An average of 4 out of 24 patients in which enhancement was not identified in LGE images were classified as demonstrating enhancement on $\Delta S/S_o$ maps (Figure 2.9). Among the 23 patients demonstrating enhanced tissue at LGE, an average of 3.5 were classified as normal by readers interpreting $\Delta S/S_o$ maps (Figure 2.10). In all such cases, enhancement patterns were consistent with small sub-endocardial enhancement at LGE.

Discussion

In this study we present a new 2-point bSSFP method for gadolinium free CMR. In 47 patients undergoing clinical LGE examination, 2-point bSSFP demonstrated a strong association between elevated $\Delta S/S_o$ and enhanced regions in LGE across a range of cardiomyopathies. Further, 2-point bSSFP demonstrated similar results to mapping of native-T1 relaxation times. Importantly, in this study we used a relatively simple method to generate MT contrast in bSSFP images. However, MT contrast can be further enhanced through the use of additional MT-preparation schemes, potentially increasing the sensitivity of CMR tissue characterization with MT contrast.

Heightened steady state signal in edematous cardiac tissue occurs in bSSFP images acquired with a short repetition time and high flip angle. In a study by Zhou et al. [132], edematous myocardium was visualized as hyper-

intense on bSSFP images following ischemia-reperfusion injury in dogs. By comparison to T2-prepared SSFP images, the authors concluded that edema contrast in bSSFP was dominated by changes in MT and proton density (65%), with altered relaxation times having a more modest effect (35%). Similarly, Kumar et al. [133] observed a 50% increase in bSSFP signal in infarcted tissue in dogs and patients with acute MI. While we observed increased signal intensity in edematous areas on bSSFP images, we found that visualization required significant contrast adjustments and resulted in noisy images (Figure 2.3). In 2-point bSSFP, changes in signal intensity on standard bSSFP cine images caused by increased T2 and reduced MT in tissue that enhances at LGE were extracted by normalization to images acquired with a 5° flip angle (proton density weighted). Measurement of $\Delta S/S_o$, which was elevated in enhanced tissue in patients with acute MI, was consistent with signal intensity changes seen by Kumar et al. [133] and Zhou et al. [132] and demonstrated strong spatial agreement with LGE (Figure 2.2). In addition, patterns of heightened $\Delta S/S_o$ in patients with acute-MI mirrored T2-mapping (Figure 2.3), which is widely used to identify edema [117,118]. Our results further agreed with Weber et al. [131] who demonstrated altered MT-ratio in patients with sub-acute MI by acquiring pairs of bSSFP images with different MT-weighting. In the study by Weber et al. MT-contrast was generated by altering the duration of the RF excitation pulse and the repetition time between cardiac phases causing reduced MT-ratio in edematous tissue in comparison to healthy tissue. However, elongation of the excitation pulse meant that differences in cardiac phase were present in images

used to calculate the MT ratio. We chose to change the excitation flip angle, and not duration, in order to have a consistent cardiac phase between MT-weighted and proton density weighted images. Subsequently, our measure of $\Delta S/S_o$ is heightened in tissues that would enhance with LGE.

Identification of focal fibrosis with LGE is the established clinical standard and in our study heightened $\Delta S/S_o$ occurred in tissues identified by LGE as replacement (Figure 2.4) and reactive fibrosis (Figure 2.5). Emerging techniques to image diffuse fibrosis including mapping of post-contrast T1-relaxation times and measurement of GPC or ECV [77,114] have been correlated to collagen volume fraction at biopsy [134] and demonstrated predictive value for clinically relevant outcomes [115,135,136]. In our study we did not have access to hematocrit, however GPC values measured in non-enhanced myocardium agreed with prior studies of healthy tissue [126,137,138] and were significantly elevated in regions of interest identified by LGE (Figure 2.6). Comparing $\Delta S/S_o$ to GPC revealed a strong and promising association (Figure 2.7). However, detection of diffuse fibrosis with 2-point bSSFP requires further study with a larger sample and a consistent phenotype such as hypertrophic cardiomyopathy.

In order to further examine the impact of changes in T1 relaxation times on the steady state signal intensity, a series of simulations of the steady state magnetization using the closed form equation for cine bSSFP were performed in Matlab (Figure 2.11). For all simulations we assumed that proton density is 1. Since bSSFP images are weighted by $\sqrt{T2/T1}$, increased T1 relaxation times in fibrotic scar tissue will have the opposite effect of decreased MT on the steady

state signal in the high flip angle acquisition (Figure 2.11). While this may be partially mitigated by concomitant increases in T2 relaxation times (Figure 2.11), the balance between increased T1 and reduced MT, and the potential limits this imposes upon detection via measurement of $\Delta S/S_o$, requires additional examination in a large cohort of patients with chronic MI. In addition, given the contributions of MT, T1, and T2 to $\Delta S/S_o$, it is unclear whether measurement of specific $\Delta S/S_o$ values can be used to differentiate edema from fibrosis. Additional studies with larger cohorts of acute and chronic MI patients are necessary to examine this possibility.

Mapping of native myocardial T1-relaxation times is emerging as a highly promising method for gadolinium free imaging of fibrosis [122,124,126]. Recently, several studies demonstrated increased T1-relaxation times in patients with edema [139], aortic stenosis [119], myocarditis [120], and hypertrophic and non-ischemic dilated cardiomyopathies [121]. Native T1-relaxation times measured in our study using a MOLLI acquisition scheme at 1.5T were comparable to those measured under similar settings [125,140] and were significantly elevated in enhanced myocardium (Figure 2.6). While we observed a strong association between heightened native-T1and GPC, our association was weaker than observed in prior studies [120,121]. One likely factor contributing to this difference is that unlike most prior studies that focused on patient cohorts with a specific and profound phenotype, we sampled patients with a range of cardiomyopathies and varying degrees of edema or fibrosis. Also, artifacts introduced by motion correction [128] have led many prior studies to restrict data

analysis to the interventricular septum [119,121,130]. We analyzed myocardium across an entire short-axis slice, defining regions of interest based on LGE patterns. Results from a recent multi-center T1 mapping study demonstrated considerable regional variability in segmental native-T1 values at 1.5T [126]. Thus, our results likely reflect the influence of both motion correction artifacts on T1-estimation and regional T1 heterogeneity of healthy tissue that were not included in prior studies. Additionally, our scanner was equipped only with a MOLLI acquisition scheme that has demonstrated sensitivity to MT-effects [123], and thus the sensitivity of native T1-mapping may have improved with other mapping methods now available [125], including recently developed arrhythmia insensitive T1 mapping protocols [127].

Images acquired with an excitation flip angle of 5° demonstrate low signal to noise, potentially leading to artificially elevated measurement of $\Delta S/S_o$. We sought to limit the effect of random noise by averaging over three identical end diastolic phases and applying a median filtering algorithm to reconstructed maps. However, subjective assessment of $\Delta S/S_o$ maps by two blinded expert readers resulted in the incorrect interpretation of diffuse enhancement in $\Delta S/S_o$ maps in all but one of the false positive cases (Figure 2.9). We chose to use a 5° excitation flip angle in order to maximize the potential difference in MT-weighting between images, however, the acquisition of such images with slightly higher flip angles may present a more promising route to maintaining MT-contrast between image pairs while reducing the presence of voxels with spuriously high $\Delta S/S_o$ values. Alternatively, future studies could examine MT-weighting without the use

of low flip angle acquisitions via various magnetization preparation schemes that encode greater MT-weighting directly into the steady state magnetization. In addition, subjective analysis of $\Delta S/S_o$ maps by expert readers revealed a propensity to misidentify small sub-endocardial enhancement patterns as blood instead of enhanced tissue (Figure 2.10). In future studies, the use of blood signal suppression should be investigated as a mechanism to mitigate fall negative interpretation of $\Delta S/S_o$ maps.

A limitation to our study was that due to time constraints we acquired data in only one slice per patient without prior knowledge of disease status. In several patients, the slice chosen for our study did not demonstrate LGE-enhancement (Group II), however LGE-enhancement was present in other slices. Additionally, limitations on T1 and T2-mapping protocols on our scanner resulted in acquisition of bSSFP images at slightly higher spatial resolution. Consequently, partial volume error is more likely to influence T2 maps, and to a lesser extent T1 maps, than 2-point bSSFP results. Care was taken to adjust boundaries to exclude border pixels affected by partial volume artifacts, however registration of pre and post gadolinium maps was not performed. The sensitivity to B1 inhomogeneity remains a significant concern in cine bSSFP, particularly at higher flip angles. We simulated the bSSFP signal using a range of myocardial relaxation times and excitation flip angles. Based on the results of our simulation (Figure 2.11), and prior evidence that MT is maximal and constant above excitation flip angles of 30° [131], we chose to use a 45° flip angle in order to minimize the potential effects of B1-inhomogeneity. Also, changes in through-

plane motion can modulate steady state behavior in the myocardium. For this reason we chose to focus our analysis on end-diastolic cardiac phases. In addition, the acquisition of two separate end expiratory breath-held scans increases the potential for misalignment between scans. Measurement of the DICE similarity coefficient between image pairs in our study was high, however we benefited from placement of our scans at the end of the non-contrast CMR workup, thus reducing potential misalignment that could occur if such scans were performed at the initiation of the CMR examination. Importantly, while registration algorithms can be used to compensate as they are in T1 mapping protocols, simple image intensity based algorithms would not be effective for registration of images acquired with a 5° excitation flip angle.

2-point bSSFP utilizes endogenous contrast mechanisms for gadolinium free CMR imaging. In this study, we demonstrated across a range of patients strong association between 2-point bSSFP and standard of care LGE-CMR. Importantly, since MT-contrast is an endogenous mechanism, the sensitivity to changes in MT-weighting increases with spatial resolution. In addition, MT-contrast can be further increased with MT-preparation schemes not used in this initial study. In contrast, differences in native-T1 between healthy and diseased tissue cannot be further increased without increasing the magnetic field strength. With further development, MT-weighted CMR could potentially enable diagnostic imaging similar to LGE CMR without the use of gadolinium.

Contributions

Tori Stromp was involved in study design, analysis of strain data, imaging of healthy controls, manuscript drafting, and statistical analysis. Steve W Leung performed imaging of patients, was involved in manuscript preparation and data analysis. Kristin N Andres and Linyuan Jing were involved in data analysis. Brandon K Fornwalt assisted in manuscript preparation. Richard J Charnigo performed statistical analysis and assisted in manuscript preparation. Vincent L Sorrell assisted in imaging of patients and manuscript preparation. Moriel H Vandsburger performed data analysis, conceived of the theoretical design of the study, and assisted in manuscript preparation.

Acknowledgments

We thank Vrinda Sardana MD, Joseph Jenkins, John Green, Rebecca Eghli and Dimmi Jackson RN for their help in patient care and image acquisition. This work was supported by the National Center for Advancing Translational Sciences at the National Institutes of Health through grant number UL1TR000117 (supporting Richard J Charnigo). Steve W Leung and Moriel H Vandsburger were supported through KL2TR000116. Moriel H Vandsburger was also supported by the American Heart Association National Affiliate (Dallas, TX) through grant number 14CRP20380071. There are no relationships with industry.

Table 2.1. Participant Characteristics.

Variable	Healthy Control (Group I) (n=10)	CVD without Enhancement (Group II) (n=24)	CVD with Enhancement (Groups III, IV) (n=23)	*p*-value
Demographics				
Age (yrs)	51.74 ± 4.7	47.7± 16.5	51.39 ± 15.4	.406
BMI (kg/m^2)	23.32 ± 1.5	29.3 ± 6.7	27.4 ± 3.6	.007
Female	4 (50.0)	8 (33.3)	4 (17.4)	.315
White	7 (40.0)	20 (83.3)	18 (78.3)	.815
African American	0	3 (12.5)	3 (13.0)	1.00
Hispanic or Other Race	1 (10.0)	1 (4.2)	2 (8.7)	.051
CMR Indication				
Cardiomyopathy		7 (29.2)	10 (43.5)	.371
Hypertrophic Cardiomyopathy		2 (8.3)	1 (4.3)	1.000
Pericarditis, Myocarditis		2 (8.3)	2 (8.7)	1.000
Sarcoidosis		2 (8.3)	2 (8.7)	1.000
Syncope		4 (16.7)	0	.109
Viability		3 (12.5)	5 (21.1)	.461
Other		4 (16.7)	3 (17.4)	1.000
Diagnosis				
Ischemic Cardiomyopathy		4 (16.7)	10 (43.5)	.060
Non-Ischemic Cardiomyopathy		10 (41.7)	7 (30.4)	.547
Cardiomyopathy		0	2 (8.7)	.234
No Evidence of Cardiomyopathy		8 (33.3)	0	.416
Other		2 (8.3)	4 (17.4)	.416
Ejection Fraction (%)		50.13 ± 14.4	42.57 ± 14.6	.081
End Diastolic Volume (mL)		190.6 ± 76.0	217.65 ± 81.1	.244

CVD without Enhancement: Patients referred for CMR not demonstrating LGE enhancement in imaged slice. CVD with Enhancement: Patients referred for CMR demonstrating LGE enhancement in imaged slice. BMI: Body Mass Index (kg/m^2).

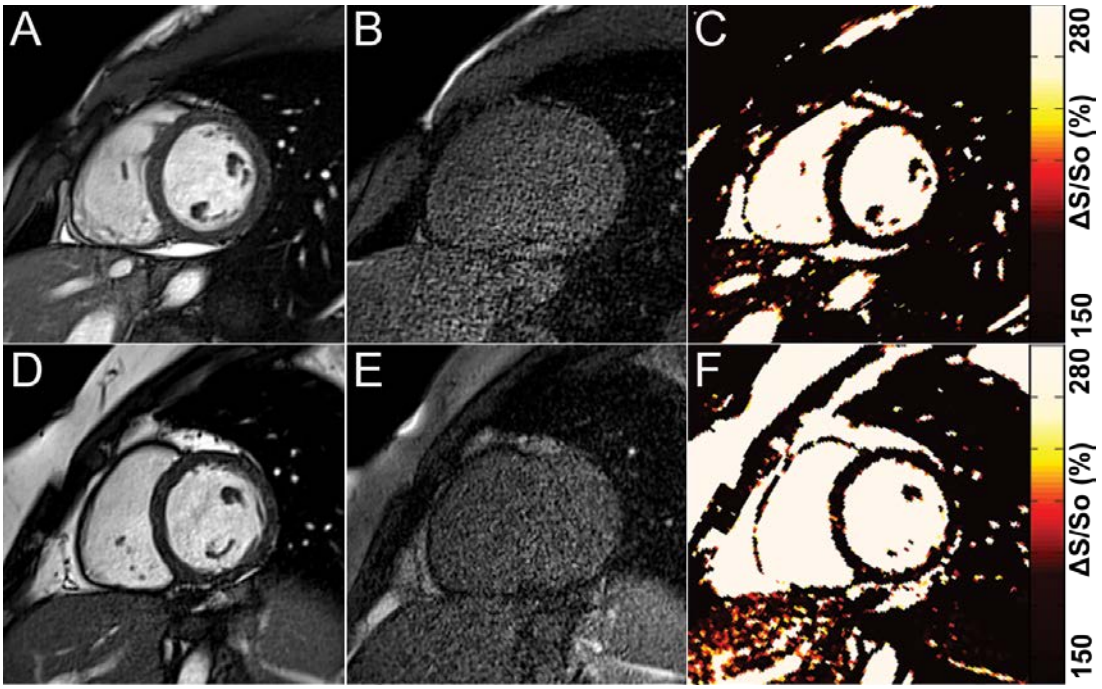

Figure 2.1. 2-pt bSSFP Imaging Method.
(A-C) Representative data from a healthy control. End-diastolic reference bSSFP images acquired with **(A)** 45° and (B) 5° flip angles provide MT-weighted and proton density reference images, respectively. **(C)** Maps of $\Delta S/S_o$ that are calculated from A and B demonstrate uniform and low values throughout the heart. **(D-F)** Representative data from a patient without LGE-enhancement. End-diastolic reference bSSFP images acquired with **(D)** 45° and **(E)** 5° flip angles. This patient demonstrated no myocardial enhancement at LGE. **(F)** Map of $\Delta S/S_o$ demonstrates uniformly low values similar to the healthy control. For all maps, the color scale was chosen to emulate LGE imaging, with areas of edema/fibrosis demonstrating signal enhancement and areas of healthy tissue appearing dark.

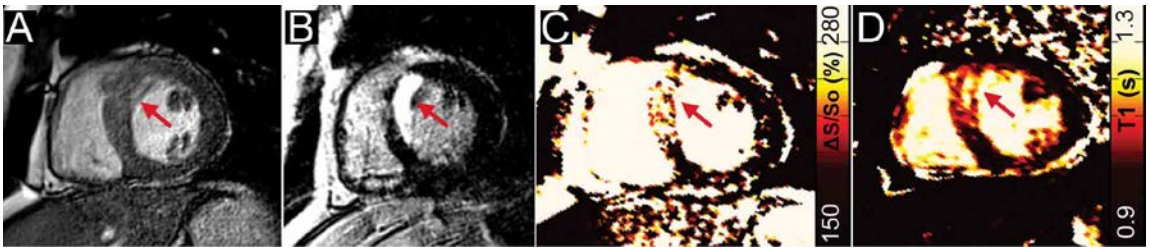

Figure 2.2. Identification of edema and necrosis in a patient with acute myocardial infarction. (A) End-diastolic reference image of a midventricular slice in which 2-point bSSFP, native T1-mapping, and LGE data were acquired. **(B)** LGE imaging reveals an area of hyper-enhancement along the septum indicative of edema and/or necrosis (red arrow). The corresponding maps of **(C)** $\Delta S/S_o$, and **(D)** native-T1 both demonstrate similar spatial patterns of elevated values to LGE (red arrow). The corresponding T2-map and windowed bSSFP image can be found in Figure 2.3.

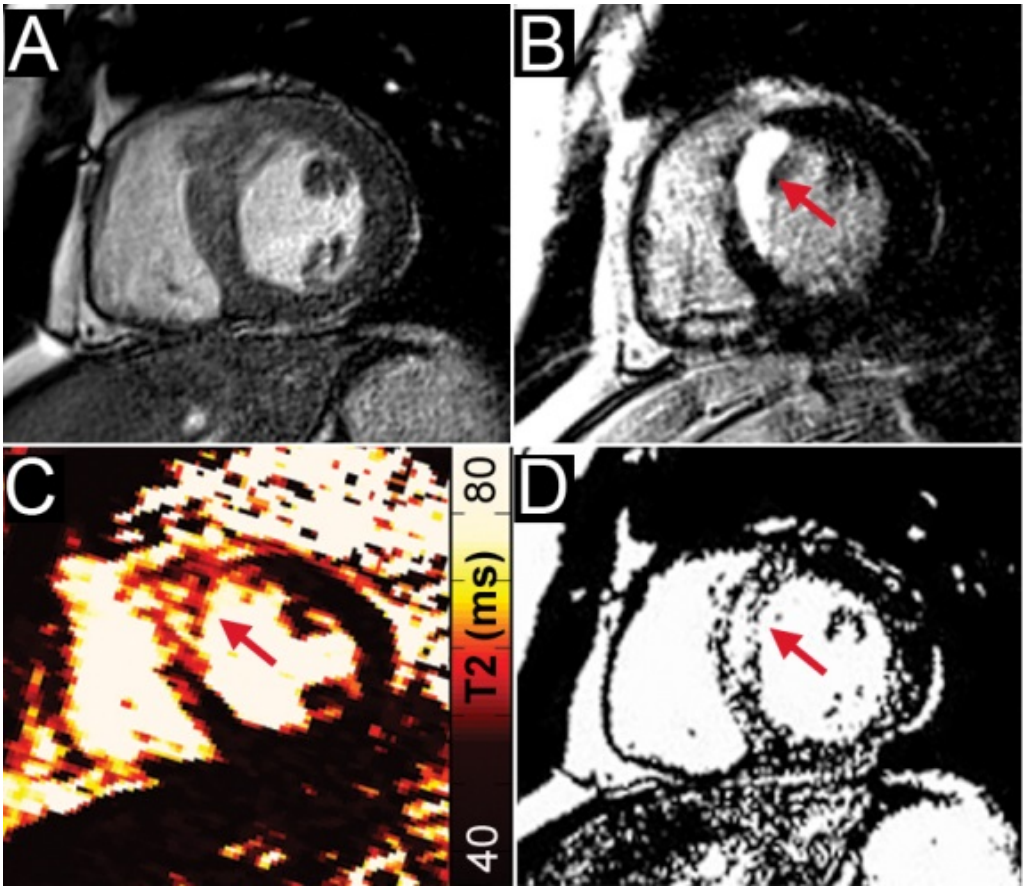

Figure 2.3. T2-Mapping and Weighting in Acute MI. (A) Anatomical reference image from same patient as shown in Figure 2.2, with **(B)** corresponding LGE image demonstrating area of edema following acute MI (red arrow). **(C)** T2-mapping revealed focally and significantly elevated T2 in the area of acute MI, corresponding to edema. **(D)**. Significant contrast manipulation through window and leveling of (A) reveals similar enhancement in the area of edema (red arrow), however scattered noise is seen in areas outside of the enhanced area.

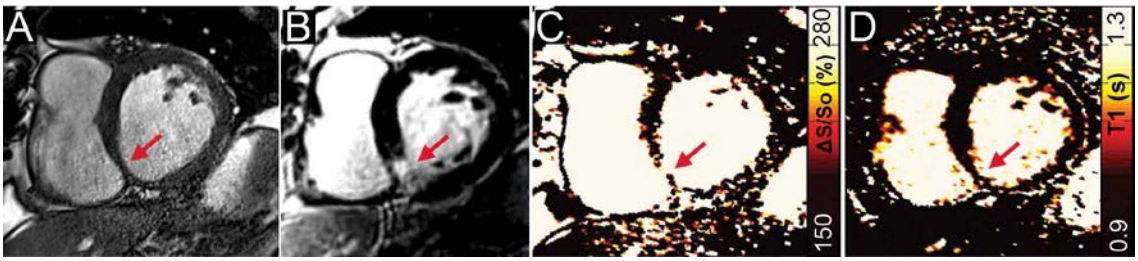

Figure 2.4. Identification of scar tissue in chronic myocardial infarction. (A) Magnitude reconstructed bSSFP image reveals a thinned wall along the inferior right ventricular insertion point (red arrow). **(B)** LGE imaging confirms the presence of primarily sub-endocardial scar tissue as an area of signal enhancement (red arrow). Mapping of **(C)** $\Delta S/S_o$ and **(D)** native-T1 both reveal increased values within the scar tissue (red arrows), and normal values throughout the remaining myocardium.

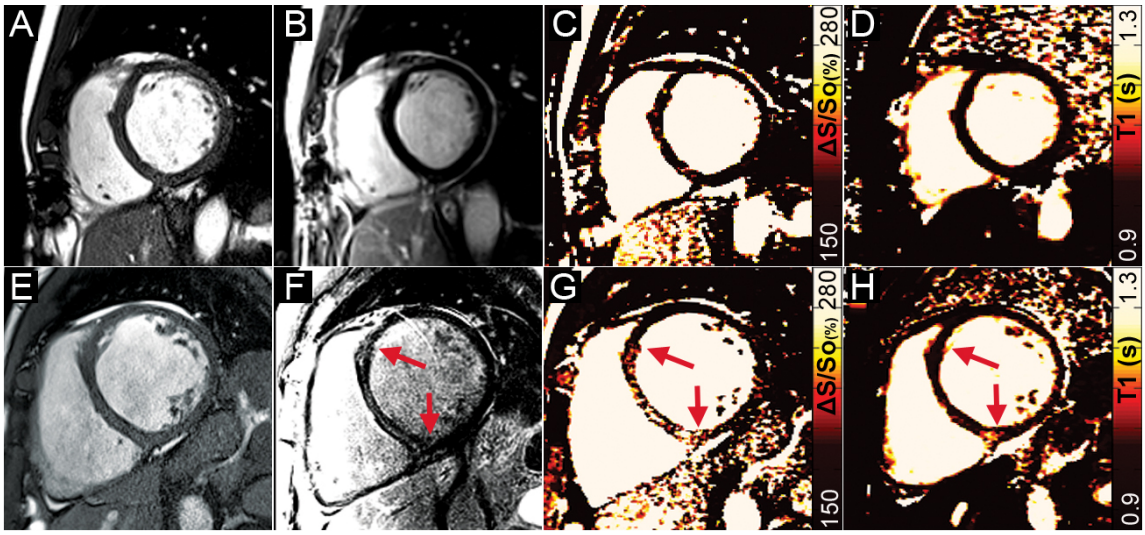

Figure 2.5. Two patients with non-ischemic dilated cardiomyopathy. (A, E) Dilation of the left ventricle is present in both patients on end-diastolic images. In the first patient, **(B)** no LGE-enhancement is present, **(C)** $\Delta S/S_0$ is normal throughout the heart as is **(D)** native-T1. In the second patient, **(F)** mid-wall septal LGE-enhancement is present (red arrows). **(G)** Heightened ΔS/So is observed in close agreement with the LGE image (red arrows), however **(H)** native-T1 values are elevated primarily at the right ventricular insertion-point.

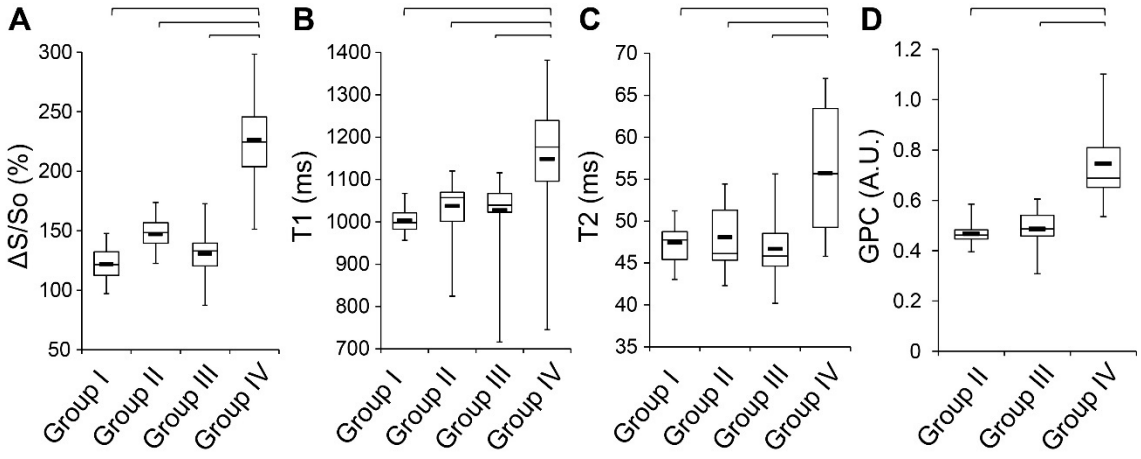

Figure 2.6. Tissue characterization parameters. (A) $\Delta S/S_o$ was significantly elevated in tissue regions that enhanced on LGE images (Group IV) compared to non-enhanced regions from the same patients (Group III), patients without any LGE enhancement (Group II), and healthy controls (Group I). Similarly, **(B)** native-T1 and **(C)** native-T2 were significantly elevated in tissue that enhanced on LGE images compared to all other groups. **(D)** GPC was significantly higher in tissue that enhanced on LGE images compared to non-enhanced tissue regions in patients. (Lines represent $p<0.05$).

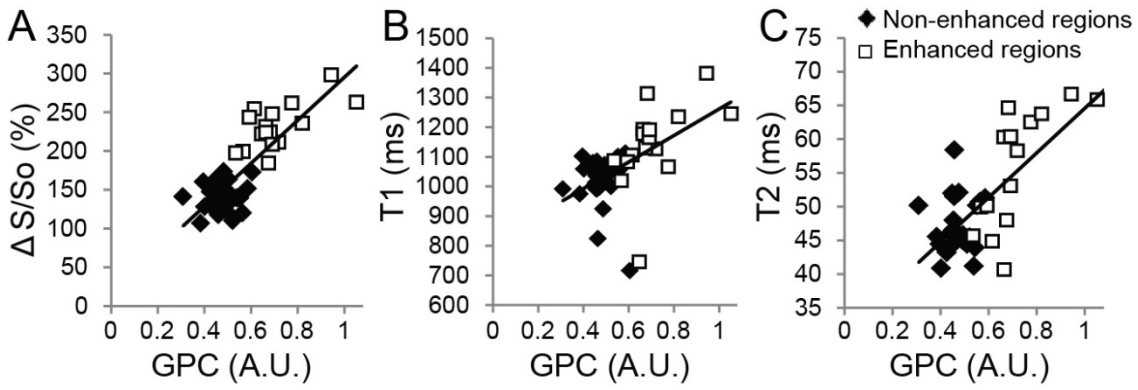

Figure 2.7. Association of tissue characterization parameters with GPC. (A) $\Delta S/S_o$ (R = 0.82), **(B)** native-T1 (R = 0.55), and **(C)** T2 (R = 0.75) all associated strongly with GPC. Data points are shown for all measurements as either enhanced on LGE images (white boxes) or non-enhanced on LGE images (black diamonds).

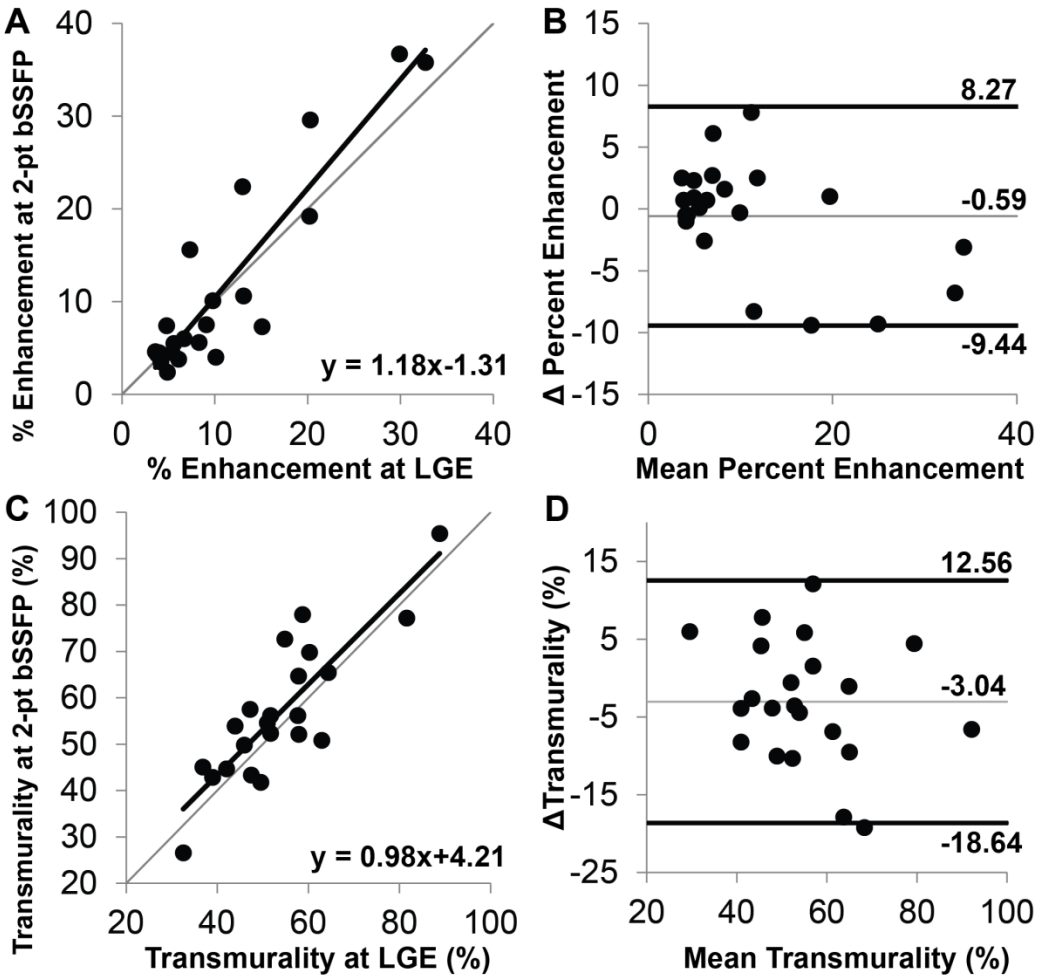

Figure 2.8. Association of enhanced area and transmurality between 2-point bSSFP and LGE. (A) Comparison of the enhanced myocardial area (represented as percent of total myocardial area) using 2-pt bSSFP and LGE revealed a strong association between the two methods (R^2 = 0.84) with a slight bias towards larger areas of enhancement with 2-point bSSFP. **(B)** Bland-Altman plot comparing the difference between enhanced areas by both methods to the mean between both methods revealed a coefficient of covariance of 0.204. **(C)** Similarly, the comparison of the transmurality of enhancement by each method revealed a strong association between 2-point bSSFP and LGE (R^2 = 0.73) with **(D)** Bland-Altman analysis demonstrating a coefficient of covariance of 0.0875.

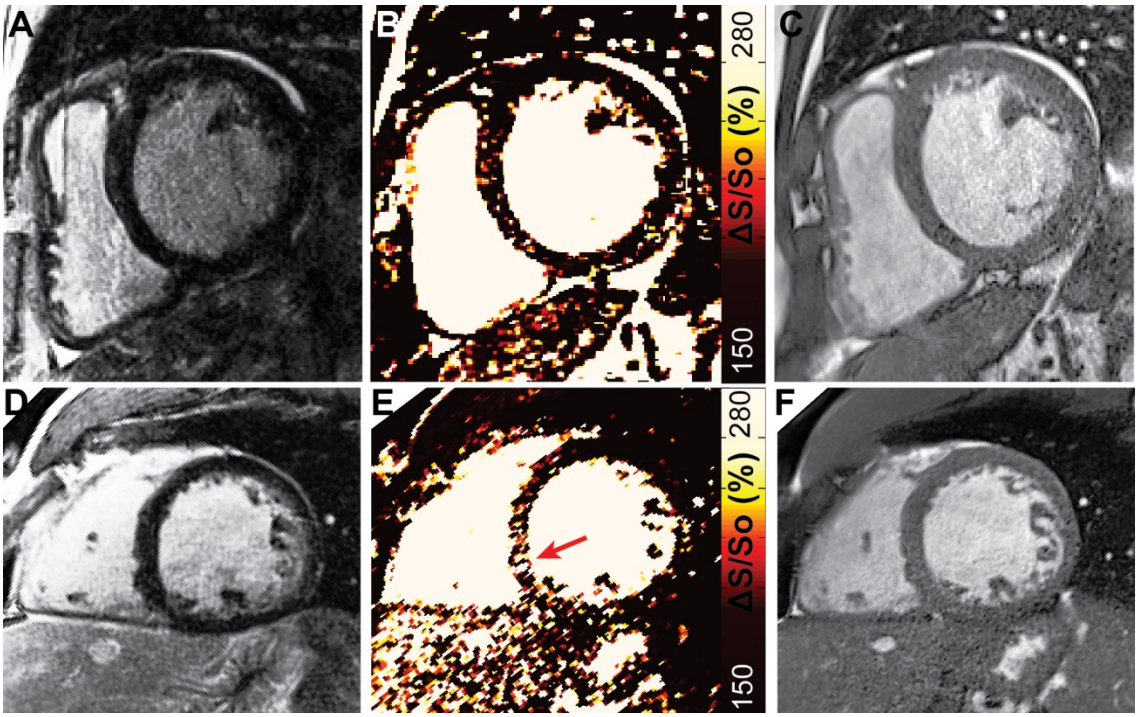

Figure 2.9. False positive identification of enhancement at $\Delta S/S_o$. (A-C) Scattered noise on ΔS/So maps led to the false identification of diffuse enhancement in 3 of the 4 false positive cases. A representative example of a patient without enhancement at LGE **(A)** that was classified by blinded readers as demonstrating diffuse enhancement at $\Delta S/S_o$ **(B)** in the septum with corresponding anatomical reference image **(C)**. **(D-F)** In one patient without enhancement at LGE **(D)**, focal enhancement (arrow) was identified on the corresponding map of $\Delta S/S_o$, with corresponding anatomical image shown in F.

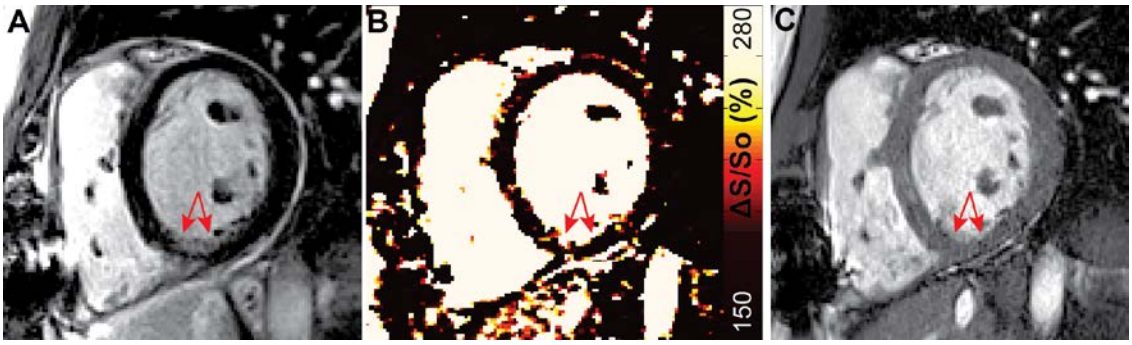

Figure 2.10. False negative identification at $\Delta S/S_o$. All cases in which blinded readers identified individuals with enhancement at LGE as normal at $\Delta S/S_o$ occurred in cases of sub-endocardial enhancement. **(A)** Representative LGE image from a patient with 50-75% sub-endocardial intermediate signal enhancement (red arrows) in the inferior wall. **(B)** The corresponding map of $\Delta S/S_o$ demonstrates elevated values in the same region (red arrows). **(C)** The corresponding anatomical reference image confirms that the elevated $\Delta S/S_o$ values in B occur in myocardial tissue.

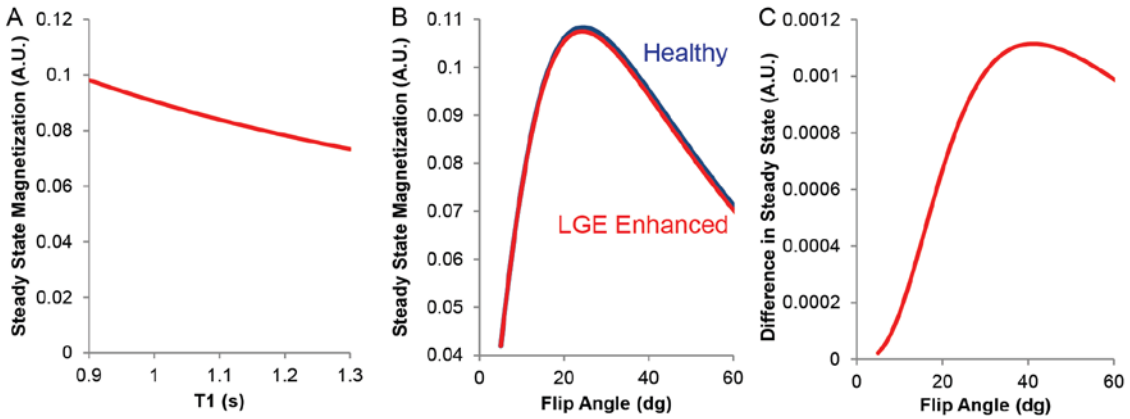

Figure 2.11. Simulations of changes in steady state signal intensity as a function of T1, T2, and flip angle. (A) Using a T2 relaxation time of 48ms (the mean amongst our healthy control cohort), and the TR and TE values from our scanning protocol, simulations confirm that lengthening of T1 relaxation times leads to a reduction in the steady state signal over a physiologically relevant range of T1 relaxation times. **(B)** However, changes in T1 relaxation times in fibrotic tissue are often accompanied by changes in T2 relaxation times that can have the opposite effect on the steady state signal. For further simulation of the steady state signal across a range of flip angles we examined healthy values (blue) using the mean T1 (1022.2 ± 48.2 (ms)) and T2 (48.2 ± 2.3 (ms)) relaxation times from our healthy cohort and previously mentioned TR/TE and proton density values. Separately, we simulated fibrotic tissue (red) using the mean T1 and T2 relaxation times from tissues that enhanced at LGE in patients that did not have acute-MI. This population included those with chronic MI and patients with enhancement determined by our cardiologist to be non-ischemic in origin. In this subset of patients (n = 12), the mean native-T1 relaxation time was 1125.6 ± 136.5 (ms), and the mean T2-relaxation time was 52.2 ± 7.7 (ms). Examination of panel B demonstrates that decreases in steady state magnetization due to increased T1 are partially mitigated by increased T2 in fibrotic tissues. **(C)** The difference in steady state signal between the two populations suggests that the contrast observed in maps of $\Delta S/S_o$ is likely heavily influenced by changes in MT.

CHAPTER 3: MAGNETIZATION TRANSFER MAGNETIC RESONANCE IMAGING IDENTIFIES CARDIAC FIBROSIS IN END STAGE RENAL DISEASE WITHOUT GADOLINIUM AND CORRELATES WITH BIOMARKERS OF COLLAGEN TURNOVER

Synopsis

***Background*:** Patients with end stage renal disease (ESRD) suffer high rates of cardiac mortality, likely from pervasive development of fibrosis. The contraindication to gadolinium contrast agents prevents the use of late gadolinium enhancement cardiac MRI (CMR) for fibrosis detection in ESRD, although it is the clinical standard for cardiac tissue characterization. Measures of hypertrophy or reduced strain are widely used as surrogates for fibrotic burden, but are not specific to the development of fibrosis. We utilized our established magnetization transfer-weighted technique, 2-point balanced steady state free precession (2-pt bSSFP) for fibrosis identification and comparison with structure, function, and biomarkers in patients with ESRD.

Methods: Patients on routine hemodialysis for ESRD (n=29) and healthy controls (n=33) were imaged on a 1.5 T MRI using the 2-pt bSSFP CMR technique. Myocardial $\Delta S/S_o$ was calculated as $\Delta S/S_o=(S_5 – S_{45})/S_5$ *100 (%) where S_i is the signal intensity per flip angle *i*. Strain and strain rates were measured in circumferential and longitudinal directions with a custom feature tacking algorithm. A standard healthy distribution of $\Delta S/S_o$ signal was generated

as a cumulative distribution function. The cumulative distribution of $\Delta S/S_o$ for each participant was compared to the healthy standard. The difference between cumulative distributions was integrated across the range of $\Delta S/S_o$ and the resulting divergence value was used as a quantitative marker of fibrosis. Pearson correlations were used to compare divergence to other widely used correlates of fibrosis and blood biomarkers.

Results: Patients with ESRD were hypertrophic but with only slightly reduced longitudinal strain compared to healthy controls. Mean $\Delta S/S_o$ and divergence were elevated in patients with ESRD (144.7 ± 17.1% and 16.3 ± 14.3 AU respectively) compared to controls (129.9 ± 12.0% and 6.5 ± 5.7 AU, $p<0.01$ for both comparisons). Divergence was only moderately correlated with left ventricular mass index (LVMI; rho=0.31, $p<0.05$) but did not correlate with strain measures. Troponin T (TnT), fibroblast growth factor 23 (FGF23), and tissue inhibitor of metalloproteinase (TIMP) 1 and 2 were elevated in the ESRD group compared to controls. All of these biomarkers correlated with divergence, but FGF23 and TnT also correlated with LVMI indicating that these biomarkers are not specific enough to measure fibrosis alone. TIMP1 and 2 did not correlate with hypertrophy or strain, suggesting that these matrix remodeling proteins may be suitable for specific identification of fibrosis and may possibly serve as molecular targets for future anti-fibrotic therapies.

Conclusions: 2-pt bSSFP CMR in patients with ESRD revealed that solely using hypertrophy or reduced mechanics as surrogate markers of fibrosis is inappropriate. While biomarkers of ischemia (TnT) and remodeling (FGF23) associated strongly with hypertrophy, they may lack specificity to cardiac fibrosis. TIMPs may emerge as both a biomarker of extracellular remodeling and potential therapeutic target specific to fibrosis in patients with ESRD.

Background

Sudden cardiac death is a leading cause of death for patients who are on routine hemodialysis for treatment of end stage renal disease (ESRD) [42]. Cardiac remodeling, which often manifests as hypertrophy in ESRD patients [47,51], and/or the development of replacement or reactive fibrosis [58,59] can lead to adverse cardiac events such as arrhythmia, heart failure, and eventually death. ESRD hemodialysis patients are contraindicated to gadolinium contrast agents [83], which are typically used for tissue characterization and fibrosis imaging with cardiac magnetic resonance imaging (CMR). Subsequently, since fibrosis and hypertrophy often occur in parallel, measurement of hypertrophy is widely used as a surrogate for fibrosis. In other studies, specific blood biomarkers including troponin T (TnT), fibroblast growth factor 23 (FGF23), and parathyroid hormone (PTH), whose levels correlate well with the degree of hypertrophy [141,142] are used as plasma biomarkers of fibrosis. Matrix metalloproteinases (MMP) and tissue inhibitor of MMP (TIMP) are under investigation as fibrosis specific markers in cardiomyopathy [143], heart failure [36,144] and cardiorenal syndrome [145-148]. Measures of reduced diastolic strain rate and global longitudinal strain (GLS) indicate stiffening of the left ventricle (LV) in kidney disease patients [60], but may only be sensitive after advanced fibrotic development. The currently employed surrogates of fibrosis—hypertrophy, contractile function, and plasma biomarkers—are all indirect measures and may not be directly correlated with the development of fibrosis as a specific disease process in all patients with ESRD. Thus detecting cardiac

fibrosis and linking it with measureable biomarkers in the ESRD population remains both a challenge and a significant obstacle to the design and evaluation of potential lifesaving therapies. Since fibrosis occurs simultaneously with the expansion of interstitial space, two point balanced steady state free precession (2-pt bSSFP) CMR, which is described in Chapter 2, is uniquely suited to overcome the existing obstacles of studying cardiac fibrosis in patients with ESRD.

In this study, we used 2-point bSSFP CMR in healthy controls and patients with ESRD on routine hemodialysis for myocardial tissue characterization. We then correlated measures of fibrosis with cardiac mechanics and blood plasma biomarkers of remodeling that are purported to reflect underlying fibrotic burden. We hypothesized that the magnitude of fibrosis will correlate more strongly with the levels of markers of matrix turnover (MMPs and TIMPs) than with the magnitude of hypertrophy, reduced strain, or levels of non-specific biomarkers TnT and FGF23.

Materials and Methods

Participants and Recruitment

Patients on routine hemodialysis for ESRD were referred from the University of Kentucky Nephrology Department and healthy volunteers were recruited with assistance from the University of Kentucky Center for Clinical and Translational Science and academic departments. All participants were prospectively enrolled. Exclusion criteria included arrhythmia, inability to hold

one's breath, and standard MRI safety and compatibility concerns. Additional exclusions for healthy volunteers were known cardiovascular disease, hypertension, diabetes, obesity, and tobacco use. A total of 31 patients with ESRD and 44 healthy controls were enrolled. Participants were excluded from data analysis due to the inability to adequately hold their breath or complete the MRI protocol (1 ESRD each) or for image quality concerns due to hardware issues (5 healthy controls). BMI > 26 (n=4), abnormal ECG (n=1) or discovery of aging related (n=1) or congenital abnormalities (n=1) in healthy controls were additional grounds for exclusion in data analysis. The research protocol was approved by the University of Kentucky Institutional Review Board and all participants gave voluntary informed consent prior to participation.

Cardiac MRI Protocol

A 12 lead electrocardiogram (ECG) was conducted prior to the MRI to detect arrhythmia or other electrical abnormalities. Participants were imaged on a 1.5T Siemens Aera scanner (Siemens Healthcare, Erlangen, Germany) using an 18 channel body coil and 12 channel chest coil and prospective ECG triggering. A 4-chamber long axis cine image was acquired during localizers for assessment of longitudinal strain. The 2-pt bSSFP method was completed as previously described (Chapter 2). During end expiratory breath holds, cine bSSFP image pairs were obtained at flip angles of 5° and 45° in a short axis stack, spanning the LV from mitral valve to apex. Additional scanning parameters include TE: 1.2

ms, TR: 3.2 ms, bandwith: 930 Hz, in plane spatial resolution: 1.02 x 1.02 mm, slice thickness: 8 mm, GRAPPA 2.

Structure and Function Analysis

Left ventricular volumes and mass were analyzed using short axis images in Argus Viewer (Siemens Healthcare, Erlangen, Germany). Left ventricular mass index (LVMI) was calculated as mass at end diastole (g) indexed to body surface area (m^2). To characterize hypertrophy, H/R ratio was calculated at end diastole in a mid-ventricular slice as H/R= septal thickness / ventricular radius (cm) similar to Grossman, et al. [149]. Blood pressure data were collected post hoc from electronic medical records, when available.

Strain Analysis

Circumferential and longitudinal strain and strain rates were assessed using a custom feature tracking algorithm [150]. Endocardial borders were manually defined and automatically segmented into 6 sectors (Figure 3.1). Sectors were followed through the cardiac cycle using feature tracking and manually corrected for errors in border definition. Peak strain was defined as the maximum circumferential or longitudinal shortening from end diastole (%). Circumferential strain was averaged across all short axis slices. Global longitudinal strain was averaged across all endocardial sectors in 1 long axis view. In each slice, average shortening across all sectors was plotted as a function of the cardiac cycle. Systolic and diastolic strain rates were then defined

as the minimum and maximum slopes during contraction and relaxation, respectively (Figure 3.1).

Image Analysis

Offline image processing was conducted offline using MATLAB version 2014a (The MathWorks Inc., Natick, MA). Cine image pairs acquired at 5° (not shown) and 45° (Figure 3.2 A and D) were assessed for misalignment and manually adjusted to realign the left ventricular myocardium when necessary. 2-pt bSSFP data was analyzed as previously described (Chapter 2). Maps of $\Delta S/S_o$ (Figure 3.2 B and E) were generated for each slice location and each cardiac phase using the formula $\Delta S/S_o=(S_{45}-S_5)/S_5 \times 100$ (%), where S_i is the signal intensity per voxel at each flip angle *i*. To reduce random noise, 1 to 3 diastolic $\Delta S/S_o$ maps without cardiac motion were averaged together when calculating $\Delta S/S_o$. The myocardium was manually defined on $\Delta S/S_o$ maps. Care was taken to exclude voxels with partial volume averaging from blood pool and pericardial fat. $\Delta S/S_o$ maps were automatically segmented into 6 sectors to calculate mean values per sector. Bullseye plots are used to demonstrate mean $\Delta S/S_o$ per sector across slices (Figure 3.2 C and F). Sectors are presented circumferentially, with slices extending radially from apex (center) to base (exterior). Quantitative analysis was completed using unfiltered $\Delta S/S_o$ maps. Figures are presented using a 2x3 median filter.

Quantification of Fibrosis

A standard distribution was defined by combining all myocardial $\Delta S/S_o$ voxel values for all healthy participants in our study. To account for variations in heart size, the standard distribution was dynamically resized to match the number of voxels in each individual heart. For each participant, a cumulative distribution function of $\Delta S/S_o$ values was compared against the appropriately-sized simulated distribution. A rightward shift in the distribution function occurs when a greater proportion of voxels demonstrate increased $\Delta S/S_o$ values consistent with tissue fibrosis. The difference between cumulative distributions was integrated across the range of $\Delta S/S_o$ and the resulting value was used as a quantitative marker of fibrosis termed *divergence*. An example of this analysis is presented **in** Figure 3.2 G. Cumulative distribution analysis was limited to voxels with 0-400% $\Delta S/S_o$ values to reduce the influence of potential region of interest errors or additional random noise. These ranges span the expected values for healthy, edematous, and fibrotic myocardium.

Blood Biomarker Analysis

In a subset of participants, blood samples were collected by standard venipuncture and allowed to clot at least 30 minutes. Samples were centrifuged at 1300g for 10 minutes at 4°C and stored at -80°C until analyzed with commercially available assay kits. Serum concentrations of TnT were analyzed by quantitative electrochemiluminescent immunoassay by ARUP Laboratories (0098803, Salt Lake City, UT, USA). MMP2 and MMP9 were measured by

enzyme-linked immunosorbent assay (ELH-MMP2, ELH-MMP9 ELISA; Ray Biotech, Norcross, GA, USA). FGF23, PTH, TIMP1 and TIMP2 were analyzed by Milliplex® magnetic bead panels (HBNMAG-51K, HTMP2MAG-54K; EMD Millipore, Billerica, MA). Assays were run in duplicate and averages were used for all analyses.

Statistical Analysis

Statistical results were computed using IBM SPSS Statistics Version 22 (IBM Corp, Armonk, NY). Shapiro-Wilk and Levene's tests were used to assess the normality and homogeneity of variance for all variables. Student's t test or Mann Whitney U tests were used where appropriate. Spearman correlations were used to compare blood biomarkers against imaging results. Continuous variables are presented as mean ± standard deviation or median [interquartile range], where appropriate. Categorical variables are presented as count (%). $P<0.05$ was considered significant for all tests.

Results

Twenty nine patients with ESRD and 33 healthy controls were included in the study. Demographic characteristics are detailed in Table 3.1. Groups were well matched in age and gender. Patients with ESRD had larger body mass index compared to controls (<0.001). Hemodialysis vintage in patients with ESRD was 4.8 ± 3.2 years. Six patients had prior kidney transplants that subsequently

failed, requiring continuation of hemodialysis. Additional clinical features of the ESRD group are described in Table 3.2.

Clinical Measures of Structure, Function, and Strain

Clinical measures from ECG and CMR are listed in Table 3.1. QRS complex duration was similar between patients with ESRD and controls ($p=0.694$), although 3 patients with ESRD had QRS duration longer than 120ms. Corrected QT interval (QTc, normalized to 60 beats per minute) was longer in patients with ESRD than controls ($p<0.001$). QTc was greater than 440ms in 18 patients with ESRD but only 6 healthy controls. The majority of patients with ESRD had preserved ejection fraction with no differences between groups, although 6 patients had EF below 55%. Mean LV mass was 112.5 ± 31.8g in controls and 189.0 ± 65.1g in patients with ESRD ($p<0.001$). LVMI, septal thickness, and H/R ratio were elevated in patients with ESRD compared to controls ($p<0.01$ for all, see Table 3.1). There were no differences in strain measurements between the ESRD and healthy control groups for circumferential peak strain, systolic, or diastolic strain rates (Figure 3.3 A-C). Longitudinal peak strain was slightly reduced in patients with ESRD (Figure 3.3 D) but did not reach statistical significance. Longitudinal systolic and diastolic strain rates were similar between groups (Figure 3.3 E-F).

Tissue Characterization by 2-pt bSSFP

Representative $\Delta S/S_o$ maps from a healthy control (Figure 3.4) depict the uniformly low $\Delta S/S_o$ values typical of healthy myocardium. An example patient with ESRD is presented in Figure 3.5. This patient demonstrates diffuse enhancements in $\Delta S/S_o$, particularly towards the base of the LV. Importantly, if this patient were to undergo myocardial tissue biopsy, the historical gold standard for fibrosis detection where a small tissue sample is extracted from the epicardial surface of the left ventricular septum at the mid-ventricle, the chance of a false negative result would be high. The longitudinal position of the tissue samples would impact the extrapolated whole-ventricle estimation of fibrotic burden, which is actually highly varied across slices. Similar to Schietinger et al. [59], we also found examples of 3 distinct patterns of fibrosis in patients with ESRD (Figure 3.6), associated with both ischemic and non-ischemic origins. From the $\Delta S/S_o$ maps generated at each short axis slice position, mean global $\Delta S/S_o$ was calculated across the LV myocardium. Patients with ESRD had significant elevation in global $\Delta S/S_o$ (144.7 ± 17.1%) compared to controls (129.9 ± 12.0%, $p<0.001$, Figure 3.7 A). Divergence was also significantly increased in the ESRD group (9.8 AU [6.0, 23.6]) compared to controls (4.7 A.U. [1.2, 11.5], $p=0.003$, Figure 3.7 B), indicating a greater fibrotic burden in these patients.

Structure and Function Alterations are not Synonymous with Fibrosis

Representative examples of LV hypertrophy in the ESRD group are shown in the anatomical cine images ($\alpha=45°$) in Figure 3.8 A-D. While each of these

example participants is considered hypertrophic, there is a wide range of fibrosis patterns, indicated by elevated signal on corresponding $\Delta S/S_o$ maps (Figure 3.8 E-H). Spearman correlations were used to investigate the association of fibrosis with hypertrophy, circumferential diastolic strain rate, and global longitudinal strain (Figure 3.9). Moderate correlations were evident when comparing divergence with LVMI (rho=0.31, p=0.014) and septal thickness (rho=0.27, p=0.035), which are commonly utilized surrogate measures of fibrosis. No correlation was found comparing divergence with diastolic strain rate (rho=0.06, p=0.646) or global longitudinal strain (rho=0.02, p=0.910). LVMI correlated with diastolic strain rate (rho=-0.26, p=0.043) and global longitudinal strain (rho=0.383, p=0.002), indicating that increased hypertrophy was associated with worsening relaxation and contraction. In patients with ESRD, hemodialysis vintage was not correlated with divergence (rho=-0.164, p=0.395), indicating that length of time on hemodialysis is also not a good indicator of fibrotic burden.

Blood Biomarkers and Correlations with LV Remodeling

We collected blood samples from a subset of healthy controls (n=25) and patients with ESRD (n=16). Serum concentrations of blood biomarkers are detailed in Table 3.3. The typical biomarkers of ischemia and cardiac remodeling, TnT and FGF23, were elevated in patients with ESRD (Figure 3.10 A-B), as was PTH. Markers of extracellular matrix turnover, TIMP1 and TIMP2 were also elevated in the ESRD group (Figure 3.10 C-D). Correlation analysis with divergence revealed moderate associations between fibrosis and TnT (rho=0.32,

p=0.043), PTH (rho=0.33, p=0.035), TIMP1 (rho=0.39, p=0.013), and TIMP2 (rho=0.40, p=0.011) but not FGF23 (Figure 3.10 E-H). Interestingly, TnT (rho=0.59, p<0.001), FGF23 (rho=0.343, p=0.030), and PTH (rho=0.37, p=0.019) also correlated with LVMI while TIMP1 and 2 did not. These overlapping correlations reveal the complex interaction between hypertrophy and fibrosis, while indicating that TnT, FGF23, and PTH may not be suitable for fibrosis detection in patients with ESRD.

Discussion

Reactive and replacement patterns of fibrosis have been previously identified in patients with ESRD using gadolinium [58,59]. Due to the risk of nephrogenic systemic fibrosis [151], patients with ESRD are now excluded from MRI examinations with gadolinium. Without the availability of safe and noninvasive fibrosis measurement techniques, surrogate measures such as hypertrophy or reduced contractility are widely used to estimate fibrotic burden for diagnostic, prognostic, and treatment efficacy purposes. In this study, we utilized 2-pt bSSFP, a magnetization transfer contrast CMR technique, to characterize myocardial fibrosis without the need for gadolinium in patients on routine hemodialysis for ESRD. We used quantitative evidence of fibrosis to challenge the current prevailing view that using hypertrophy or reduced contractility are accurate surrogates for fibrosis measurements.

$\Delta S/S_o$ values in healthy, age-equivalent controls agreed with our prior data using 2-pt bSSFP (Chapter 2, Figure 2.6). We demonstrated elevated myocardial

$\Delta S/S_o$ in patients with ESRD, corresponding to increased interstitial fibrosis and decreased magnetization transfer. Signal elevation is evident upon subjective inspection of $\Delta S/S_o$ maps (Figure 3.5, Figure 3.8) and with quantitative analysis of the distributions of $\Delta S/S_o$ (Figure 3.7). While greater than healthy tissue, mean $\Delta S/S_o$ values over the LV in patients with ESRD fell below focal values for tissue that enhanced at LGE from our previous study (Chapter 2). This is expected due to the propensity for a diffuse pathology in patients with ESRD.

Our patients with ESRD demonstrated prolonged QTc with 18 patients exceeding the standard normal cutoff of 440ms. Lengthened QT times may be demonstrative of increased ventricular fibrosis which can slow conduction times [38]. Prolonged QT is associated with the development of ventricular arrhythmia, specifically torsades de pointes [152], and is associated with mortality and sudden cardiac death in patients hemodialysis [153,154]. In addition to fibrosis, severe alterations in electrolytes may predispose patients on hemodialysis to development of arrhythmia [49,154] and time since last treatment may impact ECG recordings [154]. These confound make the detection of fibrosis a complex task by ECG alone.

Since fibrosis can lead to ventricular stiffening [35,36], strain measurements by echocardiography [165] and CMR [60] have been used to estimate fibrosis in patients with ESRD. However, the drastically fluctuating hemodynamics in patients receiving hemodialysis modify echocardiographic measures [52,68], which may not actually associate with histological measures of fibrosis in this population [51]. Strain measurements correlated with hypertrophy

but not fibrosis in this study, indicating that measures of ventricular stiffness may be a consequence of thickened LV walls and not specifically the development of fibrosis.

Previous reports indicate a varied but large proportion—up to 91%[55]—of hemodialysis patients with hypertrophy [56-58]. Hypertrophy is associated with emergence of cardiovascular disease and death in the general population [17,18] and with poorer prognosis in patients with hypertension[155], aortic stenosis[156], heart failure with preserved ejection fraction [157], and ESRD [58]. Indeed, our findings confirmed that hypertrophy was prevalent among individuals with ESRD. However, using MRI strain imaging, which is more accurate and reproducible than comparable ultrasound based methods, we observed only slightly reduced longitudinal contraction compared to healthy, age-equivalent controls (Table 3.1,Figure 3.3). Though hypertrophy is prognostic, it does not differentiate the etiology of adverse cardiac outcomes such as development of interstitial fibrosis leading to fatal arrhythmias. As described in our study, hypertrophy only moderately associated with divergence (Figure 3.9) and may not be an appropriate surrogate to detect fibrosis or probe for biomarkers specific to fibrosis. In fact, others have shown a lack of correlation between hypertrophy and fibrosis in patients with kidney disease [60] and demonstrated that fibrosis is an independent risk factor for cardiovascular mortality in ESRD above and beyond hypertrophy or contractile dysfunction [51].

Investigations of molecular mechanisms of remodeling have identified FGF23 [141,158,159], PTH [142,159,160] and serum phosphates [158,159] as

potential factors driving ventricular hypertrophy. Specifically, FGF23 is correlated with LV hypertrophy [53,141] and linked to increased risk of cardiac mortality in patients with ESRD [141,142,158]. Emerging therapies seeking to abrogate effects of elevated serum FGF23 levels through dietary intervention [53,158,161], oral phosphorous binder therapy [53,158] or use of lanthanum carbonate [162], are promising for the reduction of serum FGF23 levels over time. However, prior studies have demonstrated that phosphate binder and vitamin D therapies [141,163], and even renal transplantation [164] fail to reverse left ventricular hypertrophy, despite improving outcomes [161]. FGF receptors that are normally only activated after myocardial infarction to promote formation of fibrotic scar tissue may be activated by excess FGF23 [53], suggesting that fibrotic remodeling may play a greater role in promoting adverse cardiac events in ESRD patients. This view is substantiated by extensive interstitial fibrosis measured by biopsy [51] and LGE CMR [58,59], prior to its contraindication in ESRD patients, along with the link for cardiac fibrosis to promote arrhythmia [62], heart failure, and sudden death. In fact, increased fibrotic burden is associated with worse prognosis and predicts sudden cardiac death independent of hypertension, diabetes, ejection fraction, LV dilation, and cardiomyocyte hypertrophy in patients with ESRD [51].

Translational and early clinical trials show promise for the cardiac benefits of emerging therapies such as spironolactone [166,167], galectin 3 blockade [168], and FGF23 blockade [141,169] but with outcome measures of reduced hypertrophy, improved contraction, or decreased cardiac death. Cardiac fibrosis

has been attenuated in animal models of pressure overload hypertrophy treated with spironolactone [170] and dilated cardiomyopathy [171] and renal failure [172] treated with rapamycin. In patients with ESRD, the progress of these and other potentially lifesaving treatments is limited by the reliance on hypertrophy or reduced contraction for disease monitoring. While hypertrophy and fibrosis are interrelated, if patients are diagnosed and selected based only on hypertrophy or contractile status for clinical trials whose outcomes only measure improvements in structure or strain, the entire fibrotic disease process is overlooked. It is imperative for the design and development of targeted anti-fibrotic therapies to rely on the accurate detection of fibrosis and specific molecular mechanisms in the context of ESRD and hemodialysis, otherwise new therapeutics may effectively treat hypertrophy or contraction without affecting the independent development of fibrosis.

The patients examined in this study demonstrated significantly elevated TnT, FGF23, PTH, TIMP1, and TIMP2, reduced MMP9 and a trend toward elevated MMP2 compared to healthy controls (Table 3.3). While each of these biomarkers may indicate generic risk of arrhythmia or cardiac death, there is a complex interaction between hypertrophy and fibrosis that is not distinguished by these biomarkers. In fact, we found correlations with both hypertrophy and fibrosis for TnT, FGF23 (Figure 3.10 E-F) and PTH, indicating that none of these are specific enough to detect fibrosis alone.

MMPs play a crucial role in degrading the existing extracellular matrix, for example, in acute myocardial infarction to allow infiltration of inflammatory cells

to clear necrotic myocytes and initiate the healing process [173]. MMP2 and 9, which comprise the gelatinases, primarily degrade denatured collagen, but may also have a pro-fibrotic role in the heart [174]. TIMPs 1 and 2 are the most widely investigated inhibitors of MMPs. TIMPs bind the catalytic domain of MMPs in a 1:1 fashion, thereby preventing degradation of MMP substrates [175]. Independent of MMP interactions, TIMPs have alternative signaling roles, which can result in increased cardiac fibroblast proliferation and activation, and therefore collagen synthesis [176]. The balance between MMP and TIMP ratio is crucial for maintaining proper extracellular matrix form and function. For these reasons, MMPs and TIMPs have been investigated as molecular mechanisms of cardiac remodeling and fibrosis, and the subsequent link with contractile dysfunction in non-diseased aging populations [22] as well as hypertrophic cardiomyopathy [143], overload induced hypertrophy [177], myocardial infarction [173,178], hypertension [179], and heart failure [144]. MMPs and/or TIMPs may not only serve as prognostic or diagnostic markers, but pharmaceutical targets for adverse structural or fibrotic remodeling. A promising study in a murine model of experimental myocardial infarction demonstrated the beneficial effects of inhibiting MMP2 and MMP9 by doxycycline, an FDA approved antibiotic [180].

MMPs and TIMPs have been investigated as cardiac biomarkers in hemodialysis patients, with conflicting results [146,148,181,182] but with the goal of being easily measured parameters for non-invasive myocardial tissue characterization [183]. We have shown that patients with ESRD not only demonstrate elevated circulating TIMP1 and TIMP2, but that both of these

biomarkers correlate with measures of fibrosis, independent of hypertrophy (Figure 3.10 G-H). Importantly, it has been shown that MMPs and TIMPs are elevated in patients with deteriorating heart failure, but not end stage heart failure or normal function [144]. Thus, MMPs and TIMPs may be important indicators of cardiac disease progression, possibly through development of fibrosis. Future investigations are warranted to understand cardiac remodeling processes, tissue characterization, and MMP/TIMP involvement in hemodialysis patients, while taking into account the effects of hemodialysis treatment on the circulating concentrations of biomarkers [147,148].

Efforts to image myocardial fibrosis without gadolinium are currently under investigation, with the goal of applying non-contrast CMR to patients with kidney failure or other contraindications to gadolinium. Mapping of native T1 relaxation times [88,89] has shown promise for tissue characterization in cardiomyopathy [95,97], aortic stenosis [94], and Anderson-Fabry disease [104]. Recently, native T1 mapping has been applied to patients with ESRD [90,99,184]. Graham-Brown et al. demonstrated globally elevated T1 times as well as diffuse and non-ischemic, focal fibrosis patterns [184], similar to a previous report using LGE CMR [59] and to our results shown in Figure 3.6. The patients included in that study demonstrated reduced contractility, indicating that this sample may have had established heart failure and more advanced fibrosis compared to our patients, although the differences in T1 maps are visually subtle. Importantly, unless corrected for hematocrit, T1 times may be erroneously elevated due to anemia caused by hemodialysis and may vary depending on time since last

treatment. T1 mapping sequences are also commonly sensitive to elevated and variable heart rates, particularly for longer T1 times [91], which all routinely occur in individuals with ESRD.

A few important limitations are relevant to this study. Since 2-pt bSSFP imaging requires 2 consecutive end-expiratory breath holds, patient motion and breath hold variation between acquisitions may limit this technique. We manually registered any misaligned image pairs to adjust for inaccurate position. While this could introduce additional human error and noise in the $\Delta S/S_o$ maps, many slices were salvaged for data analysis that would otherwise be excluded from this study. While we are currently unable to collect low and high MT-weighted images simultaneously in a single breath hold, future investigations will aim to reduce table time and patient fatigue, while optimizing MT-weighting sequences to reduce analytical limitations.

Regions of interest were carefully defined to include only myocardial voxels, however it is possible that some voxels with partial volume effects from the blood pool or pericardial fat were included in our analyses. These erroneous voxels are more likely to be included for healthy controls since the myocardium is often thinner than in patients with ESRD. Thus, our calculation of $\Delta S/S_o$ may be slightly elevated in controls and true group differences may be greater than what we described. To eliminate the impact of this noise, in quantitative analysis we restricted the range of voxel values to 0-400% for $\Delta S/S_o$ which incorporates the expected physiologic ranges for normal and fibrotic myocardium.

In conclusion, we have shown that endogenous contrast mechanisms can be measured in the myocardium of patients with ESRD using 2-pt bSSFP CMR. MT-weighted CMR identifies increased fibrosis in patients with ESRD, which only moderately associated with hypertrophy but not systolic or diastolic dysfunction. The accuracy of imaging-guided biomarkers such as TIMP1 or 2 will benefit from the capacity to delineate between hypertrophy and fibrosis and may serve as potential therapeutic targets for future therapies to attenuate fibrosis in patients on hemodialysis for ESRD. Accurate and safe measurement of fibrotic burden and distribution could inform appropriate pharmaceutical interventions or serve as selection criteria for alternative treatments such as radiofrequency ablation and implantable cardioverter-defibrillator to prevent arrhythmias and ultimately reduce the risk of sudden cardiac death in patients with ESRD. We have challenged the dogmatic view that degree of hypertrophy or contractility directly represents fibrotic burden and have offered a non-contrast imaging solution to specifically measure LV fibrosis in patients with ESRD.

Contributions

Tori Stromp and Moriel Vandsburger conceived of the study design and implementation. Tori Stromp completed all imaging studies, post processing, and image analysis. Steve Leung consulted on image acquisition and quality control. Rebecca Kidney and Kristin Andres assisted with participant recruitment and, along with Tyler Spear and Joshua Kaine, assisted with structural and functional data analysis. All patients with ESRD were kindly referred by Dr. Hartmut Malluche with assistance of Nedda Hughes and Kim McLaughlin.

Acknowledgments

We thank Jennifer Moylan, PhD for the preparation and analysis of blood biomarker assays. This project was supported by the American Heart Association National Affiliate (14CRP20380071 to MHV) and the National Institutes of Health through the National Heart Lung and Blood Institute (R01HL128592) and National Center for Advancing Translational Sciences (UL1TR000117).

Table 3.1. Participant Characteristics.

Variable	**Healthy Controls** (n=33)	**Patients with ESRD** (n=29)
Demographics		
Age (yrs.)	54.0 ± 10.9	53.7 ± 12.8
Male	15 (45)	14 (48)
White/Caucasian	29 (88)	16 (55)
Black/African American	1 (3)	12 (41)
Asian	0	1 (3)
American Indian	1 (3)	0
Hispanic	2 (6)	0
Body Mass Index (kg/m^2)	24.2 ± 2.3	31.6 ± 6.8†
Cardiac Structure and Function		
Left Ventricular Mass Index (g/m^2)	60.4 ± 13.3	94.3 ± 27.8†
Septal Thickness (cm)	0.9 ± 0.2	1.3 ± .03†
H/R Ratio	0.3 ± 0.1	0.5 ± 0.2†
End Systolic Volume (mL)	34.5 [25.3, 46.0]	36.5 [31.5,54.4]
End Diastolic Volume (mL)	92.3 ± 25.3	116.5 ± 41.0*
Ejection Fraction (%)	60.5 [56.0, 64.4]	63.8 [58.4, 68.1]
Heart Rate (bpm)	60.8 ± 8.8	72.3 ± 10.8†
QRS Duration (ms)	90.0 [84.0, 98.0]	94.0 [77.0, 104.0]
QTc interval (ms)	422.7 ± 18.4	463.0 ± 37.7†
Cardiac Mechanics		
Global Diastolic Strain Rate (%/s)	174.1 ± 33.9	162.8 ± 41.7
Global Longitudinal Strain (%)	-21.8 [-26.0, -20.1]	-20.9 [-23.3, -18.7]*

Continuous variables are presented as mean ± standard deviation or median [interquartile range]. Categorical variables presented as count (%).*p<0.01, †p<0.001

Table 3.2. Clinical Features of Patients with ESRD.

Clinical Features	Results
Dialysis Duration (years)	4.8 ± 3.2
Primary Etiology of End Stage Renal Disease	
Diabetes	12 (41)
Hypertension	7 (24)
Glomerulonephritis	2 (7)
Reflux Nephropathy	2 (7)
Obstructive Nephropathy	1 (3)
Interstitial Nephritis	1 (3)
Focal Segmental Glomerulosclerosis	1 (3)
Unknown	3 (10)
Comorbidities	
Hypertension	27 (93)
Diabetes	17 (59)
Prior Myocardial Infarction	4 (14)

Continuous variable is presented as mean ± standard deviation.
Categorical variables are presented as count (%).

Table 3.3. Blood Biomarker Results

	Healthy Controls (n=25)	**Patients with ESRD** (n=16)	***p***
TnT (ng)	undetected	0.05 [0.0, 0.18]	<0.001
FGF23 (pg)	0.00 [0.00, 0.00]	521.22 [29.47, 1210.85]	0.001
PTH (pg)	139.66 [78.45, 167.61]	544.20 [340.78, 901.96]	<0.001
MMP2 (ng)	11.21 [6.89, 20.08]	23.02 [11.88, 33.35]	0.051
MMP9 (ng)	931.90 [643.31, 1201.70]	552.53 [347.87, 718.14]	0.026
TIMP1 (pg)	4336.00 [4090.50, 5757.50]	6371.00 [4323.00, 7567.00]	0.005
TIMP2 (pg)	3255.00 [2555.50, 4408.50]	4676.00 [2953.00, 5302.00]	0.035

TnT: troponin T, FGF: fibroblast growth factor, PTH: parathyroid hormone, MMP: matrix metalloproteinase, TIMP: tissue inhibitor of MMP. Values are presented as median [interquartile range]. $p < 0.05$ was considered significant by analysis with Mann-Whitney U test.

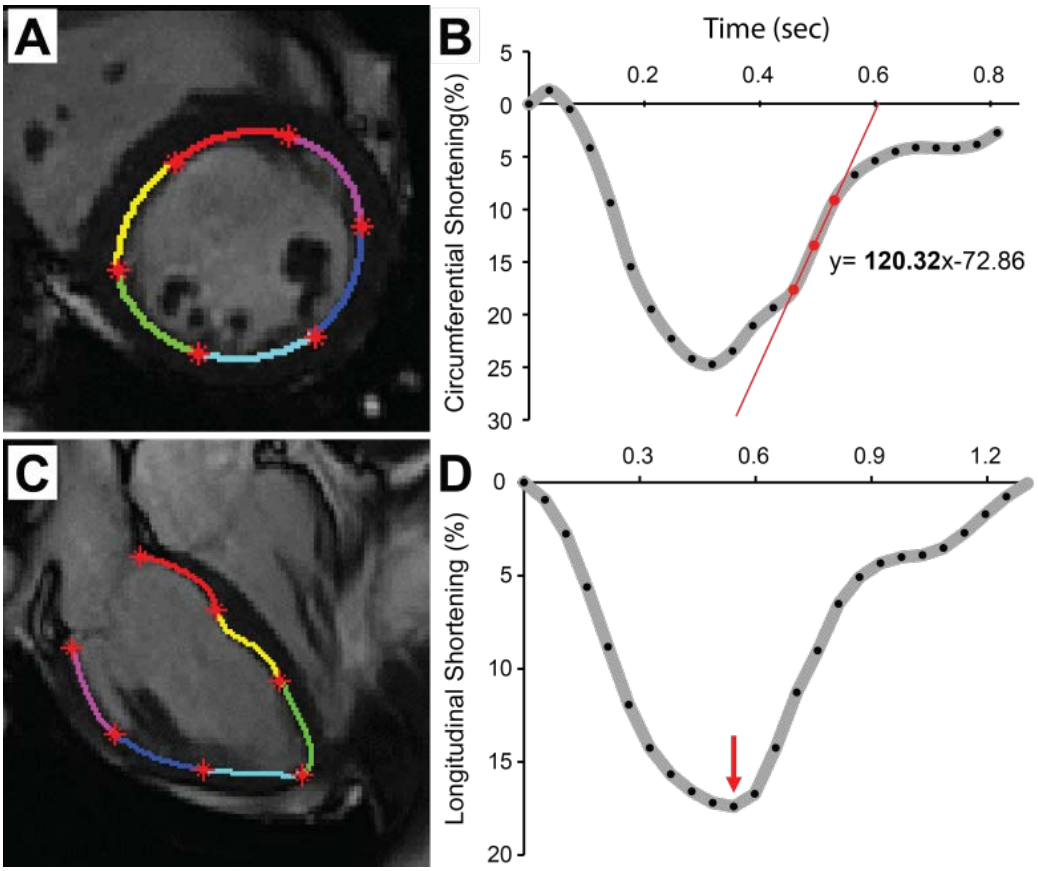

Figure 3.1. Cardiac mechanics analysis in a healthy control. **(A)** In each transverse slice, endocardial borders were manually defined at end diastole and automatically followed through the cardiac cycle using a feature tracking algorithm. **(B)** Average circumferential shortening across all sectors was plotted as a function of the cardiac cycle (grey lines), and diastolic strain rate was calculated as the maximum slope during relaxation (red line), which was 120.32%/sec for this participant. **(C)** Similarly, longitudinal strain as a function of cardiac phase was calculated from a 4 chamber longitudinal cine image. **(D)** The peak global longitudinal strain was defined by the maximum shortening value (arrow), which in this participant was 17.4%.

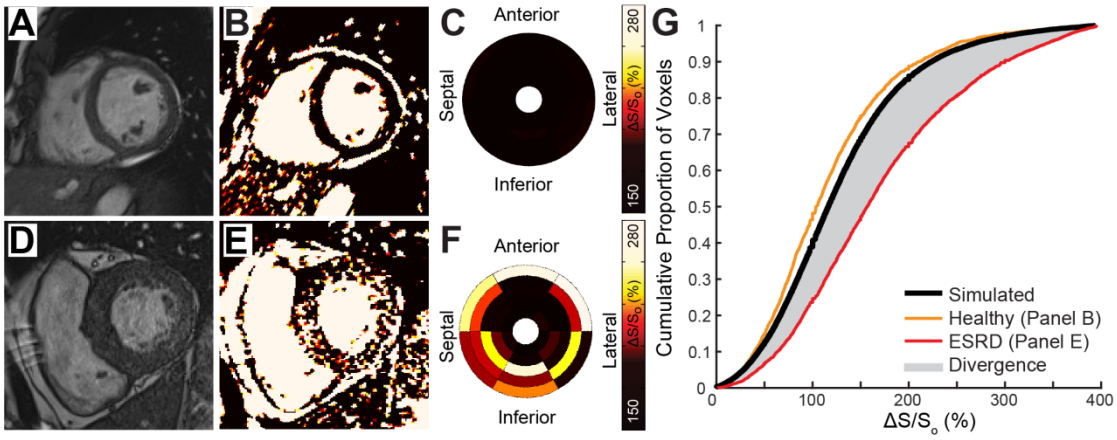

Figure 3.2. Two-pt bSSFP technique and quantitative analysis. (A) A cine bSSFP image at α=45° in a representative healthy control was paired with an image with α=5° (not shown). Maps of $\Delta S/S_o$ were generated as $\Delta S/S_o=(S_{45}-S_5)/S_5$ x 100 (%), where S_i is the signal intensity per voxel at each flip angle *i*. **(B)** A $\Delta S/S_o$ map from this healthy control demonstrates low and uniform $\Delta S/S_o$ values in a mid-ventricular slice. **(C)** Low $\Delta S/S_o$ is evident across all slices and sectors of the heart in a whole-heart bullseye plot representing mean $\Delta S/S_o$ per sector in this control. **(D)** A mid-ventricular image taken at α=45° from a representative patient with ESRD and **(E)** the corresponding $\Delta S/S_o$ map, with noticeable elevated signal intensity. **(F)** Elevated values are present throughout the ventricle, as seen in the bullseye plot. **(G)** Using all LV myocardial $\Delta S/S_o$ values from the control group, a simulated cumulative distribution function was generated (black). The simulation was dynamically resized to match the number of voxels per heart and compared to the cumulative distribution function of observed $\Delta S/S_o$ values for each individual ventricle. Cumulative distributions from the healthy control in b (orange) and patient with ESRD in e (red) are shown. We integrated the area between the simulation and each participant's distribution (here, the patient from E) to define the divergence (gray) in $\Delta S/S_o$. Divergence is a metric of fibrotic burden.

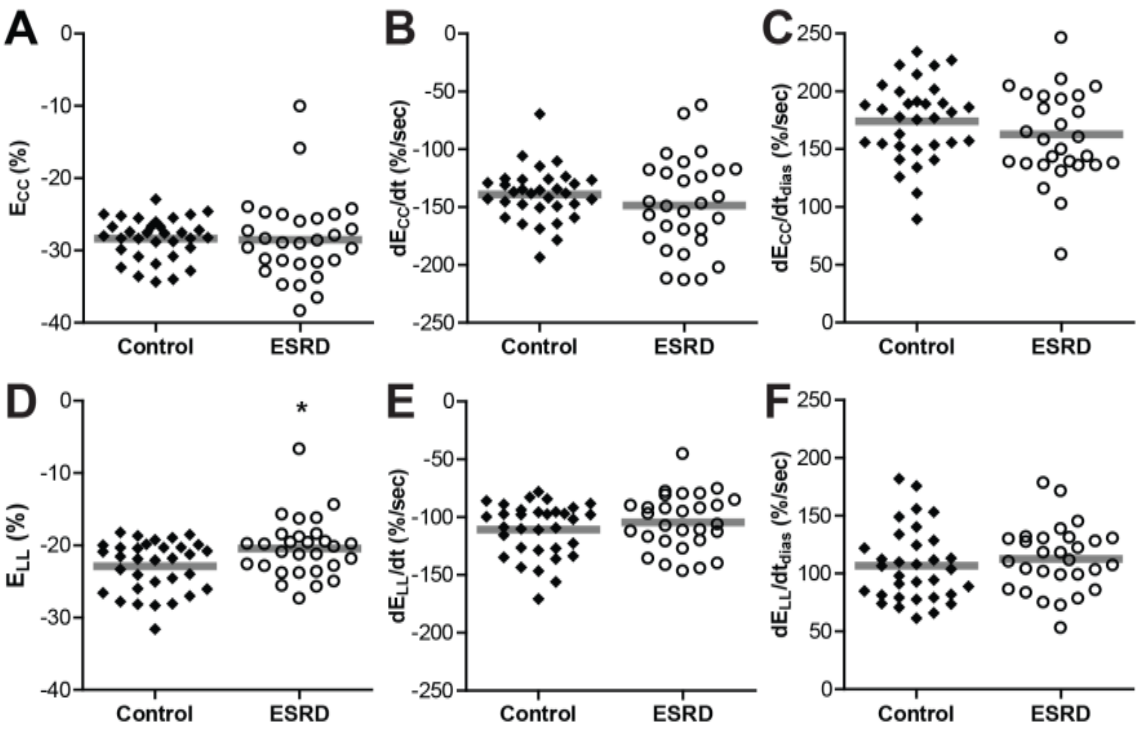

Figure 3.3. Relaxation was preserved and contractility was slightly reduced in patients with ESRD. (A) Circumferential peak strain, **(B)** systolic strain rate, and **(C)** diastolic strain rate were similar between groups (all p>0.05). **(D)** Global longitudinal strain was slightly reduced in patients with ESRD (-20.5 ± 4.1%) compared to controls (-22.9 ± 3.5%, p=0.035), while **(E)** longitudinal systolic and **(D)** diastolic strain rates were not different (p>0.05 for both). A large overlap in values indicates that global longitudinal strain is not a robust, independent predictor of increased fibrotic burden. Gray bars indicate group means. *p<0.05.

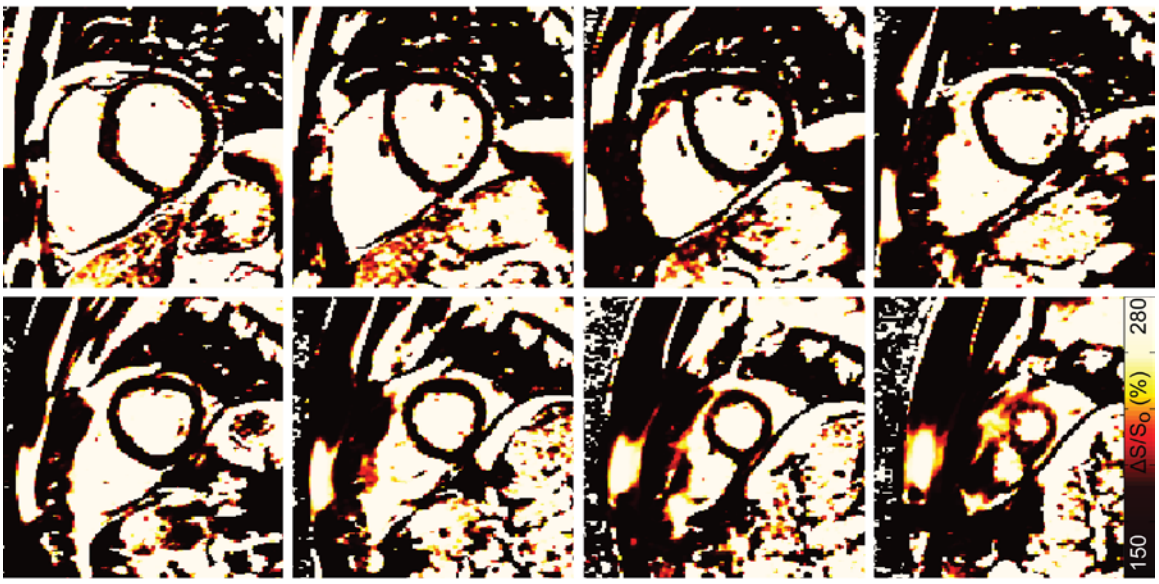

Figure 3.4. Representative images from a healthy control. In a representative healthy control, $\Delta S/S_o$ maps from base (top left) to apex (bottom right) reveal uniformly low myocardial signal throughout the LV. Low $\Delta S/S_o$ is consistent with healthy myocardial tissue.

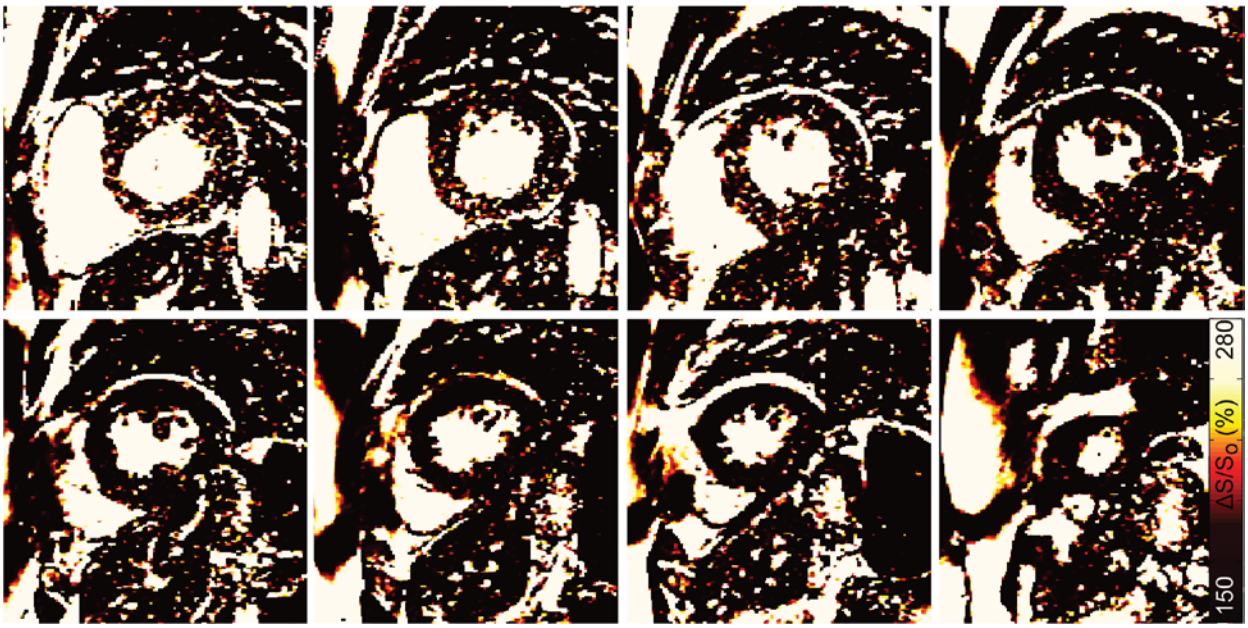

Figure 3.5. Representative images from a patient with ESRD and moderate fibrosis. $\Delta S/S_0$ maps from base (top left) to apex (bottom right) in an example patient with ESRD with moderate diffuse fibrosis. The LV was noticeably hypertrophied with scattered $\Delta S/S_0$ enhancement, indicating diffuse fibrosis, particularly in basal slices. This example demonstrates the need for accurate fibrosis mapping across the entire LV, since fibrosis burden and pattern changes drastically from base to apex of the LV.

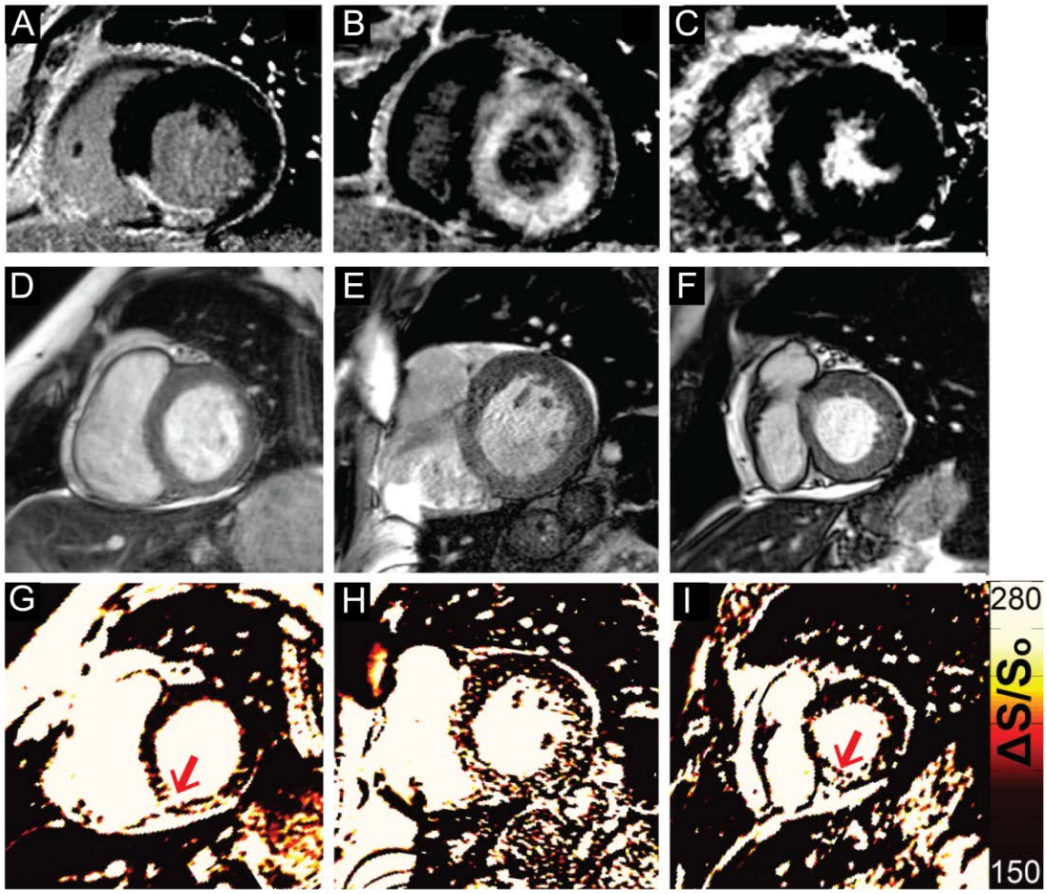

Figure 3.6. Recapitulation of three prevailing patterns of fibrotic tissue in renal failure patients. Prior to the FDA warning and contraindication of gadolinium, Schietinger et al.[59] observed 3 dominant patterns of late gadolinium enhancement in renal failure patients: **(A)** thin scar like enhancement, **(B)** diffuse subendocardial fibrosis, and **(C)** focal fibrosis at the ventricular insertion points unrelated to ischemia. (A-C adapted from [59].) MT-weighted fibrosis in renal failure patients imaging reveals similar patterns to those seen previously using late gadolinium enhancement MRI. **(D-F)** End diastolic bSSFP images in 3 renal failure patients and corresponding maps of $\Delta S/S_o$ reveal **(G)** thin enhanced tissue , **(H)** diffuse enhancement, and **(I)** focal enhancement at the ventricular insertion point.

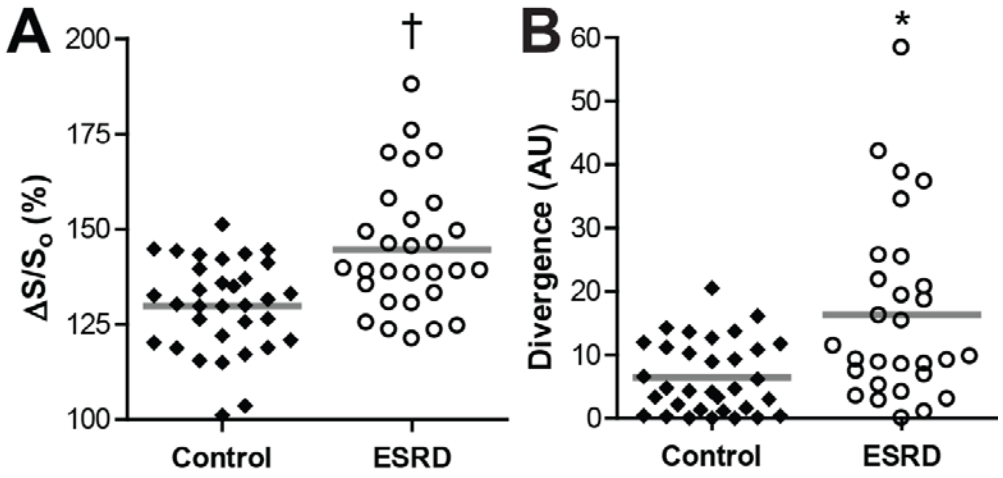

Figure 3.7. Patients with ESRD had increased signal intensity and fibrotic burden. (A) Whole-ventricle $\Delta S/S_o$ values were significantly elevated in patients with ESRD (144.7 ± 17.1%) compared to controls (129.9 ± 12.0%, p<0.001). **(B)** Divergence was increased in patients with ESRD (16.3 ± 14.3) compared to controls (6.5 ± 5.7 AU, p=0.003), indicating a greater fibrotic burden. Gray bars denote group means. *p<0.01, †p<0.001.

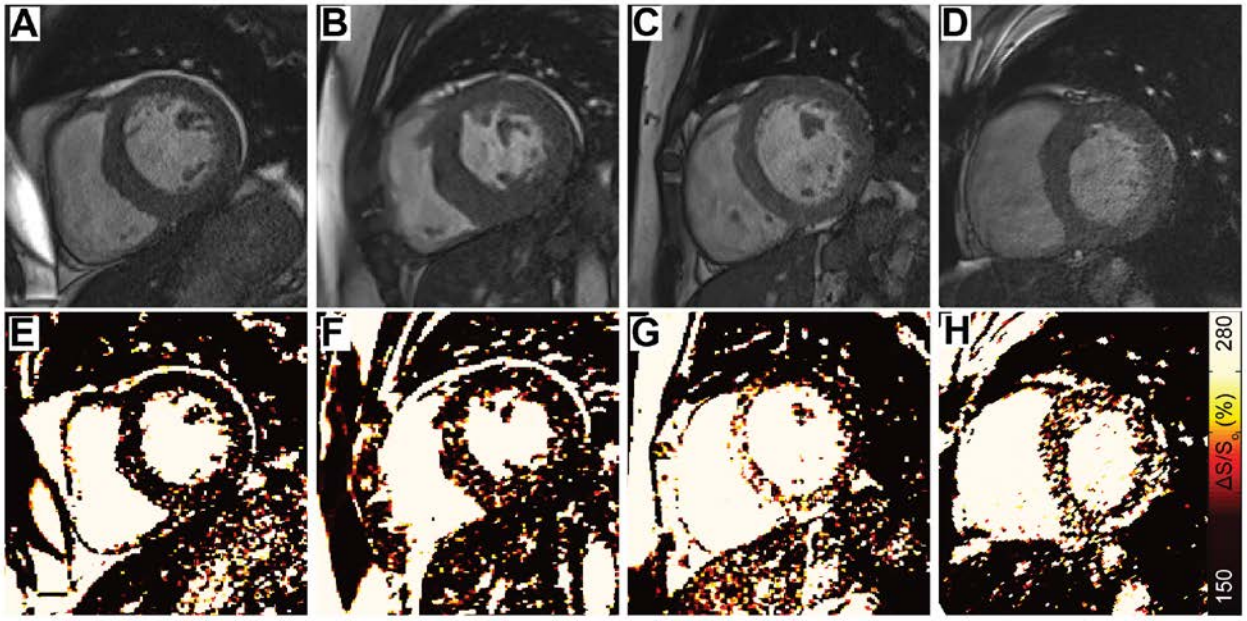

Figure 3.8. Patients with ESRD were hypertrophic but displayed a variety of fibrosis patterns. (A-D) Representative mid-ventricular images (α=45°) from 4 individual patients with ESRD who displayed hypertrophy, particularly in the interventricular septum. **(E-H)** Corresponding $\Delta S/S_o$ maps from the patients in a-d demonstrated a wide range of signal elevation in these patients, indicating that hypertrophy alone is not a good predictor of fibrotic burden in patients with ESRD.

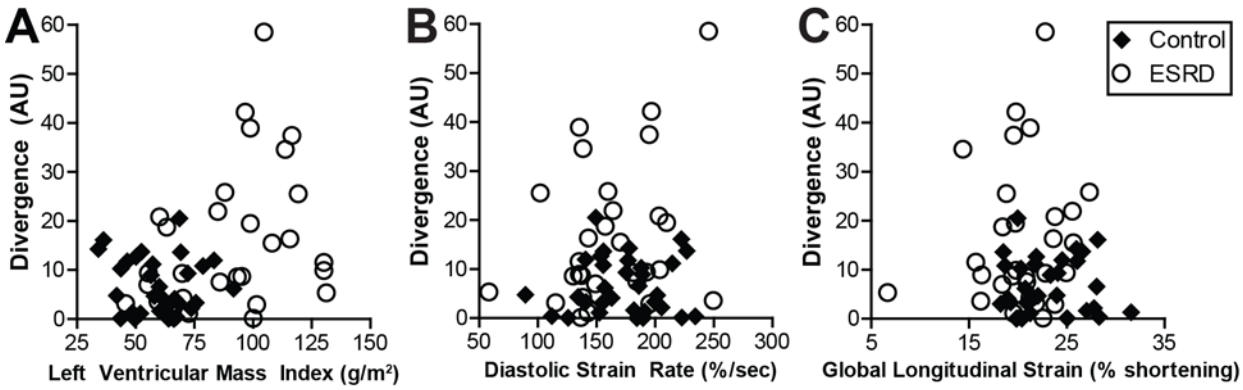

Figure 3.9. Fibrosis moderately associated with hypertrophy but did not correlate with strain. (A) Left ventricular mass index (LVMI) demonstrated a moderate correlation with divergence (rho=0.31, p=0.01). Notably, the correlation between LVMI and divergence was not linear. Patients with the highest values of either variable did not regularly demonstrate the highest values in the other. **(B)** Neither diastolic strain rate nor **(C)** global longitudinal strain correlated with divergence (p>0.05 for both).

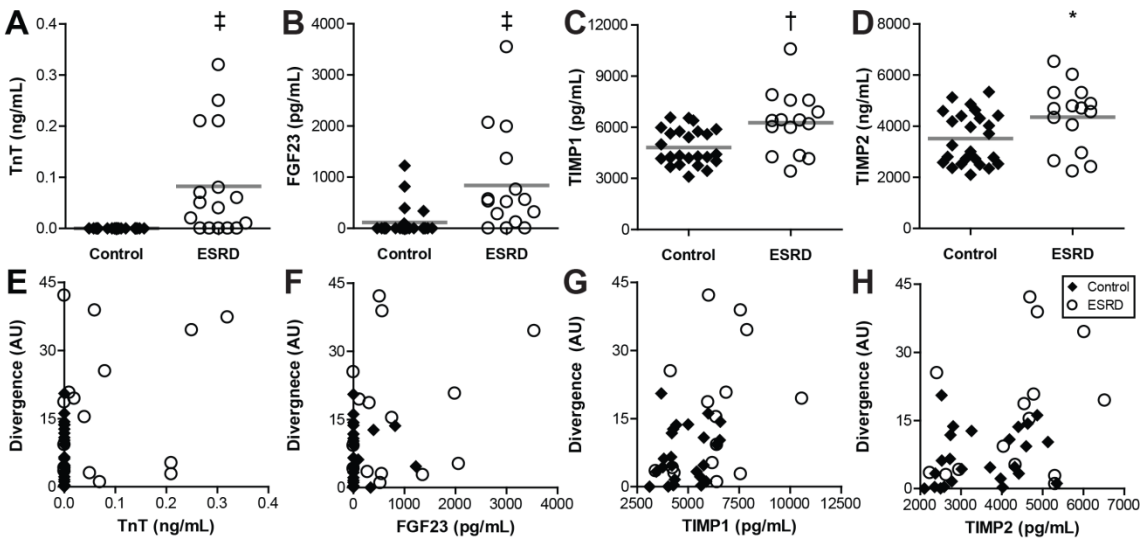

Figure 3.10. Patients with ESRD had elevated blood biomarkers with moderate correlations to fibrosis. Patients with ESRD demonstrated elevated concentrations of **(A)** troponin T (TnT), **(B)** fibroblast growth factor (FGF) 23, **(C)** tissue inhibitor of metalloproteinase (TIMP) 1 and **(D)** TIMP2. See Table 3.3 for complete biomarker results. **(E)** Spearman correlation analysis revealed a moderate association between divergence and TnT (rho=0.32, p=0.04). **(F)** FGF23 did not correlate with divergence (p=0.12). **(G)** TIMP1 and **(H)** TIMP2 demonstrated a moderate correlation with divergence (rho=0.39, p=0.01 for each). *p<0.05, †p<0.01, ‡p<0.001.

CHAPTER 4: LONGITUDINAL MONITORING OF CARDIAC FIBROSIS PROGRESSION USING MAGNETIZATION TRANSFER CARDIAC MRI IN PATIENTS ON HEMODIALYSIS FOR END STAGE RENAL DISEASE

Synopsis

Background: Chronic hemodialysis treatment is associated with a time-dependent increased risk of cardiac mortality, up to 20 times greater than the general population. Ventricular fibrosis may be a leading cause of higher death rates, yet the exclusion from gadolinium enhancement cardiac MRI (CMR) excludes patients with end stage renal disease (ESRD) from noninvasive fibrosis identification. Progressive hypertrophy and ventricular stiffness are currently utilized as alternate measures of fibrotic burden but are more likely measures of structural and functional alterations irrespective of the development of fibrosis. We employed our non-contrast, 2 point balanced steady state free precession (2-pt bSSFP) CMR technique to test the hypothesis that fibrosis progresses over 1 year in patients with ESRD independent of any changes in hypertrophy or contractility.

Methods: Patients on routine hemodialysis for treatment of ESRD who completed our previous study were invited to participate in a follow up 1 year later. $\Delta S/S_o$ and strain were calculated using our standard techniques. Using the healthy standard distribution of $\Delta S/S_o$ established in our prior study, we compared cumulative distributions of $\Delta S/S_o$ acquired in follow up scans to

calculate divergence, a metric of fibrotic burden. Measures of structure, function, and fibrosis were compared between the 2 time points with paired t tests.

Results: Six patients completed follow up 2-pt bSSFP imaging. All patients were hypertrophic at baseline but demonstrated minimal alterations in hypertrophy over time. Changes in circumferential and longitudinal strain were varied, but not significantly altered from baseline. $\Delta S/S_o$ and divergence were considerably increased at follow up by an average of 10.3 ± 16.0% and 7.1 ± 13.7% AU, respectively.

Conclusions: Patients with ESRD did not demonstrate significant changes in hypertrophy nor contractility over a 1 year follow up period. The phenotypes of fibrosis progression were varied, which demonstrates the heterogeneous development of fibrosis in this population and the need for fibrosis specific monitoring independent of structural and functional alterations. Non contrast fibrosis imaging may serve as a better prognostic tool than the current alternatives of hypertrophy and stiffness, aiding in more appropriate monitoring and treatment selection for patients with ESRD.

Background

One in 4 patients on hemodialysis for treatment of end stage renal disease (ESRD) will die from sudden cardiac death [44]. For long term hemodialysis patients (up to at least 6 years), risk of cardiovascular mortality is 10-20 times greater than the general population [47]. Over the last 30 years, post-mortem histological studies have repeatedly established high prevalence of cardiac fibrosis in deceased ESRD patients [55,58,59]. It is now appreciated that the progressive development of cardiac fibrosis is associated with increased risk of arrhythmia [69], heart failure [64], and sudden cardiac death in ESRD [51]. Cardiac fibrotic burden may be correlated with time on dialysis [55] while cardiac death rates increase steadily over multiple years of treatment [185].

Patients with ESRD are excluded from late gadolinium enhancement (LGE) cardiac magnetic resonance imaging (CMR) due to the risk of developing nephrogenic systemic fibrosis [186]. The inability to noninvasively visualize and monitor fibrosis progression impedes the ability to develop and test targeted treatments for the attenuation of cardiac fibrosis in this high risk population. Visually and quantitatively monitoring cardiac fibrosis over time has applications for clinical trials of anti-fibrotic therapies such as spironolactone [170,187] or fibroblast growth factor receptor blockade [141,188] as well as patient selection for pharmaceutical intervention, radiofrequency ablation, or implantable cardioverter-defibrillator placement. Collagen volume fraction from myocardial tissue biopsy has been the historical gold standard for detecting and quantifying

fibrosis but is prone to false negatives [65] and is undesirable for serial measurements.

Over years of hemodialysis treatment, patients with ESRD have an increasing risk of cardiac mortality [185], which may be due to advancing fibrosis. We hypothesized that over 1 year, cardiac fibrosis progresses in patients on routine hemodialysis for treatment of ESRD, irrespective of structure or function alterations. Chapter 3 described a baseline study of fibrosis identification using our 2-pt bSSFP method (described in Chapter 2) in patients with ESRD. Here we report a 1-year follow up study conducted in a subset of these patients with ESRD. We measured the progression of left ventricular (LV) fibrosis using 2-pt bSSFP along with structural and functional correlates of heart failure.

Materials and Methods

Participants

All patients with ESRD from our previous study (Chapter 3) were invited to return for a second study visit 1 year after their initial scan. Participants were considered eligible for this follow up study if they were presently on hemodialysis treatment, had no MRI-unsafe implants or devices and had not developed arrhythmia (for proper ECG gating of sequences). This study was approved by the local Institutional Review Board and all participants were consented for the initial study and re-consented for the follow-up, if necessary. Since this was a repeated measures design, each patient served as his/her own internal control, thus reducing variability and increasing statistical power.

Cardiac Imaging Protocol and Image Analysis

All baseline characteristics were collected during the initial visit for completion of this prior study and reported in this chapter only for patients who participated in the follow up study visit. All cardiac imaging and offline image analysis including structure, function, and strain was completed exactly as described in Chapter 3: *Materials and Methods*. All quantitative analysis was completed on raw data from $\Delta S/S_o$ maps. Figures are displayed using a 2x3 median filter to reduce noise. We used the healthy standard cumulative distribution function generated from healthy controls in the initial study (Chapter 3) as the reference standard for analysis of $\Delta S/S_o$ signal enhancement in follow up images. Thus, both baseline and follow up scans were compared against the same healthy standard distribution for the calculation of divergence, as a metric of fibrotic burden.

Statistical Analysis

IBM SPSS Statistics Version 22 (IBM Corp, Armonk, NY) or MATLAB (MathWorks Inc., Natick, MA) were used to complete all statistical analyses. Paired t-tests were used to compare baseline and follow up measures. Data are presented as mean (range) or count (%) where appropriate. All comparisons were considered significant at the $p<0.05$ level.

Results

Patient Characteristics

From the initial study, 11 patients were eligible to complete a 1-year follow up scan. Of these, 1 patient had received a kidney transplant and discontinued dialysis and 4 others declined to participate for medical or other reasons. Six patients completed follow up CMR visits for this study. Demographic information is detailed in Table 4.1. Primary cause for kidney failure was hypertension (50%), diabetes (33%) or unknown (17%). All 6 patients were concurrently hypertensive and 4 patients (67%) had Type 2 diabetes. One patient had a failed kidney transplant and subsequently started hemodialysis, prior to the baseline scan. Average time on hemodialysis was 4.5 years at baseline. All participants completed the follow up CMR visit approximately 1 year after the initial visit (average=12.3 months since baseline, range: 11.1-14.4 months).

Clinical Cardiac Measures of Structure, Function, and Strain

Clinical features at baseline and follow up are detailed in Table 4.2. Neither body mass index (BMI) nor body surface area (BSA) was significantly changed. On ECG, corrected QT (QTc) interval shortened from 487.5 ± 36.4 ms to 439.2 ± 11.3 ms ($p<0.05$). End diastolic volume (EDV) did not change, but there was a trend toward reduced end systolic volumes (from 56.7 ± 26.6 mL to 47.747 ± 25.0 mL, $p=0.053$) which contributed to increased ejection fraction (EF) from 61.2 ± 8.8% to 65.9 ± 10.4% ($p=0.044$) over the follow up period. Average LV mass, LVMI, septal thickness, and H/R ratio were not significantly changed

over the follow up year (Figure 4.1), although 5 of the 6 patients demonstrated slightly reduced EDV, reduced ESV, and increased EF (Table 4.2). While this cohort was hypertrophic at baseline, as a group, LV mass did not significantly increase over the follow up period and H/R ratio decreased slightly. Between baseline and follow up, changes in circumferential diastolic strain rate (from 174. 3 ± 45.9%/s to 177.2 ± 52.9%/s, $p > 0.05$) and longitudinal strain (from -20.6%/s to -21.5%, $p>0.05$) were varied, but not significantly different (Figure 4.2).

Examples of Fibrosis Development

Among the six individuals recruited to date for a 1-year follow up scan, diverse phenotypes were observed with respect to progressive changes in the magnitude of cardiac fibrosis. Some patients demonstrated low levels of $\Delta S/S_o$ at baseline with progressively increased $\Delta S/S_o$ over time, which is seen in Figure 4.3. This example patient had received hemodialysis treatment for approximately 2 years at baseline. Low and uniform $\Delta S/S_o$ values are seen across the LV in baseline images (Figure 4.3 A-C). Globally, this patient demonstrates normal baseline $\Delta S/S_o$ values throughout the entire myocardium in line with those established for healthy controls in Chapter 3 (Figure 4.3 D). At the time of the follow up visit, diffusely elevated $\Delta S/S_o$ values were evident across the 3 example slices (Figure 4.3 E-G) primarily in basal and septal regions of the heart (Figure 4.3 H). Divergence increased from 9.8 AU (within the bounds of healthy controls) to 27.6 AU (well outside the range of normal values), indicating advanced fibrosis progression in this patient.

In contrast to the prior individual, some patients who were imaged demonstrated negligible alterations in $\Delta S/S_o$ during the follow up period. Baseline scans from another representative patient on hemodialysis (4.3 years) reveal low and uniform $\Delta S/S_o$ in example slices (Figure 4.4 A-C) and across the entire LV (Figure 4.4 D). In follow up images (Figure 4.4 E-G), minimal $\Delta S/S_o$ elevations are detected, mainly in the mid ventricle but not elsewhere throughout the LV (Figure 4.4 H). A small increase of 3.9 AU in total LV divergence demonstrates the minor progression of fibrosis in this patient.

Longitudinal Monitoring of Fibrosis Progression

Five patients demonstrated increased $\Delta S/S_o$ (Figure 4.5 A) and divergence values (Figure 4.5 B) with an average group increase of 7.1 ± 13.7 AU in divergence from baseline to follow up. Cumulative distribution functions for all patients are shown in Figure 4.5 C. The baseline rightward shifts in $\Delta S/S_o$ (quantified by divergence) are visually evident compared to the healthy standard. Over the follow up period a further shift in $\Delta S/S_o$ distribution is noticeable for most patients, indicating increased fibrosis over time.

Discussion

Here we described a small follow up study using non-contrast 2-pt bSSFP CMR to monitor fibrosis progression in patients on hemodialysis for treatment of ESRD. The rate of sudden cardiac death increases over time with chronic hemodialysis [185], indicating that fibrosis may be progressing unchecked,

without proper measurement or treatment options for these patients. LGE CMR has become the clinical standard to identify for focal fibrosis and with the addition of T1 mapping can detect diffuse fibrosis through calculation of the extracellular volume content [77]. The exclusion from gadolinium enhanced CMR, however, has severely limited the ability to detect, monitor, and treat fibrosis progression in patients with ESRD.

While risk of cardiac mortality increases with time on chronic hemodialysis, we have previously shown that fibrotic burden does not directly correlate with hemodialysis vintage (Chapter 3). This is evident in the example participants in this study. At follow up, the patient in Figure 4.3 had received hemodialysis treatment for 3 years and demonstrated a large fibrotic burden, compared to over 5 years of treatment for the patient in Figure 4.4, who had a lower fibrotic burden. This lack of association is consistent with a previous gadolinium based CMR study, which found no correlation between fibrotic burden and hemodialysis vintage [58]. So while chronic hemodialysis increases mortality risk over time, it is necessary to delineate the etiology by determining whether fibrosis is progressing in the individual patient.

Since cardiac structural [51,56-58] and functional [60,90] alterations are highly prevalent in the ESRD population, increased hypertrophy and reduced LV function have been used as surrogate indicators of cardiac fibrosis. While prognostic in the cardiac and ESRD populations, it is unclear whether these associate specifically with fibrosis. In fact, fibrosis may precede hypertrophy in some patients [34]. In this study we showed pervasive progression of fibrosis in

our patients with ESRD over 1 year (Figure 4.5) without concurrent alterations in hypertrophy (Figure 4.1), strain (Figure 4.2), or ejection fraction (Table 4.2). It is surprising that while fibrosis increased, the typical indicators of heart failure progression—reduced contractility and EF—did not change over this follow up period. Thus we may be able to distinguish small variations in fibrosis before a patient has advanced to LV stiffness severe enough to be detected by other clinical measures.

It is clear that the development of hypertrophy should be considered a separate disease process from fibrosis progression. Moreover, deterioration of LV function may only arise after advanced cardiac disease progression, well after high levels of fibrosis have developed. Thus identification of fibrosis, independent of structural or functional deficits, could improve prognosis for patients with ESRD [51].

Patterns of fibrosis have been previously described in hemodialysis patients [58,59], prior to the ban on gadolinium use. Gadolinium free replication of these results is now possible and could aid in the understanding of both global and focal patterns of disease, while monitoring changes over time. Global fibrotic burden determination may assist in overall cardiac risk stratification [51], however the visualization of potentially arrhythomogenic fibrotic foci could improve selection for alternative therapies such as radiofrequency ablation and implantable cardioverter defibrillators. While nearly 40% of all ESRD deaths are attributable to arrhythmia and sudden cardiac death, less than 1% of the hemodialysis population receives implantable defibrillators or resynchronization

therapies [185]. Noninvasive and safe detection of fibrotic patterns in patients with ESRD may assist in tapping these underutilized and potentially lifesaving treatment options to improve the high rates of sudden cardiac death.

While overwhelming increases in $\Delta S/S_o$ and divergence were evident in this study, a small sample size has limited the ability for us to detect statistically significant elevations in fibrosis. Measurement of fibrosis progression in patients on hemodialysis warrants further investigation with a larger sample and multiple time points. Future analyses should examine the magnitude of change in fibrosis and correlations to advancing hypertrophy, dilation, or ventricular stiffness in patients with ESRD. We were also limited by the need for 2 consecutive breath holds to acquire pairs of images for the 2-pt bSSFP method. Alterations in breath hold position can introduce misalignment of the myocardium. While we manually corrected for these shifts, it is possible that erroneous voxels from the blood pool or pericardium were included in these analyses.

In conclusion, we have shown that patients on hemodialysis for ESRD nearly ubiquitously developed increased fibrotic burden, even in a short 1 year period. Fibrosis development is independent of alterations in hypertrophy or deteriorating contraction or relaxation. The ability to safely monitor patients with ESRD without the use of gadolinium may assist in more comprehensive risk stratification, improved treatment selection, and eventually a reduction in cardiac mortality rates.

Contributions

This study was designed by Tori Stromp and Moriel Vandsburger. Tori Stromp completed all imaging studies, post processing, image analysis, and statistical analysis. Steve Leung consulted on image acquisition and quality control. Rebecca Kidney assisted with participant recruitment and, along with Kristin Andres, aided in structural and functional data analysis.

Acknowledgments

This project was supported by the National Institutes of Health through the National Heart Lung and Blood Institute (R01HL128592).

Table 4.1. Baseline Participant Demographics.

Variable	Result
Age (yrs)	54.2 (31.2-79.7)
Male	3 (50)
White	2 (33)
Black/African American	4 (67)
Hemodialysis vintage (yrs)	4.5 (2.0-7.5)
Systolic Blood Pressure (mmHg)	160 (144-182)
Diastolic Blood Pressure (mmHg)	85 (65-98)
Primary Cause of ESRD	
Hypertension	3 (50)
Diabetes	2 (33)
Unknown/Unsure	1 (17)
Comorbidities	
Hypertension	6 (100)
Diabetes	4 (66)

Numerical variables are presented as mean (range).
Categorical variables are presented as count (%).

Table 4.2. Clinical Cardiac Measurements.

Variable	Baseline	Follow Up	*p*
Heart Rate (bpm)	71.8 (59-91)	67.8 (54-86)	0.303
BMI (kg/m^2)	31.6 (27.3-39.1)	31.6 (27.3-38.1)	0.934
BSA (m^2)	2.1 (1.8-2.2)	2.1 (1.8-2.3)	0.896
QRS Duration (ms)	90 (76-98)	90 (78-100)	0.681
QTc Interval (ms)	487.5 (444-518)	439.2 (427-456)	0.050*
EDV (mL)	140.6 (95.0-214.0)	131.8 (88.1-185.5)	0.114
ESV (mL)	56.2 (24.9-96.4)	47.7 (18.0-76.2)	0.053
EF (mL)	61.2 (48.6-73.8)	65.9 (52.0-79.6)	0.044*
Cardiac Output (L/min)	6.1 (4.4-8.1)	5.7 (4.5-7.3)	0.419
LV Mass (g)	222.4 (160.9-287.6)	208.4 (163.0-260.1)	0.135
LVMI (g/m^2)	110.3 (86.2-130.5)	102.6 (93.2-118.1)	0.157
Septal Thickness (cm)	1.3 (1.1-1.6)	1.2 (1.0-1.5)	0.565
H/R Ratio	0.5 (0.3-0.6)	0.4 (0.3-0.5)	0.138

Data are presented as mean (range). BMI: body mass index, BSA: body surface area, QTc: corrected QT (standardized to 60 beats per min), EDV: end diastolic volume, ESV: end systolic volume, EF: ejection fraction, LV: left ventricle, LVMI: left ventricular mass index (indexed to BSA), H/R ratio: septal thickness/chamber radius. *$p<0.05$ was considered significant using a paired t test.

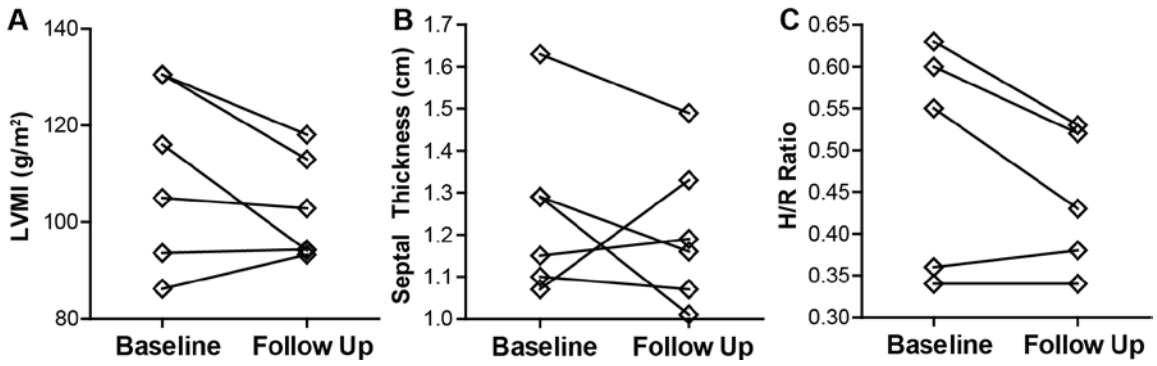

Figure 4.1. Hypertrophy did not progress over time in patients with ESRD. Patients with ESRD had elevated **(A)** LVMI, **(B)** interventricular septal thickness, and **(C)** H/R ratio at baseline but no significant alterations in these measures of hypertrophy at follow up (all $p>0.05$). LVMI: left ventricular mass index.

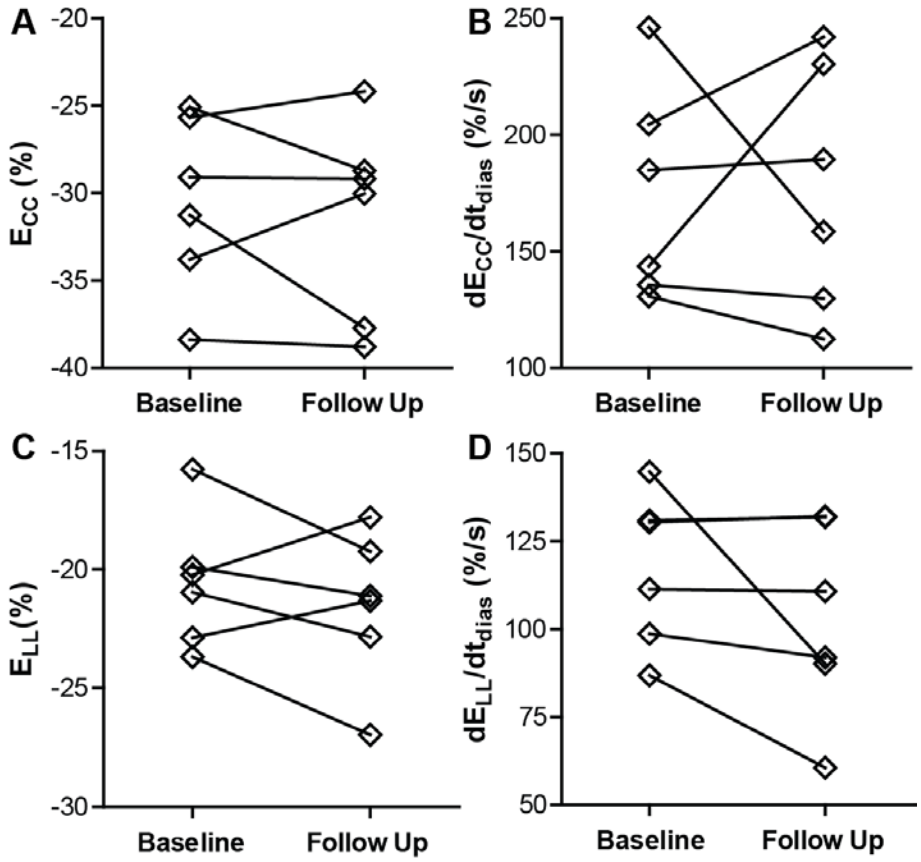

Figure 4.2. Measures of contraction and relaxation. (A) Circumferential peak strain and **(B)** diastolic strain rate show varied, but not significant changes from baseline to follow up in patients with ESRD. **(C)** Peak strain and **(D)** diastolic strain rate in the longitudinal direction showed no significant changes over time. These results indicate that LV function did not deteriorate in the follow up period. All $p>0.05$.

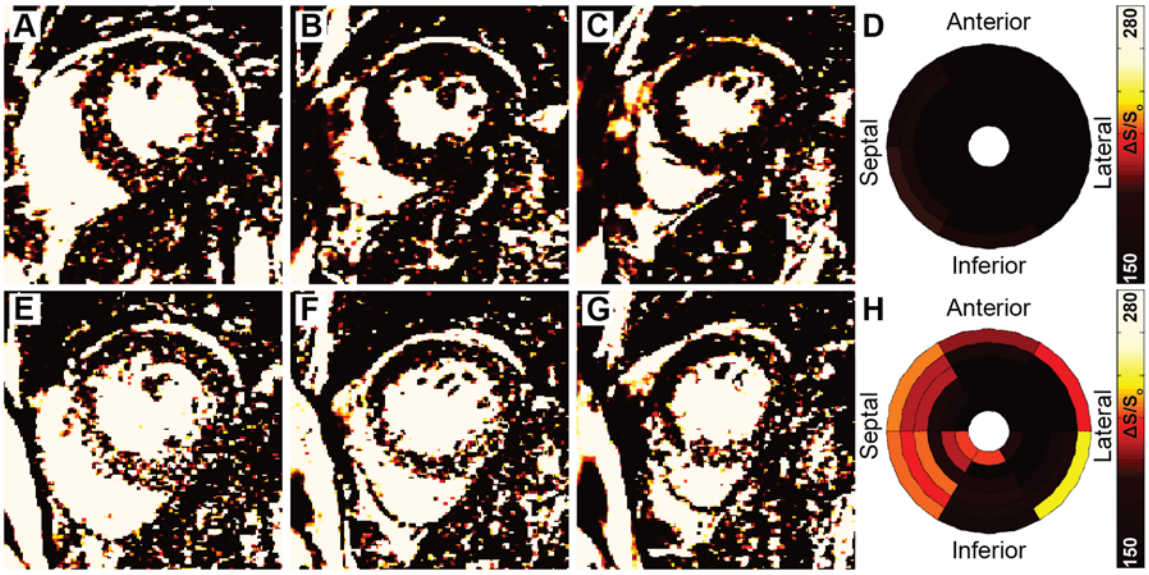

Figure 4.3. Representative patient with large increases in fibrosis. Representative $\Delta S/S_o$ maps at the **(A)** base, **(B)** mid ventricle, and **(C)** apex of a patient on hemodialysis for ESRD. **(D)** The bullseye plot revealed low $\Delta S/S_o$ values across the entire ventricle in this patient at baseline. At the follow up visit, $\Delta S/S_o$ maps demonstrated elevations in the **(E)** base and septal regions of the **(F)** mid ventricle and **(G)** apex of the LV. **(H)** Diffuse elevation was evident across many slices of the LV, indicating that this patient had developed significant amounts of fibrosis over the follow up period. Divergence increased by 22.0 AU in this patient.

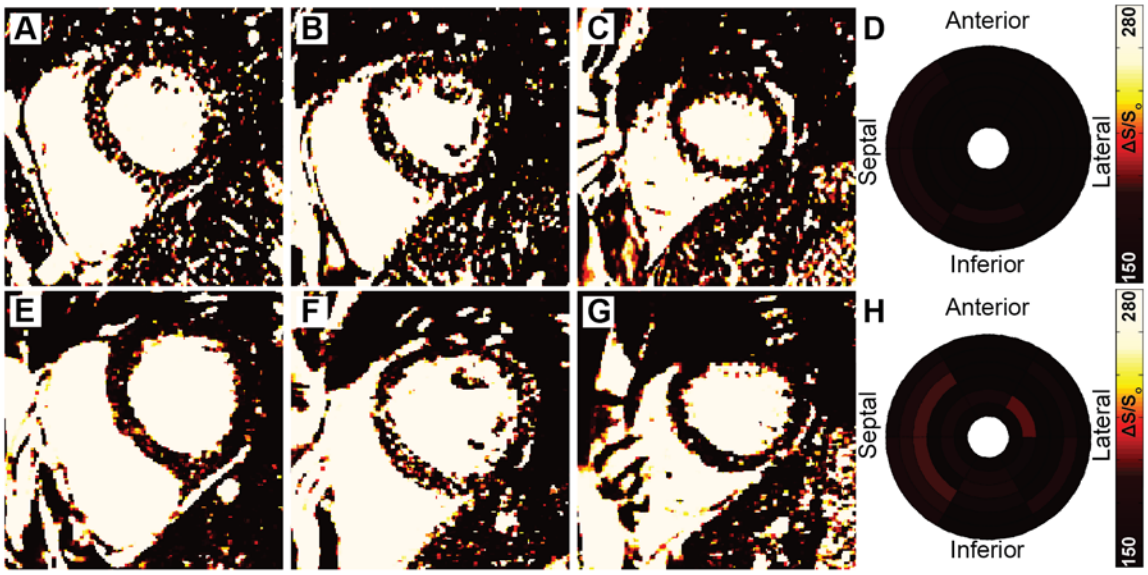

Figure 4.4. Minimal increases in fibrosis over time. At baseline, $\Delta S/S_o$ maps from this representative patient revealed minor scattered enhancement patterns in **(A)** basal, **(B)** mid ventricular, and **(C)** apical slices. **(D)** Average $\Delta S/S_o$ values remained low across the entire ventricle in this patient. At follow up, myocardial $\Delta S/S_o$ remained low in the **(E)** base and **(G)** apex, with some increased values developing in the **(F)** mid ventricle. **(H)** The corresponding bullseye plot demonstrated patterns of minor elevations in this patient. Across the 2 study visits, divergence increased by 3.9 AU, which was the minimal increase in this group.

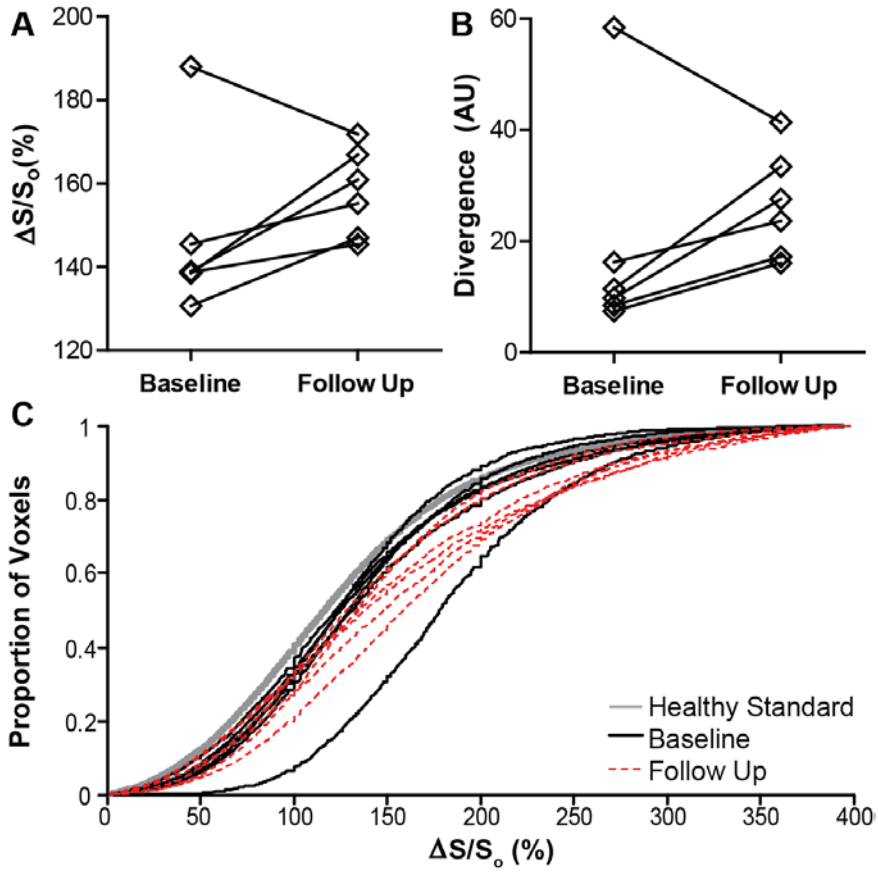

Figure 4.5. Measurements of increased fibrosis in patients with ESRD. (A) Whole ventricle $\Delta S/S_o$ values increased in all but 1 patient from baseline to follow up. **(B)** Divergence values increased in all but 1 patient, indicating a greater rightward shift in the distribution of $\Delta S/S_o$ values and increased fibrotic burden over time. **(C)** Cumulative distribution functions of the healthy simulated standard (gray), baseline (black), and follow up scans (red). All patients were shifted from the healthy standard at baseline, corresponding to an increased fibrotic burden compared to healthy individuals. All but 1 patient demonstrated a greater shift at follow up, corresponding to further progression of fibrosis.

CHAPTER 5: CONCLUSIONS AND PERSPECTIVES

Summary of Key Findings

Contrast-enhanced CMR has become an invaluable tool for myocardial tissue characterization, advancing our ability to detect and monitor various forms of fibrosis [64,69-71,74,88]. Unfortunately, the risk of developing nephrogenic systemic fibrosis has limited the use of gadolinium in individuals with reduced kidney function [84-86]. This exclusion has thwarted the ability to use our most powerful CMR techniques in patients with ESRD, who are at high risk of developing myocardial fibrosis [51,58], arrhythmias, heart failure, and sudden cardiac death [185]. Without a suitable diagnostic technique, the ability to understand underlying mechanisms of heart failure in ESRD is hindered, further limiting the development and testing of appropriate therapeutics. A gadolinium free and quantitative method for fibrosis detection could overcome these obstacles and offer a suitable diagnostic and monitoring option with applications in trials of new therapeutics. The projects in this dissertation have described the development of a quantitative gadolinium-free CMR technique, subsequent measurement of cardiac fibrosis in patients with ESRD, and a preliminary study in longitudinal monitoring of changes in cardiac fibrosis in ESRD patients.

Following previous development in a mouse model of experimentally induced myocardial infarction [111], we translated 2-pt bSSFP CMR to a cohort of 47 cardiac patients referred for standard of care LGE CMR plus 10 healthy age-equivalent controls (Chapter 2). Using high and low MT-weighted cine

bSSFP image pairs, we were able to extract endogenous contrast from the alterations in magnetization transfer (MT) arising from extracellular matrix remodeling. 2-pt bSSFP identified areas of necrosis and edema in acute myocardial infarction (Figure 2.2), replacement fibrosis in chronic myocardial infarction (Figure 2.4), and reactive fibrosis in non-ischemic dilated cardiomyopathy (Figure 2.5). Along with T1 and T2 times, $\Delta S/S_o$ was elevated in regions of enhancement at LGE compared to myocardium without enhancement (Figure 2.7). Using gadolinium partition coefficient (GPC) as a contrast based standard for fibrosis quantification, there was a stronger correlation with $\Delta S/S_o$ (R=0.82) than with other non-contrast techniques (Figure 2.8). There was strong agreement in percent of enhanced myocardium ($R^2 = 0.84$) and transmurality of enhancement ($R^2 = 0.73$) between 2-pt bSSFP and LGE techniques (Figure 2.9). Agreement was also achieved during subjective assessment by blinded reviewers of $\Delta S/S_o$ maps compared to LGE images (Figure 2.8), with a few cases of false positive (Figure 2.10) and false negative (Figure 2.11) identification of enhancement. Representing a known limitation of LGE CMR, small patterns of subendocardial signal enhancement were missed in 4 patients using $\Delta S/S_o$ maps. Time limitations restricted us to the acquisition of only 1 mid ventricular slice in this cohort, which may have also missed areas of enhancement in some patients' hearts.

Extending 2-pt bSSFP to patients on hemodialysis for ESRD, Chapter 3 detailed visual and quantitative fibrosis detection without gadolinium along with correlations to blood biomarkers that are commonly used to assess ischemia,

cardiac remodeling, and extracellular matrix turnover. We imaged the entire LV of 29 patients with ESRD and 33 healthy controls of similar age using 2-pt bSSFP CMR. While we found no differences in ejection fraction nor diastolic strain rate and only small decreases in global longitudinal strain (Table 3.1, Figure 3.3), there was widespread LV hypertrophy in the ESRD group (Figure 3.8). Using cumulative distribution function analysis, we quantified the extent of $\Delta S/S_o$ signal elevation, to represent a metric of fibrotic burden. Patients with ESRD demonstrated increased fibrotic burden (divergence=9.8 AU [6.0, 23.6]) compared to controls (4.7 A.U. [1.2, 11.5], p = 0.003). We identified 3 patterns of fibrosis without gadolinium (Figure 3.6) that were previously described using LGE [59] in patients with ESRD. Hypertrophy demonstrated only a modest correlation with fibrosis, while strain did not correlate with fibrosis at all (Figure 3.9). The existing dogma in the field of heart failure in ESRD patients dictates that hypertrophy and strain are robust surrogate markers of fibrosis because of the increased tensile characteristics of fibrotic tissue. Our findings offer compelling evidence that structural and functional measures are not sensitive to diffuse extracellular matrix remodeling and interstitial fibrosis. We utilized our capacity to identify fibrosis to compare fibrotic burden with blood biomarkers of cardiac stress, ischemia, and extracellular matrix turnover. TnT, FGF23, PTH, and TIMPs were elevated in patients with ESRD (Table 3.3). The interplay between hypertrophy and fibrosis was evident in biomarker analysis, as the commonly employed TnT and FGF23 displayed stronger correlations to hypertrophy than fibrosis in our cohort. TIMPs, however, were moderately correlated with fibrosis

but showed no association with hypertrophy. With the ability to distinguish between hypertrophy and fibrosis, imaging guided biomarkers such as TIMPs may emerge as fibrosis-specific diagnostic measures and therapeutic targets for patients with ESRD.

Extension of our findings for the purpose of longitudinal monitoring is described in Chapter 4 where a preliminary study to detect progression of fibrosis over time was performed in patients on hemodialysis for ESRD. Patients from the study in Chapter 3 were asked to return for a follow up exam using 2-pt bSSFP CMR. Six patients completed the follow-up exam. These patients were overwhelmingly hypertensive and hypertrophic at baseline (Table 4.1). Over the follow up period, they demonstrated increased EF (61.2 ± 8.8% to 65.9 ± 10.4%, p=0.044) but with no corresponding increases in hypertrophy (Table 4.2, Figure 4.1) nor decreases in strain measurements (Figure 4.2). Although no clinically relevant alterations in structure or function were identified, all but 1 patient demonstrated an increase in fibrosis over the 1 year follow up period (Figure 4.5). Fibrotic burden and progression may add prognostic value above and beyond the minimal alterations seen in structure and function to aid in risk stratification and therapeutic selection for patients on hemodialysis.

Non-contrast CMR techniques for measurement of fibrosis will empower the investigation of noninvasive biomarkers, molecular targets, and treatment efficacy in patients with ESRD. Unlike LGE, 2-pt bSSFP can detect both focal and diffuse disease patterns using a single technique while simultaneously providing images for clinically important structural and functional measures. We

are more directly measuring fibrosis in cardiac and kidney patients than the options currently available to patients with ESRD. We have also challenged the current dogma and provided evidence that structural and functional alterations may not be sensitive to the development of interstitial fibrosis which is a critical substrate for arrhythmias and sudden cardiac death.

Clinical Perspective

Myocardial tissue biopsy has served as the standard for fibrosis detection via calculation of the collagen volume fraction, primarily in epicardial tissue samples. Without the use of contrast enhanced CMR, biopsy is the only reliable alternative for fibrosis measurement in patients with ESRD. Unfortunately, biopsy is prone to underreporting true fibrotic burden [65], obligates clinicians to extrapolate the fibrotic content of non-sampled regions, and is invasive and undesirable for repeated measurements. With 2-pt bSSFP CMR, we have the ability to observe spatiotemporal changes in the magnitude and pattern of fibrosis across the entire LV in a way that is not possible with biopsy nor safe with gadolinium enhanced CMR.

Fibrosis development is a dynamic process that requires complex molecular cues with unique patterns of activation in order to reorganize existing extracellular matrix and increase collagen production by fibroblasts [26]. Specific molecular players in these processes could serve as biomarkers of fibrosis development and potential treatment targets for attenuation or prevention of fibrosis. Since hypertrophic and fibrotic remodeling often occur in tandem for

patients with ESRD, the etiology of cardiac disease development is complex. Using 2-pt bSSFP we are now able to begin untangling the fibrotic disease process from structural alterations and investigate the specific underlying mechanisms and appropriate biomarkers of fibrotic remodeling. For instance, TnT is widely used to indicate recent myocardial infarction and cardiomyocyte death, but is often detected in patients with ESRD [189], indicating myocardial damage from non-ischemic causes. Some have suggested a correlation between elevated TnT and fibrosis in non-ischemic cardiomyopathy [190] and prognostic value in ESRD [189,191]. Our results indicate that while TnT correlates with fibrosis it also correlates with hypertrophy. While it may be prognostic, TnT is unsuitable as a fibrosis-specific biomarker and may instead reflect a combination of structural hypertrophy and fibrosis development. Similarly, FGF23 has been explored as molecular mechanism [53,141,192,193], biomarker [159,194], and therapeutic target [141,169] of remodeling in patients with ESRD. It has been extensively correlated with hypertrophy, as we have also shown, yet is also associated with fibrosis detected by 2-pt bSSFP, rendering FGF 23 unable to distinguish fibrosis from the associated—but independent—hypertrophic remodeling process.

The extracellular matrix remodeling process offers alternate molecular targets that may be more specific to fibrosis development. 2-pt bSSFP allows us to probe the relationship between MMPs, TIMPs, fibrosis, and heart failure in ESRD in a safe, noninvasive way. In fact, we have found that TIMPs correlated with fibrosis but not hypertrophy, which offers promising evidence that these

peptides may be more specific to fibrosis. Investigations are emerging for the use of MMP inhibition to attenuate cardiac fibrosis development in animal models of ESRD [180,195]. 2-pt bSSFP could serve as a method to both interrogate biomarkers of extracellular matrix turnover and eventually determine the efficacy of emerging treatments, such as exogenous MMP inhibitors, that are currently under consideration.

Limitations and Future Opportunities

A few pertinent limitations are present across these studies, which represent important opportunities for future investigations. As with most CMR acquisitions, 2-pt bSSFP requires patients to sustain multiple end-expiratory breath holds. In addition, to achieve maximal resolution we attempt to minimize voxel size, which can require lengthy breath hold time. Due to need for 2 separate images to complete the 2-pt bSSFP method, the total number of breath holds and length of time can be limiting for some patients. To begin addressing breath hold limitations, our lab has investigated the use of 3 dimensional (3D) cine bSSFP. 3D bSSFP allows for the acquisition of a slab of multiple short axis slices, spanning a larger portion of the left ventricle during a single breath hold. This technique has the potential to reduce the total number of breath holds while maintaining myocardial steady state signal and collecting data across the whole LV (Figure 5.1). Future investigations could adapt 3D bSSFP to acquire slabs at flip angles of 5° and 45° for use in 2-pt bSSFP fibrosis imaging with the benefit of reduced number and total time of breath holds.

Between the 2 image acquisitions for 2-pt bSSFP, there is a possibility for patient motion or inconsistent breath holds leading to misalignment of the myocardium in the image pair. If the myocardium is not aligned, voxels outside of the myocardium could be included in the analysis of MT and erroneously alter the measured fibrotic burden. As described in chapters 3 and 4, we manually registered any image pairs that were not aligned. While this allowed us to salvage many slices for image analysis, it is possible we introduced other noise into our analysis. Ideally, a non-contrast imaging technique would achieve magnetization transfer weighting in a single image, requiring only 1 breath hold per slice position. Stemming from the need to create better contrast between endocardial scar and blood pool in LGE images (discussed in Chapter 2), new techniques are emerging for dark-blood imaging during LGE, using **F**low-**I**ndependent **D**ark-blood **D**e**L**ayed **E**nhancement (FIDDLE) [196] and **T**1(**R**ho) **A**nd **M**agnetization transfer and **IN**v**E**rsion **R**ecovery (TRAMINER) sequences [197,198]. In their current uses, these sequences null the blood pool to turn it black, which allows for enhancement at LGE—especially near the blood pool—to become more easily visualized after injection of gadolinium. As evident within the name TRAMINER, these imaging sequences incorporate an MT preparation scheme that encodes MT within the image. When modified and used without gadolinium, TRAMINER can extract endogenous contrast via MT weighting within a single image and therefore single breath hold (Figure 5.2). Studies within our lab are comparing TRAMINER to LGE in cardiac patients, including patients with myocardial infarction (Figure 5.2), who are referred for gadolinium based

CMR. If successful, these preliminary TRAMINER studies could be extended to non-contrast fibrosis imaging in ESRD patients while lowering the breath hold burden and eliminating image registration issues that currently exist in our current techniques. This technique has the added benefit of reducing manual image correction and post processing time, which are important when evaluating clinical patients in near real time and for future ambitions to automate image analysis.

Sub-endocardial scar identification has been a challenge in LGE CMR due to the low contrast to noise present when a scar is near the bright signal from blood. This has been the motivation for development of FIDDLE [196] and TRAMINER [198] described above. Similar limitations exist in 2-pt bSSFP CMR and were discussed in Chapter 2 and presented in Figure 2.11. Another example arose in the study from Chapter 3 and is presented in Figure 5.3. This patient had a history of known myocardial infarction with comorbid hypertension, type 2 diabetes mellitus, and ESRD which requires hemodialysis. Thus, this patient could not complete gadolinium based CMR to monitor stability of the established replacement fibrosis nor the presence or progression of additional reactive fibrosis. Wall thinning is ready apparent in this patient, but it is difficult to define a fibrotic scar, due to its location near the blood pool. Future development of magnetization transfer imaging will need to address this issue. One possible option is to mask the myocardium (as shown in Figure 5.2 B and D) to only present voxels of interest within the LV. This is limited by the contrast achieved in anatomical images (e.g. Figure 5.3 A) and accuracy of manual region of interest

definition, and removes other anatomical features for reference. While the CMR field is moving to improve the contrast between myocardium and blood pool in LGE, MT CMR must go in parallel to limit the uncertainty in sub-endocardial scar identification. Importantly, similar to extracellular volume (ECV) calculation, MT CMR has the advantageous ability to image multiple types of fibrosis within 1 imaging technique, as seen in Figure 5.3 B, but without the need for gadolinium. This is crucial for monitoring patients with prior myocardial infarction who may develop diffuse reactive fibrosis in remote regions [31,32] and for patients with multiple risk factors, like those with ESRD, who are at high risk for both ischemic and non-ischemic fibrosis development [58,59] but who cannot receive gadolinium.

Additional Future Directions

As 2-pt bSSFP continues to develop, it will be important to assess the practical clinical utility of this technique and its ability to recapitulate findings from gadolinium based CMR techniques. In our initial clinical study (Chapter 2) $\Delta S/S_o$ was highly correlated with gadolinium partition coefficient (R=0.82) and blinded reviewers with only minimal training were correctly able to identify elevations in $\Delta S/S_o$ with about 73% agreement to LGE. This was in a sample of patients with known cardiac disease, demonstrating a variety of fibrosis patterns. It will be important to determine whether 2-pt bSSFP can be used diagnostically to identify previously unknown cardiac disease in patients at risk for developing fibrosis. In the ESRD population, there is a high prevalence of diffuse interstitial fibrosis [51].

This pattern is difficult to identify with LGE [63], but can be identified with T1 mapping techniques through ECV calculation [74-76] for patients in which it is safe to deliver gadolinium. We are currently investigating the ability for 2-pt bSSFP to identify diffuse fibrosis comparable to ECV in patients with type 2 diabetes with no history of myocardial infarction nor reduced kidney function. These patients often develop expanded ECM [199] and diffuse myocardial fibrosis but are still able to receive gadolinium contrast. Importantly, type 2 diabetes is a leading risk factor of ESRD [185] so these patients have similar medical conditions and comorbidities to many patients with ESRD and may in fact experience renal complications in the future. While this group is more homogenous than patients included in Chapter 2, they likely have a less established cardiac history with less predictable fibrotic burden. We have scanned 30 patients with type 2 diabetes mellitus and 10 age equivalent healthy volunteers using 2-pt bSSFP and pre and post-contrast T1 mapping (Figure 5.4). There are no differences in standard clinical measures of structure and function between groups but preliminary analysis shows promise for elevated $\Delta S/S_o$, native T1, and ECV in the diabetes group. With blinded review, we will now be able to compare 2-pt bSSFP, native T1 mapping, and ECV quantification across the entire LV for the *de* novo identification of diffuse fibrosis. It is important that 2-pt bSSFP perform well against current standard contrast techniques both quantitatively and subjectively if it is to progress toward clinical utility, especially for the identification of diffuse fibrosis, which is difficult to detect with other CMR techniques.

We are also interested in utilizing 2-pt bSSFP to begin understanding the exceedingly high death rates experienced at the initiation of hemodialysis in patients with ESRD. There is a severe peak in all cause and cardiac mortality at month 2 of hemodialysis [185], with a currently unknown cause. Due to the drastic, hyperphysiologic alterations in hemodynamics [90] we speculate that early cardiac remodeling and acute fibrosis development might be a risk factor in this early timeframe. Future studies could utilize 2-pt bSSFP in a large cohort of ESRD patients who plan to initiate hemodialysis. Imaging before and at multiple time points within the first year of treatment initiation would offer evidence of early cardiac fibrosis development—with or without concomitant structure or function alterations—that could be compared to clinical measures of structure and function. Cardiac outcomes such as development of arrhythmia, heart failure, and sudden cardiac death within the first year could be correlated to fibrosis development to begin to understand the potentially modifiable risk factors in this critical period for patients beginning hemodialysis.

Blood biomarkers are a promising but complex opportunity for diagnostic and therapeutic targets in the ESRD population. With limited sample sizes in our current study (Chapter 3), analyses of blood biomarkers and their correlations with fibrosis and hypertrophy are modest but promising. Markers of extracellular matrix remodeling such as MMPs and TIMPs may prove to be more specific to cardiac fibrosis than the currently employed TnT, FGF23, and PTH which are confounded by hypertrophy. Larger cohorts of ESRD patients are necessary for more complex multiple correlation analysis to parcel out the interaction between

hypertrophy, fibrosis, and individual biomarkers. While MMPs and TIMPs are imbalanced in patients with ESRD compared to healthy individuals and CKD patients prior to hemodialysis [148], studies have reported both increases [146,181,182,200] and decreases [148] in these peptides compared to healthy controls. This may be a manifestation of the heterogeneous pathophysiology of cardiac fibrosis in this population. Additional studies are warranted to begin understanding whether MMP or TIMP concentrations are indicative of either replacement or reactive fibrosis separately. There is evidence that MMPs and TIMPs are associated with worsening, but not end stage, heart failure [144]. Serial measurements of these peptides in ESRD patients along with longitudinal monitoring of cardiac structure, function, and fibrosis by CMR would provide evidence for the utility of these biomarkers as predictors of heart failure risk and potential molecular treatment targets for the attenuation of cardiac fibrosis.

Final Remarks

The development of 2-pt bSSFP as a non-contrast CMR technique has the potential to improve the understanding of heart failure in the context of ESRD. This safe and noninvasive technique could empower future investigations for advanced diagnostics and molecular treatment targets for cardiac fibrosis. We have successfully begun to recapitulate findings from gadolinium based CMR for quantitative and subjective identification of cardiac fibrosis in patients on hemodialysis for ESRD. The current challenges in patient burden and post

processing methods represent vital opportunities for improvements in non-contrast MT techniques that may lead to more clinically applicable CMR tools.

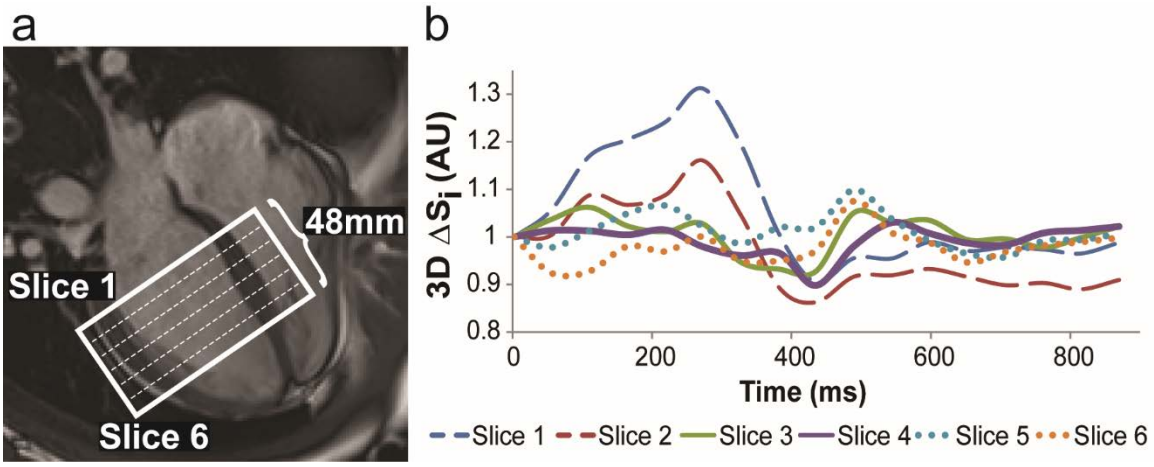

Figure 5.1. 3D bSSFP image acquisition and signal evolution. (A) Long axis, 4-chamber end diastolic image of the heart with a superimposed schematic of the slab (solid box) and slice (dashed line) architecture for one representative slab. **(B)** Normalized signal intensity waveforms for all six slices in one 3D slab are shown throughout the entire cardiac cycle. Solid lines represent the middle two slices (slice 3 and 4) which maintained the best steady state throughout the entire cardiac cycle.

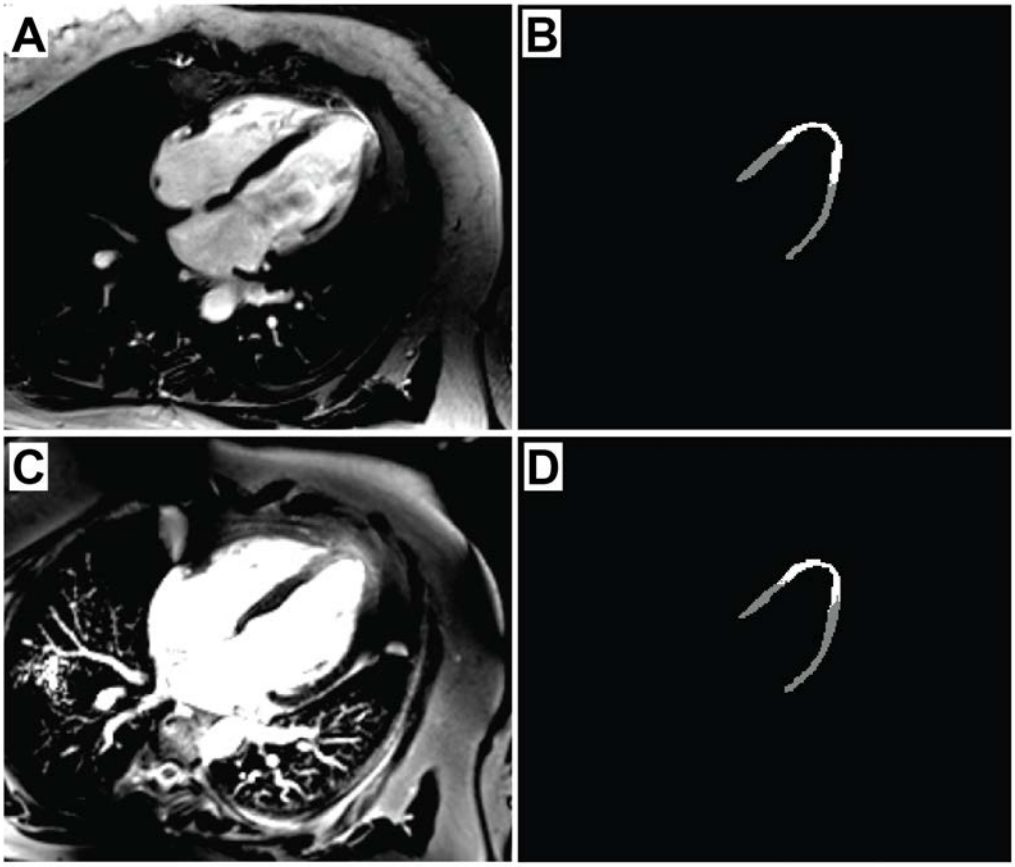

Figure 5.2. Fibrosis imaging using a single breath hold magnetization transfer weighted sequence. (A) A long axis (4-chamber) image acquired with the clinical standard LGE-CMR in a patient who suffered a myocardial infarction. Significant enhancement was evident in the apex of the LV. **(B)** Using a threshold technique (similar to Chapter 2), myocardial voxels 2 standard deviations above the average, remote (non-enhanced) myocardial signal were presented in white, overlayed on all myocardial voxels in gray. **(C)** A similar long aixs view was acquired in this patient using a non-contrast, magnetization-transfer weighted sequence (TRAMINER) in a single breathhold, which revealed significant elevations in the LV apex. **(D)** Similar to B, voxels with signal values 2 standard deviations above the mean were displayed as white with other myocardial voxels in gray. The image aqcuired without contrast using the TRAMINER technique showed extremely good spatial agreement with LGE, identifying areas of edematous and necrotic tissue folowing myocardial infarction. TRAMINER may emerge as a robust, non-contrast option for tissue characterization without gadolinium.

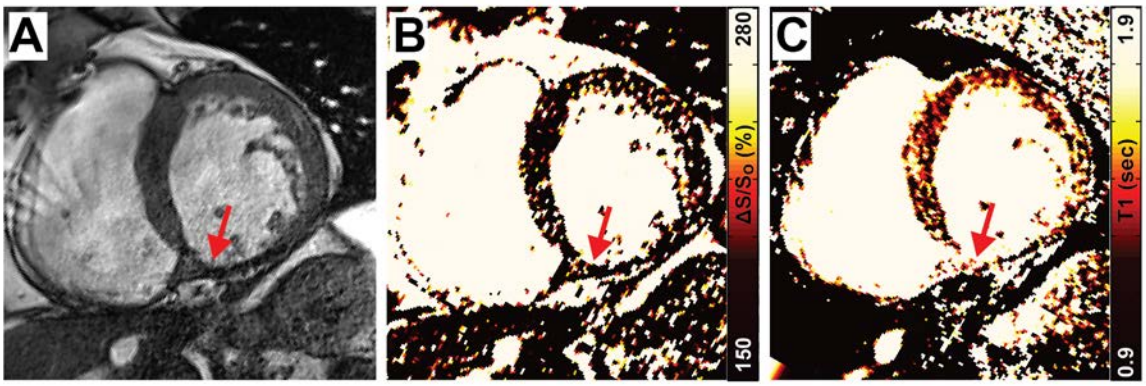

Figure 5.3. Mixed subendocardial scar and diffuse fibrosis in chronic myocardial infarction. (A) Example bSSFP image from a patient who suffered a previous myocardial infarction, which was apparent in a large area of severe myocardial thining (arrow). This patient was also hypertensive, diabetic, and was on hemodialysis for ESRD and therefore would be excluded from LGE CMR. **(B)** It was diffucult to detect a subendocardial pattern of focal scar in the corresponding $\Delta S/S_o$ map. Contrast between the blood pool and adjacent elevations in myocardial signal are a limitation of 2-pt bSSFP, as well as other CMR techniques. The $\Delta S/S_o$ map revealed areas of diffuse enhancement in this patient that would not be detectable by LGE, however. **(C)** The T1 map reveals widespread enhancement, however the myocardium, especially in areas of thinning, is difficult to resolve. While many CMR techniques share similar limitations, 2-pt bSSFP may be able to detect both focal and diffuse fibrosis in the same scanning procedure without the risks associated with gadolinium contrast agents.

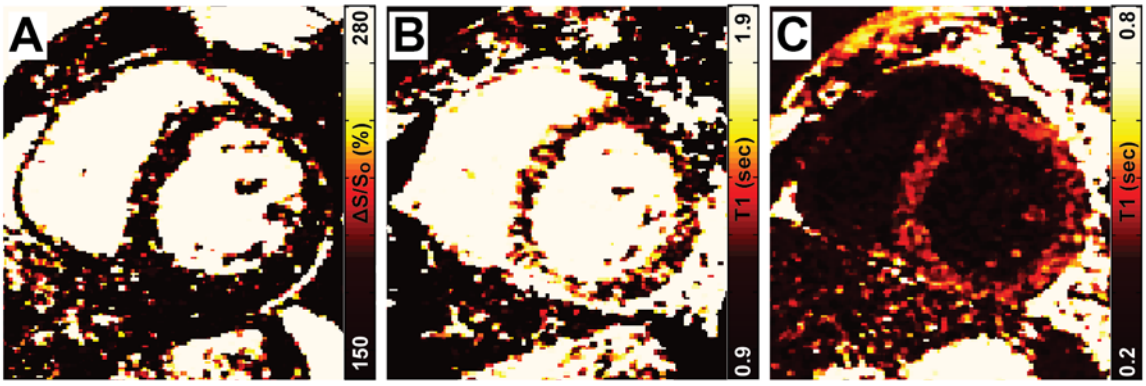

Figure 5.4. Image acquisitions in a patient with diabetes. (A) $\Delta S/S_o$ map generated at a mid ventricular slice using 2-pt bSSFP in a patients with type 2 diabetes. This patient demonstrated diffuse enhancement in this and other slices across the LV. **(B)** Elevations in T1 are apparent in the native T1 map acquired at the same slice position. **(C)** Fifteen minutes post-injection of gadolinium, a post-contrast T1 map was aquired. Maps of pre and post-contrast T1 (B and C) are compared to calculate GPC and ECV, the predominant method under investigation for diffuse fibrosis identification.

APPENDIX: LIST OF ABBREVIATIONS

2-pt bSSFP	two point balanced steady state free precession
BMI	body mass index
bSSFP	balanced steady state free precession
CKD	chronic kidney disease
CMR	cardiac magnetic resonance imaging
CVD	cardiovascular disease
ECG	electrocardiogram
Echo	echocardiography
ECV	extracellular volume (fraction)
EDV	end diastolic volume
EF	ejection fraction
ESRD	end stage renal disease
ESV	end systolic volume
FGF	fibroblast growth factor
FIDDLE	Flow-Independent Dark-blood DeLayed Enhancement
GPC	gadolinium partition coefficient
LGE	late gadolinium enhancement
LVMI	left ventricular mass index
MMP	matrix metalloproteinase
MOLLI	modified Look Locker imaging
MRI	magnetic resonance imaging

MT	magnetization transfer
PTH	parathyroid hormone
RF	radio frequency
ROI	region of interest
SD	standard deviation
TE	echo time
TIMP	tissue inhibitor of metalloproteinase
TnT	troponin T
TR	repetition time
TRAMINER	T1(Rho) And Magnetization transfer and Inversion Recovery

REFERENCES

1 Kochanek KD MS, Xu JQ,Tejada-Vera B: Deaths: Final data for 2014. National vital statistics reports 2016;65

2 Mozaffarian D, Benjamin EJ, Go AS, Arnett DK, Blaha MJ, Cushman M, Das SR, de Ferranti S, Despres JP, Fullerton HJ, Howard VJ, Huffman MD, Isasi CR, Jimenez MC, Judd SE, Kissela BM, Lichtman JH, Lisabeth LD, Liu S, Mackey RH, Magid DJ, McGuire DK, Mohler ER, 3rd, Moy CS, Muntner P, Mussolino ME, Nasir K, Neumar RW, Nichol G, Palaniappan L, Pandey DK, Reeves MJ, Rodriguez CJ, Rosamond W, Sorlie PD, Stein J, Towfighi A, Turan TN, Virani SS, Woo D, Yeh RW, Turner MB: Heart disease and stroke statistics-2016 update: A report from the american heart association. Circulation 2016;133:e38-360.

3 Heidenreich PA, Albert NM, Allen LA, Bluemke DA, Butler J, Fonarow GC, Ikonomidis JS, Khavjou O, Konstam MA, Maddox TM, Nichol G, Pham M, Pina IL, Trogdon JG: Forecasting the impact of heart failure in the united states: A policy statement from the american heart association. Circulation Heart failure 2013;6:606-619.

4 Yancy CW, Jessup M, Bozkurt B, Butler J, Casey Jr DE, Drazner MH, Fonarow GC, Geraci SA, Horwich T, Januzzi JL, Johnson MR, Kasper EK, Levy WC, Masoudi FA, McBride PE, McMurray JJV, Mitchell JE, Peterson PN, Riegel B, Sam F, Stevenson LW, Tang WHW, Tsai EJ, Wilkoff BL: 2013 accf/aha guideline for the management of heart failure: A report of the american college of cardiology foundation/american heart association task force on practice guidelines. Journal of the American College of Cardiology 2013;62:e147-e239.

5 McMurray JJ, Adamopoulos S, Anker SD, Auricchio A, Bohm M, Dickstein K, Falk V, Filippatos G, Fonseca C, Gomez-Sanchez MA, Jaarsma T, Kober L, Lip GY, Maggioni AP, Parkhomenko A, Pieske BM, Popescu BA, Ronnevik PK, Rutten FH, Schwitter J, Seferovic P, Stepinska J, Trindade PT, Voors AA, Zannad F, Zeiher A, Bax JJ, Baumgartner H, Ceconi C, Dean V, Deaton C, Fagard R, Funck-Brentano C, Hasdai D, Hoes A, Kirchhof P, Knuuti J, Kolh P, McDonagh T, Moulin C, Popescu BA, Reiner Z, Sechtem U, Sirnes PA, Tendera M, Torbicki A, Vahanian A, Windecker S, McDonagh T, Sechtem U, Bonet LA, Avraamides P, Ben Lamin HA, Brignole M, Coca A, Cowburn P, Dargie H, Elliott P, Flachskampf FA, Guida GF, Hardman S, Iung B, Merkely B, Mueller C, Nanas JN, Nielsen OW, Orn S, Parissis JT, Ponikowski P: Esc guidelines for the diagnosis and treatment of acute and chronic heart failure 2012: The task force for the diagnosis and treatment of acute and chronic heart failure 2012 of the european society of cardiology. Developed in collaboration with the heart failure association (hfa) of the esc. European journal of heart failure 2012;14:803-869.

6 Heart Failure Society of America: Executive summary: Hfsa 2010 comprehensive heart failure practice guideline. Journal of cardiac failure 2010;16:475-539.

7 Cohn JN, Ferrari R, Sharpe N: Cardiac remodeling—concepts and clinical implications: A consensus paper from an international forum on cardiac remodeling. Journal of the American College of Cardiology 2000;35:569-582.

8 Eaton LW, Bulkley BH: Expansion of acute myocardial infarction: Its relationship to infarct morphology in a canine model. Circulation research 1981;49:80-88.
9 McKay RG, Pfeffer MA, Pasternak RC, Markis JE, Come PC, Nakao S, Alderman JD, Ferguson JJ, Safian RD, Grossman W: Left ventricular remodeling after myocardial infarction: A corollary to infarct expansion. Circulation 1986;74:693-702.
10 Weisman HF, Bush DE, Mannisi JA, Weisfeldt ML, Healy B: Cellular mechanisms of myocardial infarct expansion. Circulation 1988;78:186-201.
11 Cerqueira MD, Weissman NJ, Dilsizian V, Jacobs AK, Kaul S, Laskey WK, Pennell DJ, Rumberger JA, Ryan T, Verani MS: Standardized myocardial segmentation and nomenclature for tomographic imaging of the heart. A statement for healthcare professionals from the cardiac imaging committee of the council on clinical cardiology of the american heart association. Circulation 2002;105:539-542.
12 Rumberger JA, Behrenbeck T, Breen JR, Reed JE, Gersh BJ: Nonparallel changes in global left ventricular chamber volume and muscle mass during the first year after transmural myocardial infarction in humans. Journal of the American College of Cardiology 1993;21:673-682.
13 Weisman HF, Bush DE, Mannisi JA, Bulkley BH: Global cardiac remodeling after acute myocardial infarction: A study in the rat model. Journal of the American College of Cardiology 1985;5:1355-1362.
14 Gaudron P, Eilles C, Kugler I, Ertl G: Progressive left ventricular dysfunction and remodeling after myocardial infarction. Potential mechanisms and early predictors. Circulation 1993;87:755-763.
15 Nadruz W: Myocardial remodeling in hypertension. Journal of human hypertension 2015;29:1-6.
16 Ganau A, Devereux RB, Roman MJ, de Simone G, Pickering TG, Saba PS, Vargiu P, Simongini I, Laragh JH: Patterns of left ventricular hypertrophy and geometric remodeling in essential hypertension. Journal of the American College of Cardiology 1992;19:1550-1558.
17 Kannel WB, Cobb J: Left ventricular hypertrophy and mortality--results from the framingham study. Cardiology 1992;81:291-298.
18 Levy D, Garrison RJ, Savage DD, Kannel WB, Castelli WP: Prognostic implications of echocardiographically determined left ventricular mass in the framingham heart study. New England Journal of Medicine 1990;322:1561-1566.
19 Lorell BH, Carabello BA: Left ventricular hypertrophy. Pathogenesis, Detection, and Prognosis 2000;102:470-479.
20 Piano MR, Phillips SA: Alcoholic cardiomyopathy: Pathophysiologic insights. Cardiovascular toxicology 2014;14:291-308.
21 Gersh BJ, Maron BJ, Bonow RO, Dearani JA, Fifer MA, Link MS, Naidu SS, Nishimura RA, Ommen SR, Rakowski H, Seidman CE, Towbin JA, Udelson JE, Yancy CW: 2011 accf/aha guideline for the diagnosis and treatment of hypertrophic cardiomyopathy: Executive summary: A report of the american college of cardiology foundation/american heart association task force on practice guidelines. The Journal of thoracic and cardiovascular surgery 2011;142:1303-1338.

22 Horn MA, Trafford AW: Aging and the cardiac collagen matrix: Novel mediators of fibrotic remodelling. Journal of Molecular and Cellular Cardiology 2016;93:175-185.
23 Kim HE, Dalal SS, Young E, Legato MJ, Weisfeldt ML, D'Armiento J: Disruption of the myocardial extracellular matrix leads to cardiac dysfunction. The Journal of clinical investigation 2000;106:857-866.
24 Marijianowski MM, Teeling P, Becker AE: Remodeling after myocardial infarction in humans is not associated with interstitial fibrosis of noninfarcted myocardium. Journal of the American College of Cardiology 1997;30:76-82.
25 Pfeffer MA, Braunwald E: Ventricular remodeling after myocardial infarction. Experimental observations and clinical implications. Circulation 1990;81:1161-1172.
26 Mewton N, Liu CY, Croisille P, Bluemke D, Lima JA: Assessment of myocardial fibrosis with cardiovascular magnetic resonance. Journal of the American College of Cardiology 2011;57:891-903.
27 Law B, Fowlkes V, Goldsmith JG, Carver W, Goldsmith EC: Diabetes-induced alterations in the extracellular matrix and their impact on myocardial function. Microscopy and Microanalysis 2012;18:22-34.
28 Weber KT, Janicki JS, Shroff SG, Pick R, Chen RM, Bashey RI: Collagen remodeling of the pressure-overloaded, hypertrophied nonhuman primate myocardium. Circulation research 1988;62:757-765.
29 Ellims AH, Iles LM, Ling LH, Hare JL, Kaye DM, Taylor AJ: Diffuse myocardial fibrosis in hypertrophic cardiomyopathy can be identified by cardiovascular magnetic resonance, and is associated with left ventricular diastolic dysfunction. Journal of cardiovascular magnetic resonance : official journal of the Society for Cardiovascular Magnetic Resonance 2012;14:76.
30 Brooks A, Schinde V, Bateman AC, Gallagher PJ: Interstitial fibrosis in the dilated non-ischaemic myocardium. Heart (British Cardiac Society) 2003;89:1255-1256.
31 Bishop JE, Greenbaum R, Gibson DG, Yacoub M, Laurent GJ: Enhanced deposition of predominantly type i collagen in myocardial disease. J Mol Cell Cardiol 1990;22:1157-1165.
32 Volders PG, Willems IE, Cleutjens JP, Arends JW, Havenith MG, Daemen MJ: Interstitial collagen is increased in the non-infarcted human myocardium after myocardial infarction. J Mol Cell Cardiol 1993;25:1317-1323.
33 Tanaka M, Fujiwara H, Onodera T, Wu DJ, Hamashima Y, Kawai C: Quantitative analysis of myocardial fibrosis in normals, hypertensive hearts, and hypertrophic cardiomyopathy. British heart journal 1986;55:575-581.
34 Ho CY, Lopez B, Coelho-Filho OR, Lakdawala NK, Cirino AL, Jarolim P, Kwong R, Gonzalez A, Colan SD, Seidman JG, Diez J, Seidman CE: Myocardial fibrosis as an early manifestation of hypertrophic cardiomyopathy. The New England journal of medicine 2010;363:552-563.
35 Cheng XW, Okumura K, Kuzuya M, Jin Z, Nagata K, Obata K, Inoue A, Hirashiki A, Takeshita K, Unno K, Harada K, Shi G-P, Yokota M, Murohara T: Mechanism of diastolic stiffening of the failing myocardium and its prevention by angiotensin receptor and calcium channel blockers. Journal of cardiovascular pharmacology 2009;54:47-56.

36 Martos R, Baugh J, Ledwidge M, O'Loughlin C, Conlon C, Patle A, Donnelly SC, McDonald K: Diastolic heart failure: Evidence of increased myocardial collagen turnover linked to diastolic dysfunction. Circulation 2007;115:888-895.
37 Conrad CH, Brooks WW, Hayes JA, Sen S, Robinson KG, Bing OH: Myocardial fibrosis and stiffness with hypertrophy and heart failure in the spontaneously hypertensive rat. Circulation 1995;91:161-170.
38 Nguyen TP, Qu Z, Weiss JN: Cardiac fibrosis and arrhythmogenesis: The road to repair is paved with perils. J Mol Cell Cardiol 2014;70:83-91.
39 Gulati A, Jabbour A, Ismail TF, et al.: Association of fibrosis with mortality and sudden cardiac death in patients with nonischemic dilated cardiomyopathy. Jama 2013;309:896-908.
40 US Renal Data System: Usrds 2014 annual data report: An overview of the epidemiology of kidney disease in the united states. Bethesda, MD, National Instituties of Health, National Institute of Diabetes and Digestive and Kidney Failure, 2014, 1,
41 System URD: Annual data report: Atlas of chronic kidney disease and end-stage renal disease in the united states. Bethesda, md:. National Institute of Health, National Isntitute of Diabetes and Digestive and Kidney Diseases 2013
42 Saran R, Li Y, Robinson B, Ayanian J, Balkrishnan R, Bragg-Gresham J, Chen JT, Cope E, Gipson D, He K, Herman W, Heung M, Hirth RA, Jacobsen SS, Kalantar-Zadeh K, Kovesdy CP, Leichtman AB, Lu Y, Molnar MZ, Morgenstern H, Nallamothu B, O'Hare AM, Pisoni R, Plattner B, Port FK, Rao P, Rhee CM, Schaubel DE, Selewski DT, Shahinian V, Sim JJ, Song P, Streja E, Kurella Tamura M, Tentori F, Eggers PW, Agodoa LY, Abbott KC: Us renal data system 2014 annual data report: Epidemiology of kidney disease in the united states. American journal of kidney diseases : the official journal of the National Kidney Foundation 2015;66:Svii, S1-305.
43 Collins AJ, Foley RN, Herzog C, Chavers B, Gilbertson D, Herzog C, Ishani A, Johansen K, Kasiske B, Kutner N, Liu J, St Peter W, Ding S, Guo H, Kats A, Lamb K, Li S, Li S, Roberts T, Skeans M, Snyder J, Solid C, Thompson B, Weinhandl E, Xiong H, Yusuf A, Zaun D, Arko C, Chen SC, Daniels F, Ebben J, Frazier E, Hanzlik C, Johnson R, Sheets D, Wang X, Forrest B, Constantini E, Everson S, Eggers P, Agodoa L: Us renal data system 2012 annual data report. American journal of kidney diseases : the official journal of the National Kidney Foundation 2013;61:A7, e1-476.
44 Collins AJ, Foley RN, Chavers B, Gilbertson D, Herzog C, Ishani A, Johansen K, Kasiske BL, Kutner N, Liu J, St Peter W, Guo H, Hu Y, Kats A, Li S, Li S, Maloney J, Roberts T, Skeans M, Snyder J, Solid C, Thompson B, Weinhandl E, Xiong H, Yusuf A, Zaun D, Arko C, Chen SC, Daniels F, Ebben J, Frazier E, Johnson R, Sheets D, Wang X, Forrest B, Berrini D, Constantini E, Everson S, Eggers P, Agodoa L: Us renal data system 2013 annual data report. American journal of kidney diseases : the official journal of the National Kidney Foundation 2014;63:A7.
45 McCullough PA, Kellum JA, Haase M, Muller C, Damman K, Murray PT, Cruz D, House AA, Schmidt-Ott KM, Vescovo G, Bagshaw SM, Hoste EA, Briguori C, Braam B, Chawla LS, Costanzo MR, Tumlin JA, Herzog CA, Mehta RL, Rabb H,

Shaw AD, Singbartl K, Ronco C: Pathophysiology of the cardiorenal syndromes: Executive summary from the eleventh consensus conference of the acute dialysis quality initiative (adqi). Contributions to nephrology 2013;182:82-98.
46 Larsen T NK, McCullough PA: Type 4 cardiorenal syndrome: Myocardial dysfunction, fibrosis, and heart failure in patients with chronic kidney disease. J Clinic Experiment Cardiol 2012;3
47 Foley RN, Parfrey PS, Harnett JD, Kent GM, Martin CJ, Murray DC, Barre PE: Clinical and echocardiographic disease in patients starting end-stage renal disease therapy. Kidney international 1995;47:186-192.
48 Pun PH, Lehrich RW, Honeycutt EF, Herzog CA, Middleton JP: Modifiable risk factors associated with sudden cardiac arrest within hemodialysis clinics. Kidney international 2011;79:218-227.
49 Middleton JP: Predisposition to arrhythmias: Electrolytes, uremic fibrosis, other factors. Semin Dial 2011;24:287-289.
50 Chiu DY, Sinha S, Kalra PA, Green D: Sudden cardiac death in haemodialysis patients: Preventative options. Nephrology (Carlton, Vic) 2014;19:740-749.
51 Aoki J, Ikari Y, Nakajima H, Mori M, Sugimoto T, Hatori M, Tanimoto S, Amiya E, Hara K: Clinical and pathologic characteristics of dilated cardiomyopathy in hemodialysis patients. Kidney international 2005;67:333-340.
52 Hunold P, Vogt FM, Heemann UW, Zimmermann U, Barkhausen J: Myocardial mass and volume measurement of hypertrophic left ventricles by mri--study in dialysis patients examined before and after dialysis. Journal of cardiovascular magnetic resonance : official journal of the Society for Cardiovascular Magnetic Resonance 2003;5:553-561.
53 Gutierrez OM, Januzzi JL, Isakova T, Laliberte K, Smith K, Collerone G, Sarwar A, Hoffmann U, Coglianese E, Christenson R, Wang TJ, deFilippi C, Wolf M: Fibroblast growth factor 23 and left ventricular hypertrophy in chronic kidney disease. Circulation 2009;119:2545-2552.
54 Verma A, Anavekar NS, Meris A, Thune JJ, Arnold JM, Ghali JK, Velazquez EJ, McMurray JJ, Pfeffer MA, Solomon SD: The relationship between renal function and cardiac structure, function, and prognosis after myocardial infarction: The valiant echo study. Journal of the American College of Cardiology 2007;50:1238-1245.
55 Mall G, Huther W, Schneider J, Lundin P, Ritz E: Diffuse intermyocardiocytic fibrosis in uraemic patients. Nephrology Dialysis Transplantation 1990;5:39-44.
56 Wald R, Goldstein MB, Wald RM, Harel Z, Kirpalani A, Perl J, Yuen DA, Wolf MS, Yan AT: Correlates of left ventricular mass in chronic hemodialysis recipients. The international journal of cardiovascular imaging 2014;30:349-356.
57 Patel RK, Oliver S, Mark PB, Powell JR, McQuarrie EP, Traynor JP, Dargie HJ, Jardine AG: Determinants of left ventricular mass and hypertrophy in hemodialysis patients assessed by cardiac magnetic resonance imaging. Clinical journal of the American Society of Nephrology : CJASN 2009;4:1477-1483.
58 Mark PB, Johnston N, Groenning BA, Foster JE, Blyth KG, Martin TN, Steedman T, Dargie HJ, Jardine AG: Redefinition of uremic cardiomyopathy by contrast-enhanced cardiac magnetic resonance imaging. Kidney international 2006;69:1839-1845.

59 Schietinger BJ, Brammer GM, Wang H, Christopher JM, Kwon KW, Mangrum AJ, Mangrum JM, Kramer CM: Patterns of late gadolinium enhancement in chronic hemodialysis patients. JACC Cardiovascular imaging 2008;1:450-456.
60 Edwards NC, Moody WE, Yuan M, Hayer MK, Ferro CJ, Townend JN, Steeds RP: Diffuse interstitial fibrosis and myocardial dysfunction in early chronic kidney disease. The American Journal of Cardiology 2015
61 Mall G, Huther W, Schneider J, Lundin P, Ritz E: Diffuse intermyocardiocytic fibrosis in uraemic patients. Nephrology, dialysis, transplantation : official publication of the European Dialysis and Transplant Association - European Renal Association 1990;5:39-44.
62 Huang SY, Chen YC, Kao YH, Hsieh MH, Chen YA, Chen WP, Lin YK, Chen SA, Chen YJ: Renal failure induces atrial arrhythmogenesis from discrepant electrophysiological remodeling and calcium regulation in pulmonary veins, sinoatrial node, and atria. International journal of cardiology 2016;202:846-857.
63 de Meester de Ravenstein C, Bouzin C, Lazam S, Boulif J, Amzulescu M, Melchior J, Pasquet A, Vancraeynest D, Pouleur A-C, Vanoverschelde J-LJ, Gerber BJ: Histological validation of measurement of diffuse interstitial myocardial fibrosis by myocardial extravascular volume fraction from modified look-locker imaging (molli) t1 mapping at 3 t. Journal of Cardiovascular Magnetic Resonance 2015;17
64 Iles L, Pfluger H, Phrommintikul A, Cherayath J, Aksit P, Gupta SN, Kaye DM, Taylor AJ: Evaluation of diffuse myocardial fibrosis in heart failure with cardiac magnetic resonance contrast-enhanced t1 mapping. Journal of the American College of Cardiology 2008;52:1574-1580.
65 Becker AE, Heijmans CD, Essed CE: Chronic non-ischaemic congestive heart disease and endomyocardial biopsies. Worth the extra? European heart journal 1991;12:218-223.
66 Abraham TP, Dimaano VL, Liang H-Y: Role of tissue doppler and strain echocardiography in current clinical practice. Circulation 2007;116:2597-2609.
67 Dandel M, Lehmkuhl H, Knosalla C, Suramelashvili N, Hetzer R: Strain and strain rate imaging by echocardiography – basic concepts and clinical applicability. Current Cardiology Reviews 2009;5:133-148.
68 Stewart GA, Foster J, Cowan M, Rooney E, McDonagh T, Dargie HJ, Rodger RS, Jardine AG: Echocardiography overestimates left ventricular mass in hemodialysis patients relative to magnetic resonance imaging. Kidney international 1999;56:2248-2253.
69 Bello D, Shah DJ, Farah GM, Di Luzio S, Parker M, Johnson MR, Cotts WG, Klocke FJ, Bonow RO, Judd RM, Gheorghiade M, Kim RJ: Gadolinium cardiovascular magnetic resonance predicts reversible myocardial dysfunction and remodeling in patients with heart failure undergoing beta-blocker therapy. Circulation 2003;108:1945-1953.
70 Rogers WJ, Jr., Kramer CM, Geskin G, Hu YL, Theobald TM, Vido DA, Petruolo S, Reichek N: Early contrast-enhanced mri predicts late functional recovery after reperfused myocardial infarction. Circulation 1999;99:744-750.
71 Kramer CM, Rogers WJ, Jr., Mankad S, Theobald TM, Pakstis DL, Hu YL: Contractile reserve and contrast uptake pattern by magnetic resonance imaging

and functional recovery after reperfused myocardial infarction. Journal of the American College of Cardiology 2000;36:1835-1840.
72 Parsai C, O'Hanlon R, Prasad SK, Mohiaddin RH: Diagnostic and prognostic value of cardiovascular magnetic resonance in non-ischaemic cardiomyopathies. Journal of Cardiovascular Magnetic Resonance 2012;14:54-54.
73 de Meester de Ravenstein C, Bouzin C, Lazam S, Boulif J, Amzulescu M, Melchior J, Pasquet A, Vancraeynest D, Pouleur AC, Vanoverschelde JL, Gerber BL: Histological validation of measurement of diffuse interstitial myocardial fibrosis by myocardial extravascular volume fraction from modified look-locker imaging (molli) t1 mapping at 3 t. Journal of cardiovascular magnetic resonance : official journal of the Society for Cardiovascular Magnetic Resonance 2015;17:48.
74 Messroghli DR, Nordmeyer S, Buehrer M, Kozerke S, Dietrich T, Kaschina E, Becher PM, Hucko T, Berger F, Klein C, Kuehne T: Small animal look-locker inversion recovery (salli) for simultaneous generation of cardiac t1 maps and cine and inversion recovery-prepared images at high heart rates: Initial experience. Radiology 2011;261:258-265.
75 Ugander M, Oki AJ, Hsu L-Y, Kellman P, Greiser A, Aletras AH, Sibley CT, Chen MY, Bandettini WP, Arai AE: Extracellular volume imaging by magnetic resonance imaging provides insights into overt and sub-clinical myocardial pathology. European heart journal 2012;33:1268-1278.
76 Broberg CS, Chugh SS, Conklin C, Sahn DJ, Jerosch-Herold M: Quantification of diffuse myocardial fibrosis and its association with myocardial dysfunction in congenital heart disease. Circulation: Cardiovascular Imaging 2010;3:727-734.
77 Kellman P, Wilson J, Xue H, Bandettini WP, Shanbhag SM, Druey KM, Ugander M, Arai AE: Extracellular volume fraction mapping in the myocardium, part 2: Initial clinical experience. Journal of Cardiovascular Magnetic Resonance 2012;14
78 Iles LM, Ellims AH, Llewellyn H, Hare JL, Kaye DM, McLean CA, Taylor AJ: Histological validation of cardiac magnetic resonance analysis of regional and diffuse interstitial myocardial fibrosis. European heart journal cardiovascular Imaging 2015;16:14-22.
79 Wong TC, Piehler K, Meier CG, Testa SM, Klock AM, Aneizi AA, Shakesprere J, Kellman P, Shroff SG, Schwartzman DS, Mulukutla SR, Simon MA, Schelbert EB: Association between extracellular matrix expansion quantified by cardiovascular magnetic resonance and short-term mortality. Circulation 2012;126:1206-1216.
80 Ellims AH, Shaw JA, Stub D, Iles LM, Hare JL, Slavin GS, Kaye DM, Taylor AJ: Diffuse myocardial fibrosis evaluated by post-contrast t1 mapping correlates with left ventricular stiffness. Journal of the American College of Cardiology 2014;63:1112-1118.
81 Schelbert EB, Piehler KM, Zareba KM, Moon JC, Ugander M, Messroghli DR, Valeti US, Chang CC, Shroff SG, Diez J, Miller CA, Schmitt M, Kellman P, Butler J, Gheorghiade M, Wong TC: Myocardial fibrosis quantified by extracellular volume is associated with subsequent

hospitalization for heart failure, death, or both across the spectrum of ejection fraction and heart failure stage. J Am Heart Assoc 2015;4
82 Food and Drug Administration: Public health advisory. Gadolinium-containing contrast agents for magnetic resonance imaging (mri):Omniscan, optimark, magnevist,prohance, and multihance. 2006
83 Food and Drug Administration: Public health advisory. Gadolinium-containing contrast agents for magnetic resonance imaging (mri). 2006
84 Grobner T: Gadolinium--a specific trigger for the development of nephrogenic fibrosing dermopathy and nephrogenic systemic fibrosis? Nephrology, dialysis, transplantation : official publication of the European Dialysis and Transplant Association - European Renal Association 2006;21:1104-1108.
85 Marckmann P, Skov L, Rossen K, Dupont A, Damholt MB, Heaf JG, Thomsen HS: Nephrogenic systemic fibrosis: Suspected causative role of gadodiamide used for contrast-enhanced magnetic resonance imaging. Journal of the American Society of Nephrology : JASN 2006;17:2359-2362.
86 Grant D, Johnsen H, Juelsrud A, Lovhaug D: Effects of gadolinium contrast agents in naive and nephrectomized rats: Relevance to nephrogenic systemic fibrosis. Acta radiologica (Stockholm, Sweden : 1987) 2009;50:156-169.
87 Bardin T, Richette P: Nephrogenic systemic fibrosis. Current opinion in rheumatology 2010;22:54-58.
88 Moon JC, Messroghli DR, Kellman P, Piechnik SK, Robson MD, Ugander M, Gatehouse PD, Arai AE, Friedrich MG, Neubauer S, Schulz-Menger J, Schelbert EB: Myocardial t1 mapping and extracellular volume quantification: A society for cardiovascular magnetic resonance (scmr) and cmr working group of the european society of cardiology consensus statement. Journal of cardiovascular magnetic resonance : official journal of the Society for Cardiovascular Magnetic Resonance 2013;15:92.
89 Baksi AJ, Pennell DJ: T1 mapping in heart failure: From technique to prognosis, toward altering outcome. Circulation Cardiovascular imaging 2013;6:861-863.
90 Rutherford E, Talle MA, Mangion K, Bell E, Rauhalammi SM, Roditi G, McComb C, Radjenovic A, Welsh P, Woodward R, Struthers AD, Jardine AG, Patel RK, Berry C, Mark PB: Defining myocardial tissue abnormalities in end-stage renal failure with cardiac magnetic resonance imaging using native t1 mapping. Kidney international 2016
91 Kellman P, Hansen MS: T1-mapping in the heart: Accuracy and precision. Journal of cardiovascular magnetic resonance : official journal of the Society for Cardiovascular Magnetic Resonance 2014;16:2.
92 Messroghli DR, Radjenovic A, Kozerke S, Higgins DM, Sivananthan MU, Ridgway JP: Modified look-locker inversion recovery (molli) for high-resolution t1 mapping of the heart. Magnetic resonance in medicine : official journal of the Society of Magnetic Resonance in Medicine / Society of Magnetic Resonance in Medicine 2004;52:141-146.
93 Messroghli DR, Walters K, Plein S, Sparrow P, Friedrich MG, Ridgway JP, Sivananthan MU: Myocardial t1 mapping: Application to patients with acute and chronic myocardial infarction. Magnetic resonance in medicine : official journal of

the Society of Magnetic Resonance in Medicine / Society of Magnetic Resonance in Medicine 2007;58:34-40.
94 Bull S, White SK, Piechnik SK, Flett AS, Ferreira VM, Loudon M, Francis JM, Karamitsos TD, Prendergast BD, Robson MD, Neubauer S, Moon JC, Myerson SG: Human non-contrast t1 values and correlation with histology in diffuse fibrosis. Heart (British Cardiac Society) 2013;99:932-937.
95 Puntmann VO, Voigt T, Chen Z, Mayr M, Karim R, Rhode K, Pastor A, Carr-White G, Razavi R, Schaeffter T, Nagel E: Native t1 mapping in differentiation of normal myocardium from diffuse disease in hypertrophic and dilated cardiomyopathy. JACC Cardiovascular imaging 2013;6:475-484.
96 Dabir D, Child N, Kalra A, Rogers T, Gebker R, Jabbour A, Plein S, Yu CY, Otton J, Kidambi A, McDiarmid A, Broadbent D, Higgins DM, Schnackenburg B, Foote L, Cummins C, Nagel E, Puntmann VO: Reference values for healthy human myocardium using a t1 mapping methodology: Results from the international t1 multicenter cardiovascular magnetic resonance study. Journal of cardiovascular magnetic resonance : official journal of the Society for Cardiovascular Magnetic Resonance 2014;16:69.
97 Shah RV, Kato S, Roujol S, Murthy V, Bellm S, Kashem A, Basha T, Jang J, Eisman AS, Manning WJ, Nezafat R: Native myocardial t1 as a biomarker of cardiac structure in non-ischemic cardiomyopathy. The American Journal of Cardiology 2016;117:282-288.
98 van Oorschot JWM, Güçlü F, de Jong S, Chamuleau SAJ, Luijten PR, Leiner T, Zwanenburg JJM: Endogenous assessment of diffuse myocardial fibrosis in patients with t1ρ-mapping. Journal of Magnetic Resonance Imaging 2016:n/a-n/a.
99 Graham-Brown MP, Burton JO, McCann GP: The use of t1 mapping to define myocardial fibrosis in haemodialysis patients. European heart journal cardiovascular Imaging 2016
100 Roujol S, Weingartner S, Foppa M, Chow K, Kawaji K, Ngo LH, Kellman P, Manning WJ, Thompson RB, Nezafat R: Accuracy, precision, and reproducibility of four t1 mapping sequences: A head-to-head comparison of molli, shmolli, sasha, and sapphire. Radiology 2014;272:683-689.
101 Liu S, Han J, Nacif MS, Jones J, Kawel N, Kellman P, Sibley CT, Bluemke DA: Diffuse myocardial fibrosis evaluation using cardiac magnetic resonance t1 mapping: Sample size considerations for clinical trials. Journal of Cardiovascular Magnetic Resonance 2012;14:90.
102 Nacif MS, Turkbey EB, Gai N, Nazarian S, van der Geest RJ, Noureldin RA, Sibley CT, Ugander M, Liu S, Arai AE, Lima JA, Bluemke DA: Myocardial t1 mapping with mri: Comparison of look-locker and molli sequences. Journal of magnetic resonance imaging : JMRI 2011;34:1367-1373.
103 Rogers T, Puntmann VO: T1 mapping - beware regional variations. European heart journal cardiovascular Imaging 2014;15:1302.
104 Sado DM, White SK, Piechnik SK, Banypersad SM, Treibel T, Captur G, Fontana M, Maestrini V, Flett AS, Robson MD, Lachmann RH, Murphy E, Mehta A, Hughes D, Neubauer S, Elliott PM, Moon JC: Identification and assessment of

anderson-fabry disease by cardiovascular magnetic resonance noncontrast myocardial t1 mapping. Circulation Cardiovascular imaging 2013;6:392-398.
105 Silverberg DS, Wexler D, Iaina A: The role of anemia in the progression of congestive heart failure. Is there a place for erythropoietin and intravenous iron? Journal of nephrology 2004;17:749-761.
106 Wolff SD, Balaban RS: Magnetization transfer imaging: Practical aspects and clinical applications. Radiology 1994;192:593-599.
107 Bieri O, Scheffler K: On the origin of apparent low tissue signals in balanced ssfp. Magnetic Resonance in Medicine 2006;56:1067-1074.
108 Weber OM, Speier P, Scheffler K, Bieri O: Assessment of magnetization transfer effects in myocardial tissue using balanced steady-state free precession (bssfp) cine mri. Magnetic resonance in medicine : official journal of the Society of Magnetic Resonance in Medicine / Society of Magnetic Resonance in Medicine 2009;62:699-705.
109 van Oorschot JWM, Gho JMIH, van Hout GPJ, Froeling M, Jansen of Lorkeers SJ, Hoefer IE, Doevendans PA, Luijten PR, Chamuleau SAJ, Zwanenburg JJM: Endogenous contrast mri of cardiac fibrosis: Beyond late gadolinium enhancement. Journal of Magnetic Resonance Imaging 2014:n/a-n/a.
110 Scholz TD, Hoyt RF, DeLeonardis JR, Ceckler TL, Balaban RS: Water-macromolecular proton magnetization transfer in infarcted myocardium: A method to enhance magnetic resonance image contrast. Magnetic resonance in medicine : official journal of the Society of Magnetic Resonance in Medicine / Society of Magnetic Resonance in Medicine 1995;33:178-184.
111 Vandsburger M, Vandoorne K, Oren R, Leftin A, Mpofu S, Delli Castelli D, Aime S, Neeman M: Cardio-chemical exchange saturation transfer magnetic resonance imaging reveals molecular signatures of endogenous fibrosis and exogenous contrast media. Circulation: Cardiovascular Imaging 2015;8
112 Vandsburger M, Epstein F: Emerging mri methods in translational cardiovascular research. J of Cardiovasc Trans Res 2011;4:477-492.
113 Wu KC, Weiss RG, Thiemann DR, Kitagawa K, Schmidt A, Dalal D, Lai S, Bluemke DA, Gerstenblith G, Marbán E, Tomaselli GF, Lima JAC: Late gadolinium enhancement by cardiovascular magnetic resonance heralds an adverse prognosis in nonischemic cardiomyopathy. Journal of the American College of Cardiology 2008;51:2414-2421.
114 Kellman P, Wilson J, Xue H, Ugander M, Arai AE: Extracellular volume fraction mapping in the myocardium, part 1: Evaluation of an automated method. Journal of Cardiovascular Magnetic Resonance 2012;14
115 Wong TC, Piehler KM, Kang IA, Kadakkal A, Kellman P, Schwartzman DS, Mulukutla SR, Simon MA, Shroff SG, Kuller LH, Schelbert EB: Myocardial extracellular volume fraction quantified by cardiovascular magnetic resonance is increased in diabetes and associated with mortality and incident heart failure admission. European Heart Journal 2014;35:657-664.
116 Broome DR: Nephrogenic systemic fibrosis associated with gadolinium based contrast agents: A summary of the medical literature reporting. European Journal of Radiology 2008;66:230-234.

117 Giri S, Chung Y-C, Merchant A, Mihai G, Rajagopalan S, Raman S, Simonetti O: T2 quantification for improved detection of myocardial edema. Journal of Cardiovascular Magnetic Resonance 2009;11:56.
118 Verhaert D, Thavendiranathan P, Giri S, Mihai G, Rajagopalan S, Simonetti OP, Raman SV: Direct t2 quantification of myocardial edema in acute ischemic injury. JACC: Cardiovascular Imaging 2011;4:269-278.
119 Bull S, White SK, Piechnik SK, Flett AS, Ferreira VM, Loudon M, Francis JM, Karamitsos TD, Prendergast BD, Robson MD, Neubauer S, Moon JC, Myerson SG: Human non-contrast t1 values and correlation with histology in diffuse fibrosis. Heart 2013;99:932-937.
120 Ferreira VM, Piechnik SK, Dall'Armellina E, Karamitsos TD, Francis JM, Ntusi N, Holloway C, Choudhury RP, Kardos A, Robson MD, Friedrich MG, Neubauer S: T1 mapping for the diagnosis of acute myocarditis using cmr: Comparison to t2-weighted and late gadolinium enhanced imaging. JACC: Cardiovascular Imaging 2013;6:1048-1058.
121 Puntmann VO, Voigt T, Chen Z, Mayr M, Karim R, Rhode K, Pastor A, Carr-White G, Razavi R, Schaeffter T, Nagel E: Native t1 mapping in differentiation of normal myocardium from diffuse disease in hypertrophic and dilated cardiomyopathy. JACC: Cardiovascular Imaging 2013;6:475-484.
122 Baksi AJ, Pennell DJ: T1 mapping in heart failure: From technique to prognosis, toward altering outcome. Circulation: Cardiovascular Imaging 2013;6:861-863.
123 Kellman P, Hansen M: T1-mapping in the heart: Accuracy and precision. Journal of Cardiovascular Magnetic Resonance 2014;16:2.
124 Moon J, Messroghli D, Kellman P, Piechnik S, Robson M, Ugander M, Gatehouse P, Arai A, Friedrich M, Neubauer S, Schulz-Menger J, Schelbert E: Myocardial t1 mapping and extracellular volume quantification: A society for cardiovascular magnetic resonance (scmr) and cmr working group of the european society of cardiology consensus statement. Journal of Cardiovascular Magnetic Resonance 2013;15:92.
125 Roujol S, Weingärtner S, Foppa M, Chow K, Kawaji K, Ngo LH, Kellman P, Manning WJ, Thompson RB, Nezafat R: Accuracy, precision, and reproducibility of four t1 mapping sequences: A head-to-head comparison of molli, shmolli, sasha, and sapphire. Radiology 2014;272:683-689.
126 Dabir D, Child N, Kalra A, Rogers T, Gebker R, Jabbour A, Plein S, Yu C, Otton J, Kidambi A, McDiarmid A, Higgins DM, Schnackbenburg B, Foote L, Cummins C, Nagel E, Puntmann V: Reference values for healthy human myocardium using a t1 mapping methodology: Results from the international t1 multicenter cardiovascular magnetic resonance study. Journal of Cardiovascular Magnetic Resonance 2014;16:69.
127 Fitts M, Breton E, Kholmovski EG, Dosdall DJ, Vijayakumar S, Hong KP, Ranjan R, Marrouche NF, Axel L, Kim D: Arrhythmia insensitive rapid cardiac t1 mapping pulse sequence. Magnetic Resonance in Medicine 2013;70:1274-1282.
128 Rogers T, Puntmann V: T1 mapping - beware regional variations. European Heart Journal Cardiovascular Imaging 2014;15:1302.
129 Sado DM, White SK, Piechnik SK, Banypersad SM, Treibel T, Captur G, Fontana M, Maestrini V, Flett AS, Robson MD, Lachmann RH, Murphy E, Mehta A,

Hughes D, Neubauer S, Elliott PM, Moon JC: Identification and assessment of anderson-fabry disease by cardiovascular magnetic resonance noncontrast myocardial t1 mapping. Circulation: Cardiovascular Imaging 2013;6:392-398.
130 Thompson RB, Chow K, Khan A, Chan A, Shanks M, Paterson I, Oudit GY: T1 mapping with cardiovascular mri is highly sensitive for fabry disease independent of hypertrophy and sex. Circulation: Cardiovascular Imaging 2013;6:637-645.
131 Weber OM, Speier P, Scheffler K, Bieri O: Assessment of magnetization transfer effects in myocardial tissue using balanced steady-state free precession (bssfp) cine mri. Magnetic Resonance in Medicine 2009;62:699-705.
132 Zhou X, Rundell V, Liu Y, Tang R, Shah S, Zuehlsdorff S, Li D, Dharmakumar R: On the mechanisms enabling myocardial edema contrast in bssfp-based imaging approaches. Magnetic Resonance in Medicine 2011;66:187-191.
133 Kumar A, Beohar N, Arumana JM, Larose E, Li D, Friedrich MG, Dharmakumar R: Cmr imaging of edema in myocardial infarction using cine balanced steady-state free precession. JACC: Cardiovascular Imaging 2011;4:1265-1273.
134 Sibley CT, Noureldin RA, Gai N, Nacif MS, Liu S, Turkbey EB, Mudd JO, van der Geest RJ, Lima JAC, Halushka MK, Bluemke DA: T1 mapping in cardiomyopathy at cardiac mr: Comparison with endomyocardial biopsy. Radiology 2012:724-732.
135 Wong TC, Piehler K, Meier CG, Testa SM, Klock AM, Aneizi AA, Shakesprere J, Kellman P, Shroff SG, Schwartzman DS, Mulukutla SR, Simon MA, Schelbert EB: Association between extracellular matrix expansion quantified by cardiovascular magnetic resonance and short-term mortality. Circulation 2012;126:1206-1216.
136 Mascherbauer J, Marzluf BA, Tufaro C, Pfaffenberger S, Graf A, Wexberg P, Panzenböck A, Jakowitsch J, Bangert C, Laimer D, Schreiber C, Karakus G, Hülsmann M, Pacher R, Lang IM, Maurer G, Bonderman D: Cardiac magnetic resonance postcontrast t1 time is associated with outcome in patients with heart failure and preserved ejection fraction. Circulation: Cardiovascular Imaging 2013;6:1056-1065.
137 Salerno M, Janardhanan R, Jiji RS, Brooks J, Adenaw N, Mehta B, Yang Y, Antkowiak P, Kramer CM, Epstein FH: Comparison of methods for determining the partition coefficient of gadolinium in the myocardium using t1 mapping. Journal of Magnetic Resonance Imaging 2013:217-224.
138 Liu C-Y, Liu Y-C, Wu C, Armstrong A, Volpe GJ, van der Geest RJ, Liu Y, Hundley WG, Gomes AS, Liu S, Nacif M, Bluemke DA, Lima JAC: Evaluation of age-related interstitial myocardial fibrosis with cardiac magnetic resonance contrast-enhanced t1 mapping: Mesa (multi-ethnic study of atherosclerosis). Journal of the American College of Cardiology 2013;62:1280-1287.
139 Ferreira V, Piechnik S, Dall'Armellina E, Karamitsos T, Francis J, Choudhury R, Friedrich M, Robson M, Neubauer S: Non-contrast t1-mapping detects acute myocardial edema with high diagnostic accuracy: A comparison to t2-weighted cardiovascular magnetic resonance. Journal of Cardiovascular Magnetic Resonance 2012;14:42.

140 Messroghli DR, Radjenovic A, Kozerke S, Higgins DM, Sivananthan MU, Ridgway JP: Modified look-locker inversion recovery (molli) for high-resolution t1 mapping of the heart. Magnetic Resonance in Medicine 2004;52:141-146.
141 Faul C, Amaral AP, Oskouei B, Hu MC, Sloan A, Isakova T, Gutierrez OM, Aguillon-Prada R, Lincoln J, Hare JM, Mundel P, Morales A, Scialla J, Fischer M, Soliman EZ, Chen J, Go AS, Rosas SE, Nessel L, Townsend RR, Feldman HI, St John Sutton M, Ojo A, Gadegbeku C, Di Marco GS, Reuter S, Kentrup D, Tiemann K, Brand M, Hill JA, Moe OW, Kuro OM, Kusek JW, Keane MG, Wolf M: Fgf23 induces left ventricular hypertrophy. The Journal of clinical investigation 2011;121:4393-4408.
142 Isakova T, Xie H, Yang W, Xie D, Anderson AH, Scialla J, Wahl P, Gutierrez OM, Steigerwalt S, He J, Schwartz S, Lo J, Ojo A, Sondheimer J, Hsu CY, Lash J, Leonard M, Kusek JW, Feldman HI, Wolf M: Fibroblast growth factor 23 and risks of mortality and end-stage renal disease in patients with chronic kidney disease. Jama 2011;305:2432-2439.
143 Lombardi R, Betocchi S, Losi MA, Tocchetti CG, Aversa M, Miranda M, D'Alessandro G, Cacace A, Ciampi Q, Chiariello M: Myocardial collagen turnover in hypertrophic cardiomyopathy. Circulation 2003;108:1455-1460.
144 Barton PJ, Birks EJ, Felkin LE, Cullen ME, Koban MU, Yacoub MH: Increased expression of extracellular matrix regulators timp1 and mmp1 in deteriorating heart failure. The Journal of heart and lung transplantation : the official publication of the International Society for Heart Transplantation 2003;22:738-744.
145 Gluba-Brzozka A, Michalska-Kasiczak M, Franczyk-Skora B, Nocun M, Banach M, Rysz J: Markers of increased cardiovascular risk in patients with chronic kidney disease. Lipids in health and disease 2014;13:135.
146 Pawlak K, Mysliwiec M, Pawlak D: Peripheral blood level alterations of mmp-2 and mmp-9 in patients with chronic kidney disease on conservative treatment and on hemodialysis. Clinical biochemistry 2011;44:838-843.
147 Chou FP, Chu SC, Cheng MC, Yang SF, Cheung WN, Chiou HL, Hsieh YS: Effect of hemodialysis on the plasma level of type iv collagenases and their inhibitors. Clinical biochemistry 2002;35:383-388.
148 Rysz J, Banach M, Stolarek RA, Mikhailidis DP, Cialkowska-Rysz A, Pokoca L, Piechota M, Baj Z: Serum metalloproteinases mmp-2, mmp-9 and metalloproteinase tissue inhibitors timp-1 and timp-2 in patients on hemodialysis. International urology and nephrology 2011;43:491-498.
149 Grossman W, Jones D, McLaurin LP: Wall stress and patterns of hypertrophy in the human left ventricle. The Journal of clinical investigation 1975;56:56-64.
150 Jing L, Haggerty CM, Suever JD, Alhadad S, Prakash A, Cecchin F, Skrinjar O, Geva T, Powell AJ, Fornwalt BK: Patients with repaired tetralogy of fallot suffer from intra- and inter-ventricular cardiac dyssynchrony: A cardiac magnetic resonance study. European heart journal cardiovascular Imaging 2014;15:1333-1343.
151 Food and Drugh Administration: Fda drug safety communication: New warnings for using gadolinium-based contrast agents in patients with kidney dysfunction; in Association FaD (ed), 2010,

152 Kaye AD, Volpi-Abadie J, Bensler JM, Kaye AM, Diaz JH: Qt interval abnormalities: Risk factors and perioperative management in long qt syndromes and torsades de pointes. Journal of Anesthesia 2013;27:575-587.
153 Hage FG, de Mattos AM, Khamash H, Mehta S, Warnock D, Iskandrian AE: Qt prolongation is an independent predictor of mortality in end-stage renal disease. Clinical cardiology 2010;33:361-366.
154 Genovesi S, Rossi E, Nava M, Riva H, De Franceschi S, Fabbrini P, Vigano MR, Pieruzzi F, Stella A, Valsecchi MG, Stramba-Badiale M: A case series of chronic haemodialysis patients: Mortality, sudden death, and qt interval. Europace : European pacing, arrhythmias, and cardiac electrophysiology : journal of the working groups on cardiac pacing, arrhythmias, and cardiac cellular electrophysiology of the European Society of Cardiology 2013;15:1025-1033.
155 McLenachan JM, Henderson E, Morris KI, Dargie HJ: Ventricular arrhythmias in patients with hypertensive left ventricular hypertrophy. The New England journal of medicine 1987;317:787-792.
156 Rader F, Sachdev E, Arsanjani R, Siegel RJ: Left ventricular hypertrophy in valvular aortic stenosis: Mechanisms and clinical implications. Am J Med 2015;128:344-352.
157 Shah AM, Claggett B, Sweitzer NK, Shah SJ, Anand IS, O'Meara E, Desai AS, Heitner JF, Li G, Fang J, Rouleau J, Zile MR, Markov V, Ryabov V, Reis G, Assmann SF, McKinlay SM, Pitt B, Pfeffer MA, Solomon SD: Cardiac structure and function and prognosis in heart failure with preserved ejection fraction: Findings from the echocardiographic study of the treatment of preserved cardiac function heart failure with an aldosterone antagonist (topcat) trial. Circulation Heart failure 2014;7:740-751.
158 Gutierrez OM, Mannstadt M, Isakova T, Rauh-Hain JA, Tamez H, Shah A, Smith K, Lee H, Thadhani R, Juppner H, Wolf M: Fibroblast growth factor 23 and mortality among patients undergoing hemodialysis. The New England journal of medicine 2008;359:584-592.
159 Isakova T, Wahl P, Vargas GS, Gutierrez OM, Scialla J, Xie H, Appleby D, Nessel L, Bellovich K, Chen J, Hamm L, Gadegbeku C, Horwitz E, Townsend RR, Anderson CA, Lash JP, Hsu CY, Leonard MB, Wolf M: Fibroblast growth factor 23 is elevated before parathyroid hormone and phosphate in chronic kidney disease. Kidney international 2011;79:1370-1378.
160 Block GA, Kilpatrick RD, Lowe KA, Wang W, Danese MD: Ckd-mineral and bone disorder and risk of death and cardiovascular hospitalization in patients on hemodialysis. Clinical journal of the American Society of Nephrology : CJASN 2013;8:2132-2140.
161 Gutierrez OM, Muntner P, Rizk DV, McClellan WM, Warnock DG, Newby PK, Judd SE: Dietary patterns and risk of death and progression to esrd in individuals with ckd: A cohort study. American journal of kidney diseases : the official journal of the National Kidney Foundation 2014;64:204-213.
162 Isakova T, Barchi-Chung A, Enfield G, Smith K, Vargas G, Houston J, Xie H, Wahl P, Schiavenato E, Dosch A, Gutierrez OM, Diego J, Lenz O, Contreras G, Mendez A, Weiner RB, Wolf M: Effects of dietary phosphate restriction and

phosphate binders on fgf23 levels in ckd. Clinical journal of the American Society of Nephrology : CJASN 2013;8:1009-1018.
163 Thadhani R, Appelbaum E, Pritchett Y, Chang Y, Wenger J, Tamez H, Bhan I, Agarwal R, Zoccali C, Wanner C, Lloyd-Jones D, Cannata J, Thompson BT, Andress D, Zhang W, Packham D, Singh B, Zehnder D, Shah A, Pachika A, Manning WJ, Solomon SD: Vitamin d therapy and cardiac structure and function in patients with chronic kidney disease: The primo randomized controlled trial. Jama 2012;307:674-684.
164 Patel RK, Mark PB, Johnston N, McGregor E, Dargie HJ, Jardine AG: Renal transplantation is not associated with regression of left ventricular hypertrophy: A magnetic resonance study. Clinical journal of the American Society of Nephrology : CJASN 2008;3:1807-1811.
165 Pressman GS, Seetha Rammohan HR, Romero-Corral A, Fumo P, Figueredo VM, Gorcsan J, 3rd: Echocardiographic strain and mortality in black americans with end-stage renal disease on hemodialysis. Am J Cardiol 2015;116:1601-1604.
166 Cezar MDM, Damatto RL, Pagan LU, Lima ARR, Martinez PF, Bonomo C, Rosa CM, Campos DHS, Cicogna AC, Gomes MJ, Oliveira-Jr SA, Blotta DA, Okoshi MP, Okoshi K: Early spironolactone treatment attenuates heart failure development by improving myocardial function and reducing fibrosis in spontaneously hypertensive rats. Cellular Physiology and Biochemistry 2015;36:1453-1466.
167 Esposito CT, Varahan S, Jeyaraj D, Lu Y, Stambler BS: Spironolactone improves the arrhythmogenic substrate in heart failure by preventing ventricular electrical activation delays associated with myocardial interstitial fibrosis and inflammation. Journal of cardiovascular electrophysiology 2013;24:806-812.
168 Martinez-Martinez E, Calvier L, Fernandez-Celis A, Rousseau E, Jurado-Lopez R, Rossoni LV, Jaisser F, Zannad F, Rossignol P, Cachofeiro V, Lopez-Andres N: Galectin-3 blockade inhibits cardiac inflammation and fibrosis in experimental hyperaldosteronism and hypertension. Hypertension 2015;66:767-775.
169 Moe SM, Chertow GM, Parfrey PS, Kubo Y, Block GA, Correa-Rotter R, Drüeke TB, Herzog CA, London GM, Mahaffey KW, Wheeler DC, Stolina M, Dehmel B, Goodman WG, Floege J: Cinacalcet, fgf23 and cardiovascular disease in hemodialysis: The evolve trial. Circulation 2015
170 Coelho-Filho OR, Shah RV, Neilan TG, Mitchell R, Moreno H, Jr., Kwong R, Jerosch-Herold M: Cardiac magnetic resonance assessment of interstitial myocardial fibrosis and cardiomyocyte hypertrophy in hypertensive mice treated with spironolactone. J Am Heart Assoc 2014;3:e000790.
171 Yu SY, Liu L, Li P, Li J: Rapamycin inhibits the mtor/p70s6k pathway and attenuates cardiac fibrosis in adriamycin-induced dilated cardiomyopathy. The Thoracic and cardiovascular surgeon 2013;61:223-228.
172 Haller ST, Yan Y, Drummond CA, Xie J, Tian J, Kennedy DJ, Shilova VY, Xie Z, Liu J, Cooper CJ, Malhotra D, Shapiro JI, Fedorova OV, Bagrov AY: Rapamycin attenuates cardiac fibrosis in experimental uremic cardiomyopathy by reducing marinobufagenin levels and inhibiting downstream pro-fibrotic signaling. J Am Heart Assoc 2016;5

173 Vanhoutte D, Schellings M, Pinto Y, Heymans S: Relevance of matrix metalloproteinases and their inhibitors after myocardial infarction: A temporal and spatial window. Cardiovascular research 2006;69:604-613.
174 Giannandrea M, Parks WC: Diverse functions of matrix metalloproteinases during fibrosis. Disease models & mechanisms 2014;7:193-203.
175 Spinale FG: Myocardial matrix remodeling and the matrix metalloproteinases: Influence on cardiac form and function. Physiological reviews 2007;87:1285-1342.
176 Vanhoutte D, Heymans S: Timps and cardiac remodeling: 'Embracing the mmp-independent-side of the family'. J Mol Cell Cardiol 2010;48:445-453.
177 de Simone G, de Divitiis O: Extracellular matrix and left ventricular mechanics in overload hypertrophy. Advances in clinical pathology : the official journal of Adriatic Society of Pathology 2002;6:3-10.
178 Creemers EE, Davis JN, Parkhurst AM, Leenders P, Dowdy KB, Hapke E, Hauet AM, Escobar PG, Cleutjens JP, Smits JF, Daemen MJ, Zile MR, Spinale FG: Deficiency of timp-1 exacerbates lv remodeling after myocardial infarction in mice. American journal of physiology Heart and circulatory physiology 2003;284:H364-371.
179 Agrinier N, Thilly N, Boivin JM, Dousset B, Alla F, Zannad F: Prognostic value of serum piiinp, mmp1 and timp1 levels in hypertensive patients: A community-based prospective cohort study. Fundamental & clinical pharmacology 2013;27:572-580.
180 Zhu H, Sun X, Wang D, Hu N, Zhang Y: Doxycycline ameliorates aggregation of collagen and atrial natriuretic peptide in murine post-infarction heart. European journal of pharmacology 2015;754:66-72.
181 Pawlak K, Pawlak D, Mysliwiec M: Serum matrix metalloproteinase-2 and increased oxidative stress are associated with carotid atherosclerosis in hemodialyzed patients. Atherosclerosis 2007;190:199-204.
182 Musial K, Zwolinska D: Matrix metalloproteinases and soluble fas/fasl system as novel regulators of apoptosis in children and young adults on chronic dialysis. Apoptosis : an international journal on programmed cell death 2011;16:653-659.
183 Fatema K, Hirono O, Masakane I, Nitobe J, Kaneko K, Zhang X, Takeishi Y, Kubota I: Dynamic assessment of myocardial involvement in patients with end-stage renal disease by ultrasonic tissue characterization and serum markers of collagen metabolism. Clinical cardiology 2004;27:228-234.
184 Graham-Brown MP, March DS, Churchward DR, Stensel DJ, Singh A, Arnold R, Burton JO, McCann GP: Novel cardiac nuclear magnetic resonance method for noninvasive assessment of myocardial fibrosis in hemodialysis patients. Kidney international 2016;90:835-844.
185 Saran R, Li Y, Robinson B, Abbott KC, Agodoa LY, Ayanian J, Bragg-Gresham J, Balkrishnan R, Chen JL, Cope E, Eggers PW, Gillen D, Gipson D, Hailpern SM, Hall YN, He K, Herman W, Heung M, Hirth RA, Hutton D, Jacobsen SJ, Kalantar-Zadeh K, Kovesdy CP, Lu Y, Molnar MZ, Morgenstern H, Nallamothu B, Nguyen DV, O'Hare AM, Plattner B, Pisoni R, Port FK, Rao P, Rhee CM, Sakhuja A, Schaubel DE, Selewski DT, Shahinian V, Sim JJ, Song P, Streja E, Kurella Tamura M, Tentori F, White S, Woodside K, Hirth RA: Us renal data system 2015

annual data report: Epidemiology of kidney disease in the united states. American journal of kidney diseases : the official journal of the National Kidney Foundation 2016;67:A7-8.
186 Sadowski EA, Bennett LK, Chan MR, Wentland AL, Garrett AL, Garrett RW, Djamali A: Nephrogenic systemic fibrosis: Risk factors and incidence estimation. Radiology 2007;243:148-157.
187 Pitt B, Pfeffer MA, Assmann SF, Boineau R, Anand IS, Claggett B, Clausell N, Desai AS, Diaz R, Fleg JL, Gordeev I, Harty B, Heitner JF, Kenwood CT, Lewis EF, O'Meara E, Probstfield JL, Shaburishvili T, Shah SJ, Solomon SD, Sweitzer NK, Yang S, McKinlay SM: Spironolactone for heart failure with preserved ejection fraction. The New England journal of medicine 2014;370:1383-1392.
188 Di Marco GS, Reuter S, Kentrup D, Grabner A, Amaral AP, Fobker M, Stypmann J, Pavenstadt H, Wolf M, Faul C, Brand M: Treatment of established left ventricular hypertrophy with fibroblast growth factor receptor blockade in an animal model of ckd. Nephrology, dialysis, transplantation : official publication of the European Dialysis and Transplant Association - European Renal Association 2014;29:2028-2035.
189 Apple FS, Murakami MM, Pearce LA, Herzog CA: Multi-biomarker risk stratification of n-terminal pro-b-type natriuretic peptide, high-sensitivity c-reactive protein, and cardiac troponin t and i in end-stage renal disease for all-cause death. Clinical chemistry 2004;50:2279-2285.
190 Takashio S, Yamamuro M, Uemura T, Utsunomiya D, Morita K, Izumiya Y, Sugiyama S, Kojima S, Yamamoto E, Tsujita K, Tanaka T, Tayama S, Kaikita K, Hokimoto S, Yasuda O, Yamashita Y, Ogawa H: Correlation between extent of myocardial fibrosis assessed by cardiac magnetic resonance and cardiac troponin t release in patients with nonischemic heart failure. Am J Cardiol 2014;113:1697-1704.
191 Khan NA, Hemmelgarn BR, Tonelli M, Thompson CR, Levin A: Prognostic value of troponin t and i among asymptomatic patients with end-stage renal disease: A meta-analysis. Circulation 2005;112:3088-3096.
192 Touchberry CD, Green TM, Tchikrizov V, Mannix JE, Mao TF, Carney BW, Girgis M, Vincent RJ, Wetmore LA, Dawn B, Bonewald LF, Stubbs JR, Wacker MJ: Fgf23 is a novel regulator of intracellular calcium and cardiac contractility in addition to cardiac hypertrophy. American journal of physiology Endocrinology and metabolism 2013;304:E863-873.
193 Hsu HJ, Wu MS: Fibroblast growth factor 23: A possible cause of left ventricular hypertrophy in hemodialysis patients. The American journal of the medical sciences 2009;337:116-122.
194 Negishi K, Kobayashi M, Ochiai I, Yamazaki Y, Hasegawa H, Yamashita T, Shimizu T, Kasama S, Kurabayashi M: Association between fibroblast growth factor 23 and left ventricular hypertrophy in maintenance hemodialysis patients. Comparison with b-type natriuretic peptide and cardiac troponin t. Circulation journal : official journal of the Japanese Circulation Society 2010;74:2734-2740.
195 Marson BP, Poli de Figueiredo CE, Tanus-Santos JE: Imbalanced matrix metalloproteinases in cardiovascular complications of end-stage kidney disease:

A potential pharmacological target. Basic & clinical pharmacology & toxicology 2012;110:409-415.
196 Kim HW, Rehwald WG, Wendell DC, Jenista E, Assche LV, Jensen CJ, Chen E-L, Parker M, Kim R: Flow-independent dark-blood delayed enhancement (fiddle): Validation of a novel black blood technique for the diagnosis of myocardial infarction. Journal of Cardiovascular Magnetic Resonance 2016;18:O55.
197 Varga-Szemes A, Muscogiuri G, Rehwald WG, Schoepf UJ, Litwin SE, De Cecco CN, Wichmann JL, Mangold S, Caruso D, Fuller SR, Suranyi P: Accuracy of a prototype dark blood late gadolinium enhancement technique for the detection and quantification of myocardial infarction. Journal of Cardiovascular Magnetic Resonance 2016;18:Q65.
198 Muscogiuri G, Rehwald WG, Schoepf UJ, Suranyi P, Litwin SE, De Cecco CN, Wichmann JL, Mangold S, Caruso D, Fuller SR, Bayer 2nd RR, Varga-Szemes A: T(rho) and magnetization transfer and inversion recovery (traminer)-prepared imaging: A novel contrast-enhanced flow-independent dark-blood technique for the evaluation of myocardial late gadolinium enhancement in patients with myocardial infarction. Journal of magnetic resonance imaging : JMRI 2016
199 Wong TC, Piehler KM, Kang IA, Kadakkal A, Kellman P, Schwartzman DS, Mulukutla SR, Simon MA, Shroff SG, Kuller LH, Schelbert EB: Myocardial extracellular volume fraction quantified by cardiovascular magnetic resonance is increased in diabetes and associated with mortality and incident heart failure admission. European heart journal 2014;35:657-664.
200 Friese RS, Rao F, Khandrika S, Thomas B, Ziegler MG, Schmid-Schonbein GW, O'Connor DT: Matrix metalloproteinases: Discrete elevations in essential hypertension and hypertensive end-stage renal disease. Clinical and experimental hypertension (New York, NY : 1993) 2009;31:521-533.

VITA

TORI ANN STROMP

EDUCATION

2013-2016 **Doctorate of Philosophy,** Physiology (expected Dec 2016)
University of Kentucky, College of Medicine: Lexington, KY

2015-2016 **Graduate Certificate in Clinical and Translational Science**
University of Kentucky, Center for Clinical Translational Science

2005-2009 **Bachelor of Science**, Psychology
Otterbein University (Formerly Otterbein College): Westerville, OH

PROFESSIONAL RESEARCH EXPERIENCE

2012-2013 **Clinical Trials Associate II**
Monroe Carell Jr. Children's Hospital at Vanderbilt: Nashville, TN
Neurology/Pediatric Division

2010-2012 **Research Assistant I**
Vanderbilt University Kennedy Center: Nashville, TN
Psychiatry Department

2009-2010 **Clinical Research Coordinator**
Ohio State University, Nisonger Center: Columbus, OH
Research Unit on Pediatric Psychopharmacology

2009 **Lab Manager/ Research Assistant**
Otterbein University; Westerville, OH
Psychology Department

PUBLICATIONS

2016 **Stromp TA**, Kidney RM, Andres KN, Spear TJ, Kaine JC, Leung SW, Vandsburger MH. Magnetization Transfer Magnetic Resonance Imaging Identifies Cardiac Fibrosis in End Stage Renal Disease without Gadolinium and Correlates with Biomarkers of Collagen Turnover. *In preparation.*

Spear TJ, **Stromp TA**, Leung SW, Vandsburger MH. Influence of longitudinal position on the evolution of steady state signal in

cardiac cine balanced steady state free precession imaging. *Journal of Magnetic Resonance Imaging*. *Under Review.*

Kolb, SJ, Coffey, CS, Yankey, JW, Krosschell, K, Arnold, WD, Rutkove, SB, … the NeuroNEXT Clinical Trial Network and on behalf of the NN101 SMA Biomarker Investigators. (2016). Baseline results of the NeuroNEXT spinal muscular atrophy infant biomarker study. *Annals of Clinical and Translational Neurology*, *3*(2), 132–145. http://doi.org/10.1002/acn3.283. (*Member of the NN101 SMA Biomarker Investigators*)

2015 **Stromp TA**, Leung SW, Andres KN, Jing L, Fornwalt BK, Charnigo RJ, Sorrell VL, Vandsburger MH. Gadolinium Free Cardiac Magnetic Resonance Imaging with 2-point Cine Balanced Steady State Free Precession. *Journal of Cardiovascular Magnetic Resonance. 2015 Oct 29;17(1):90. doi: 10.1186/s12968-015-0194-1.*

ORAL PRESENTATIONS

2016 **Stromp TA,** Spear TJ, Kidney RM, Andres KN, Kaine JC, Leung SW, Charnigo RJ, Sorrell VL, Vandsburger MH. Differentiating Cardiac Fibrosis from Hypertrophy in Patients with End Stage Renal Disease Using Non-Contrast MRI and Imaging Guided Biomarkers. Invited trainee talk: University of Kentucky Gill Heart Institute 19th Annual Cardiovascular Research Day, Lexington, KY. November 2016.

Stromp TA, Spear TJ, Kaine JC, Andres KN, Kidney RM, Leung SW, Sorrell VL, Vandsburger MH. Quantifying Cardiac Fibrosis in Renal Failure Patients Using Gadolinium-Free Molecular MRI. *World Molecular Imaging Congress*. September 2016.

Stromp T. Non-Contrast MRI for the Identification of Cardiac Fibrosis in Hemodialysis Patients. University of Kentucky Physiology Department Seminar, April 2016.

2015 **Stromp T.** Preliminary Application of Non-Contrast Cardiac MRI for Detection of Fibrosis in Chronic Renal Failure Patients. University of Kentucky Physiology Department Seminar & University of Kentucky Muscle Forum, May 2015.

2014 **Stromp T**. Leung SW, Jing L, Fornwalt BK, Sorrell VL, Charnigo RJ, Vandsburger MH. Clinical Gadolinium-Free Magnetic Resonance Imaging with Magnetization Transfer Contrast Detects Cardiac Fibrosis with High Sensitivity and Specificity Compared to

Late Gadolinium Enhanced Imaging. *American Heart Association Scientific Sessions*, eAbstract Presentation, Chicago, IL Nov 2014.

Stromp T. Exploiting Endogenous Magnetization Transfer Contrast in Clinical Standard MRI to Identify Cardiac Fibrosis and Edema without Gadolinium. Invited trainee talk: University of Kentucky Gill Heart Institute 17th Annual Cardiovascular Research Day, Lexington, KY. October 2014.

Stromp T. Clinical MRI of Cardiac Fibrosis and Edema without Gadolinium Contrast. Invited trainee talk, University of Kentucky Physiology Department Research Retreat, Jabez, KY, Aug 2014.

ABSTRACTS

*presenting author

2016 **Stromp TA*,** Spear TJ, Kidney RM, Andres KN, Kaine JC, Charnigo RJ, Leung SW, Sorrell VL, Vandsburger MH. Differentiating cardiac fibrosis from hypertrophy in chronic kidney disease hemodialysis patients using gadolinium-free imaging and biomarkers of extracellular matrix turnover. *CCTS External Advisory Committee* and *19th Annual Gill Heart Institute Cardiovascular Research Day*, Lexington, KY; *American Heart Association Scientific Sessions,* New Orleans, LA. November 2016.

Stromp TA*, Spear, TJ, Kidney, RM, Andres KN, Kaine JC, Leung SW, Vandsburger MH. Measuring Cardiac Fibrosis in End Stage Renal Disease Patients Using Non-Contrast MRI. University of Kentucky Department of Physiology Research Retreat. Lexington, KY. August 2016.

Stromp TA*, Kaine JC, Spear, TJ, Andres KN, Fornwalt, BW, Leung SW, Sorrell VL, Vandsburger MH. Cardiac Tissue Characterization in End Stage Renal Disease Patients with Non-Contrast MRI and Myocardial Mechanics. *International Society for Magnetic Resonance In Medicine 24th Annual Meeting and Exhibition*, ePoster presentation, Singapore. May 2016.

Spear TJ, **Stromp TA**, Leung SW, Vandsburger MH. Comparing the impact of through-plane motion during the cardiac cycle on steady state signal evolution in cine 2D and 3D balanced steady state free precession. *International Society for Magnetic Resonance In Medicine 24th Annual Meeting and Exhibition*, Singapore. May 2016.

Stromp TA*, Kaine JC, Spear, TJ, Andres KN, Kidney, RM, Leung SW, Sorrell VL, Vandsburger MH. Non-Contrast MRI for Safe Assessment of Cardiac Fibrosis in End Stage Renal Disease Patients. Association for Clinical and Translation Science; *Translational Science 2016*, Washington, DC, and University of Kentucky *Center for Clinical and Translational Science Spring Conference*, Lexington, KY. Apr 2016.

Stromp TA*, Kaine JC, Andres KN, Jing L, Fornwalt BK, Leung SW, Sorrell VL, Vandsburger MH. Non-contrast Cardiac MRI for Tissue Characterization in Patients with End Stage Renal Disease. *19th Annual Society for Cardiovascular Magnetic Resonance Scientific Sessions*. Los Angeles, CA. Jan 2016.

2015 **Stromp TA***, Kaine JC, Andres KN, Leung SW, Sorrell VL, Vandsburger MH. Identifying Cardiac Remodeling in Patients with End Stage Renal Disease: A Non-Contrast MRI Study. *18th Annual Gill Heart Institute Cardiovascular Research Day*. Lexington, KY. Oct 2015.

Kaine J, **Stromp T**, Jing L, Leung S, Sorrell V, Vandsburger M. Chronic Kidney Disease patients found to have near normal cardiac mechanics using standard cardiac CINE MRI. *18th Annual Gill Heart Institute Cardiovascular Research Day*. Lexington, KY. Oct 2015.

Andres K, **Stromp T**, Spear T, Leung S, Sorrell V, Vandsburger M. Non-Contrast Cardiac Magnetic Resonance Imaging of Myocardial Fibrosis in Type 2 Diabetes Mellitus. *18th Annual Gill Heart Institute Cardiovascular Research Day*. Lexington, KY. Oct 2015.

Stromp TA*, Leung SW, Sorrell VL, Vandsburger MH. Non-contrast characterization of interstitial cardiac remodeling in chronic kidney disease patients. *International Society for Magnetic Resonance In Medicine 23rd Annual Meeting and Exhibition*. Toronto, Ontario, Canada. June 2015.

Lawless RD, Leung SW, **Stromp TA**, Thompson K, Vandsburger MH. Myocardial tissue characterization from cine bSSFP signal waveforms and longitudinal shortening identifies edematous and fibrotic myocardium in agreement with gadolinium enhanced imaging *International Society for Magnetic Resonance In Medicine 23rd Annual Meeting and Exhibition*. Toronto, Ontario, Canada. June 2015.

Kaine J, Stromp T, Jing L, Leung S, Sorrell V, Vandsburger M. MRI of Cardiac Mechanics Reveals Normal Mechanical Function in Patients with Chronic Kidney Disease. University of Kentucky College of Medicine Alpha Omega Alpha Groves Memorial MD/PhD Student Research Symposium. Lexington, KY. February 2015.

2014 **Stromp TA***, Leung SW, Jing L, Fornwalt BK, Sorrell VL, Vandsburger MH. Clinical Gadolinium-Free Magnetic Resonance Imaging with Magnetization Transfer Contrast Detects Cardiac Fibrosis with High Sensitivity and Specificity Compared to Late Gadolinium Enhanced Imaging. *American Heart Association Scientific Sessions*, Chicago, IL Nov 2014.

Stromp T*, Leung SW, Jing L, Fornwalt BK, Sorrell VL, Charnigo RJ, Vandsburger MH. Exploiting Endogenous Magnetization Transfer Contrast in Clinical Standard MRI to Identify Cardiac Fibrosis and Edema without Gadolinium. University of Kentucky/Gill Heart Institute 17th Annual Cardiovascular Research Day and University of Kentucky Center for Muscle Biology Research Day, Lexington, KY. October 2014.

Stromp TA*, Leung SW, Sorrell VL, Charnigo RJ, Vandsburger MH. Two-Point Balanced Steady State Free Precession MRI Detects Cardiac Fibrosis and Edema Without Gadolinium. *American College of Cardiology—Kentucky Chapter 10th Annual Meeting and Scientific Session: Valvular Summit 2014 with Emphasis on the Left Heart*, Louisville, KY. October 2014.

Stromp T*, Leung S, Jing L, Fornwalt B, Charnigo R, Sorrell V, Vandsburger M. Gadolinium Free 2-point Balanced SSFP MRI Correctly Identifies Cardiac Fibrosis and Edema. *UK Physiology Department Research Retreat*, Jabez, KY, Aug 2014.

2012 Corbett B, Coke C, Bingham E, **Stromp T**, Swain D, Taylor C, Wang L, Song Y. Presented by B Corbett. *International Meeting for Autism Research*, Toronto, Ontario, Canada. May 2012.

Stromp T*, Corbett B, Social Engagement in Children with and without Autism in a Natural Play Environment. *Vanderbilt Kennedy Center Science Day*, Nashville, TN. Feb 2011.

2011 Corbett B, **Stromp T*,** Swain D. Social Emotional Neuroscience Endocrinology (SENSE) Lab. *Vanderbilt University Interdisciplinary Graduate Program Neuroscience Orientation Day*, Nashville, TN. Aug 2011.

Corbett B, Schupp C, **Stromp T*,** & Sharma R. Peer Social Interactions and Cortisol Responsivity in Children with Autism. *Vanderbilt Kennedy Center Science Day*, Nashville, TN. Feb 2011.

Corbett B. Constantine L, Schupp C, **Stromp T***, Sharma R. SENSE Theatre Intervention Research Program for Children with Autism. *Vanderbilt Kennedy Center Science Day.* Nashville, TN. Feb 2011

2009 **Stromp T***, Clark N, Wendling H, Thinnes C. Impression formation based on variation in accent. *Midwestern Psychological Association Undergraduate Research Conference*, Chicago. IL. Mar 2009.

FUNDING

2015-2016 **NIH T32 Predoctoral Fellow**—TL1RR000115
Clinical and Translational Science

HONORS AND AWARDS

2016 University of Kentucky Department of Physiology Research Retreat best graduate student poster
University of Kentucky Graduate Student Congress Travel Award
ISMRM, Educational Stipend, 24th Annual Meeting; Singapore
2015 ISMRM, Educational Stipend for the 23rd Annual Meeting; Toronto, Ontario, Canada
2014 Council on Cardiovascular Radiology & Intervention (CVRI) Early Career Investigator Travel Award, AHA Scientific Sessions, Chicago, IL
Center for Muscle Biology Research Day, 1st place grad student poster
2013-2016 University of Kentucky Integrated Biomedical Sciences (IBS) Research Incentive Award
2009 Graduated *summa cum laude*, Otterbein University

2009 Otterbein University Psychology Department Leadership Award
2008-2009 Psi Chi National Honor Society in Psychology
2006-2009 Alpha Lambda Delta National Honor Society
Phi Eta Sigma National Honor Society
2005-2009 Academic Dean's List, Otterbein University
Ohio Board of Regents Academic Scholarship
Otterbein University President's Award Scholarship

PROFESSIONAL MEMBERSHIP

2016 World Molecular Imaging Society (WMIS)
2015-2016 Society for Cardiovascular Magnetic Resonance (SCMR)
2014-pres International Society for Magnetic Resonance in Medicine (ISMRM)
2014-pres American Heart Association (AHA)
2012-pres The Society of Clinical Research Associates (SoCRA)

LEADERSHIP

2016-pres Executive Board, Director of Committees (elected)
University of Kentucky Biomedical Graduate Student Organization

2016-pres Volunteer Coordinator (nominated)
Central Kentucky American Heart Association Heart Walk

2012-2013 Staff Representative (nominated)
Vanderbilt University Clinical and Translational Research Staff Council

MENTORSHIP

Medical Students:
Kristin Andres (2015-2016), Joshua Kaine (2014-2016)
Laboratory Technicians:
Rebecca Kidney (2015-pres), Tyler Spear (2015-2016)
Research Assistant:
Rahul Subbraryan (2010)

SERVICE

2016-pres University of Kentucky Biomedical Graduate Student Organization
2015 Area Health Education Centers' Health Researchers Youth Academy volunteer presentation
2014 Alpha Phi Red Dress Gala (at UK) American Heart Association benefit, invited presentation
2014-pres American Heart Association Heart Walk volunteer
2014-2015 The Sports Geeks/ SW.O.R.D. volunteer
2014-2016 Kentucky American Water Fayette County District Science Fair community judge